Diss. ETH Nr. 14803

Development of Al-Si-Mg Alloys for Semi-Solid Processing and Silicon Spheroidization Treatment (SST) for Al-Si Cast Alloys

A dissertation submitted to the

SWISS FEDERAL INSTITUTE OF TECHNOLOGY ZURICH

for the degree of

Doctor of Technical Sciences

presented by

Erhard Ogris
Dipl.-Ing., TU-Wien
born on 26th February 1975
citizen of Austria

accepted on the recommendation of

Prof. Dr. P.J. Uggowitzer, examiner
Prof. Dr. M.O. Speidel, co-examiner
Prof. Dr. S. Virtanen, co-examiner

2002

- to Elke -

ACKNOWLEDGEMENTS

I also owe my appreciation to many other members of our institute as well as to some students. Here are the names of those who have substantially contributed to the successful completion of this particular work: Roger Bachmann, Werner Blattmann, Dr. Markus Diener, Niklaus Koch, Markus (Bio) Müller, Régis Pittier, Christian Roth, Eduard Schaller, Christian Wegmann, Torsten Wulff and Pius Zihlmann.

A sincere thank you goes to Simon Kleiner with whom I had the pleasure to share the room for the most part of my time here. I thank him for many useful critical comments and helpful discussions as well as for his special sense of humour.

Last but not least I would like to express my deep gratitude to my parents who encouraged and supported me in all respects. A very big thank you goes to my sisters (Waltraud, thanks a million for reviewing the manuscript and Hedwig, thank you for being my first medical consultant) and mother-in-law as well as to my great extended family for their support and constant interest in my work.

Above all I owe an extra special thank you to my beloved wife Elke, not only for her enormous interest in my work and her critical review of my written English, but furthermore for her brave and selfless approval of an almost three-year-long weekend relationship.

ABSTRACT

The increasing need of lighter and safer cars is the driving force behind research in the area of high strength light metal safety part applications. Following the demands of the automotive industry, safety parts should have a minimum fracture elongation of 15% and a minimum yield strength of 180 MPa. The huge hurdle for Al-Si cast alloys is the 15% fracture elongation which can not be reached by conventional sand or die casting, but some relatively new alternative casting technologies, like thixocasting yield encouraging ductility values. The development of new ductile Al-Si-Mg alloys for semi-solid metal forming is the subject of the first part of the present thesis. It is generally desired to abstain from the expensive T6 treatment. During T6 solution heat treatment the silicon fibres spheroidize and therefore substantially contribute to good ductility values in T6. It is shown, though, that due to sharp-edged eutectic silicon fibres the ductility is limited when no solution heat treatment is applied (T5). Although the effect of silicon spheroidization has already been well documented, there are very few statements concerning the entire process of spheroidization and kinetics. The effect of sole spheroidization on mechanical properties has not been studied so far. The silicon spheroidization and its influence on mechanical properties is theoretically and experimentally described in the second part of the thesis. Modelling as well as experimental investigations of the silicon spheroidization show that well modified eutectic silicon spheroidizes within minutes of soaking time between 500°C and 540°C. The application of this Silicon Spheroidization Treatment (SST) to thixoformed components results in outstanding fracture elongation values (up to 18%) at good yield strength level (~230MPa). The influence of SST on static, dynamic and impact properties is also investigated. FEM simulations of the short high temperature heat treatment confirm a short process time for successful SST even for components with notably variable wall thicknesses. SST has been patented and is successfully applied to different components and alloys in industrial environment.

ZUSAMMENFASSUNG

Der steigende Bedarf an leichten und sicheren Autos ist die treibende Kraft für die Forschung an hochfesten Leichtmetallsicherheitsbauteilen. Für Sicherheitsbauteile wird von der Automobilindustrie eine minimale Bruchdehnung von 15% und eine minimale Streckgrenze von 180MPa gewünscht. Für Al-Si Gusslegierungen ist die grosse Hürde dabei die Bruchdehnung von 15%, die mit herkömmlichem Sand- oder Druckguss nicht erreicht werden kann. Bruchdehnungswerte aus Bauteilen, die mit einem relativ neuen Semi-Solid Giessverfahren wie Thixocasting hergestellt werden, geben allerdings berechtigten Anlass zur Hoffnung, die geforderten Bruchdehnungswerte zu erreichen. Der erste Teil der vorliegenden Arbeit beschäftigt sich mit der Entwicklung neuer, duktiler Al-Si-Mg Legierungen für das Thixocasting, die möglichst ohne die teure T6 Lösungsglühung hergestellt werden sollen (T5). Eine T6 Lösungsglühung sphäroidisiert das eutektische Silizium und ist somit hauptverantwortlich für die guten Bruchdehnungswerte im Zustand T6. Es wird gezeigt, dass die Duktilität ohne entsprechende Lösungsglühung wegen des scharfkantigen eutektischen Siliziums begrenzt ist. Obwohl der positive Effekt der Siliziumsphäroidisierung schon lange bekannt ist, wurden die alleinigen Auswirkungen einer Siliziumsphäroidisierung auf die mechanischen Eigenschaften bis jetzt noch nicht untersucht. Diese Sphäroidisierung des eutektischen Siliziums und ihr Einfluss auf die mechanischen Eigenschaften ist im zweiten Teil dieser Arbeit Gegenstand theoretischer und experimenteller Untersuchungen. Modellierung und experimentelle Untersuchungen ergeben, dass ein veredeltes eutektisches Silizium zwischen 500°C und 540°C innerhalb weniger Minuten vollständig sphäroidisiert ist. Die Anwendung dieses Silicon Spheroidization Treatments (SST) liefert bei Thixobauteilen bestechende Bruchdehnungswerte (bis 18%) bei guter Festigkeit (~230MPa). Weiters wird auch der positive Einfluss von SST auf andere mechanische Eigenschaften beschrieben. FEM Berechnungen bestätigen die sehr kurze SST-Gesamtprozessdauer auch für Bauteile mit beträchtlich unterschiedlichen Wanddicken. SST wurde bereits patentiert und wird an verschiedenen Bauteilen und Legierungen industriell erfolgreich angewendet.

TABLE OF CONTENTS

1
INTRODUCTION

1.1 HISTORIC PERSPECTIVE

Since Hans Christian Ørsted had succeeded at first in making aluminum on a laboratory scale in Denmark in 1825 the triumphal procession of aluminum was not to stop. In 1886 the American Charles Martin Hall and the French Paul T. Héroult independently from each other developed the electrolysis of aluminum oxide dissolved in molten cryolite [ALT98]. The coincidental invention of the dynamo by General Electric and Siemens and the development of an efficient process that used caustic soda to extract the alumina from bauxite by the Austrian Karl Joseph Bayer in 1892 have substantially contributed to the mass production of aluminum. However, since pure aluminum is a very soft metal, the development of numerous aluminum alloys became a prerequisite for their extensive technical use. Above all the epoch making discoveries of precipitation hardening of aluminum alloys by Alfred Wilm and the modification of aluminum silicon eutectic by Aladar Pacz are worth to be considered more closely.

1.1.1 THE STORY OF DURALUMIN

Around the turn of the last century, in 1901, Dr. Alfred Wilm started work to improve the strength of Al-alloys which then left much to be desired. He joined a government laboratory close to Berlin. With a background in chemistry from Berlin and Göttingen universities he knew all about the physical metallurgy of his days. He knew that steel can be hardened if the right compositions were cooled fast enough. So he mixed a very large number of Al-alloys and quenched them at different rates. To his great frustration many alloys became even softer the more rapidly they were quenched. The saga of his discovery

tells that Wilm was a devoted researcher, but a man with other hobbies too. He conducted many quenching experiments with Al-Cu-alloys with small amounts of additional elements on a saturday morning. The sun was shining and so he remembered his other hobby, interrupted his work and went out sailing on the Havel river for the whole weekend. On monday morning, first hardness measurements and then tensile tests were resumed of the quenched alloys. To his greatest astonishment, hardness had increased considerably during the two days and so did the tensile properties. The experiments were repeated systematically and by 1906 an alloy of Al with 3.5-5.5% Cu, plus less than 1% Mg and Mn was patented [WIL06]. This alloy, named DURALUMIN, is still in use 100 years later [HOR01].

1.1.2 THE STORY OF SILICON MODIFICATION

The commercial attraction of Al-Si cast alloys is based on the discovery of modification of Al-Si eutectic around 1920 from a genius named Dr. Aladar Pacz. Pacz who was born in Csokas, Hungary, on January 11th, 1882 emigrated to the United States in 1905 where he first became an engineer at General Electric Company in Cleveland. Around 1915 he developed a non-offsetting and non-sagging tungsten wire which was obtained by the addition of potassium to the tungstic oxide. This was the major

Figure 1.1: Aladar Pacz, developer of Al-Si eutectic modification and non-sag tungsten wire.

breakthrough for the successful development of the incandescent lamp. Pacz left the General Electric Company sometime in the early 1920s and established a business to develop aluminum alloys [WOO@]. There he observed that the brittle aluminum silicon eutectic changed its morphology from undesired long plates to fine acicular fibres when small amounts of alkali fluoride or sodium or potassium were added to the melt. In 1921, Pacz introduced Al-Si alloys containing up to 15% silicon in the United States under the trade name "ALPAX" [PAC21], and the development of these alloys marked the start of exten-

sive research on Al-Si alloys and subsequently deliberate investigations of the nature of the Al-Si eutectic [MAK01]. As part of the spoils of World War I, the United States were to receive a dirigible, which would be made by the famous Zeppelin Company at Friedrichshafen, Germany. Until that ship was christened in the United States, it was known as ZR-3; after the christening it became the U.S.S. Los Angeles. The delivery date was made possible, in part, because of one of Pacz's silicon-aluminum alloys. After the war, Germany was not in good financial condition, and it could not afford to use copper in its aluminum alloys. Pacz's alloy, therefore, could be used to some extent in needed castings. His alloy was used by the French in streetcars and railways, and the Belgians, British and Germans also used it. In Germany the alloy was used in motor blocks of the expensive Daimler car. That car was later renamed after the 10-year-old daughter of the businessman, Emil Jellinek. Thus, the Mercedes name on an automobile was born [WOO@].

1.2 ADVANCED PROCESSING OF ALUMINUM ALLOYS

For many years the biggest end-use market for aluminum has been the transportation sector with a major share of it going into car manufacturing. More than 80% of present aluminum applications in automobiles are accounted for by cast components, such as gear boxes, cylinder heads, pistons, and engine blocks [EAA@]. A novel casting process that has lately been the subject of much attention is thixocasting. The technique takes advantage of the thixotropic properties of some metal alloys in the partly solidified state [ALT98]. Thixotropy can be derived from the Greek words for „contact, touch", and „change, modification". Hence, thixotropy describes the property of some materials becoming fluid when stirred or shaken, and setting solid again when allowed to stand still [WAH01]. The cutting test demonstrates the thixotropic behaviour of AlSi7Mg alloy in Figure 1.2. The discovery of this shear rate dependent viscosity for metals in the solidification range in the early 1970s [SPE71] was the starting point for the development of semi-solid processing routes for light metal alloys, also known as „semi-solid metallurgy" (SSM) or „semi solid forming" [WAB02].

Over the last decade or more, the primary driving force for the development and enhancement of semi-solid forming processes has been the automotive industry in its search for
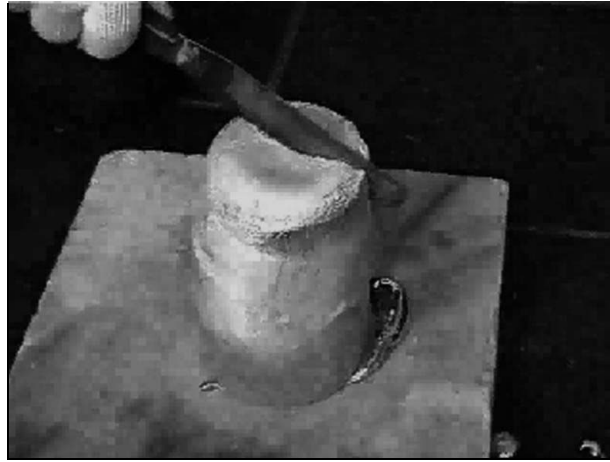
Figure 1.2: AlSi7Mg slug in its semi-solid state can be easily cut with a knife.

energy efficient automobiles. Aluminum and magnesium usage in automobiles, especially in cast form, has increased dramatically and as a consequence the need for parts of higher strength and greater reliability has increased. SSM is one of the important processes filling this niche [FLE00].

One of the major benefits from SSM is the enhanced weldability and heat treatability of SSM components. Heat treatment is a key process to improve mechanical properties and durability of metallic components. Its technology is currently facing various challenges such as environmental impact, energy conservation and the more stringent market needs such as higher performance, reliability, reduction of car weight, and production costs [FUN98]. Heat treatment standards currently being used in the cast shops were developed several years ago and need to be revised to suit current foundry practice [APE90]. Additionally to traditional heat treatment processes the advancement of new furnace design and new heat treatment technologies like fluidized bed heat treating [BIC98] or new alternative heat treatment procedures will forward effective contemporary processing of aluminum components.

The enhancement of mechanical properties via balanced development of both specific alloys for semi-solid forming and alternative cost-effective heat treatment procedures is the main object of this particular work.

2
GENERAL ASPECTS

Semi-solid forming provides several advantages compared to conventional forming techniques. In order to satisfy the increasing demands for high-strength and high-ductile light metal components, specific alloy designs for semi-solid forming combined with development of new competitive heat treatment processes are essential.

2.1 SEMI-SOLID PROCESSING

For semi-solid metal forming (SSM) the following major requirements are necessary:

- The material must have a sufficiently wide temperature range of solidification and a continuous transition from solidus to liquidus.

- The material must provide non-dendritic, globular α-grains prior to forming.

In alloys which fulfill these prerequisites the viscosity dramatically decreases when the material is sheared in the semi-solid state (Fig. 2.1).
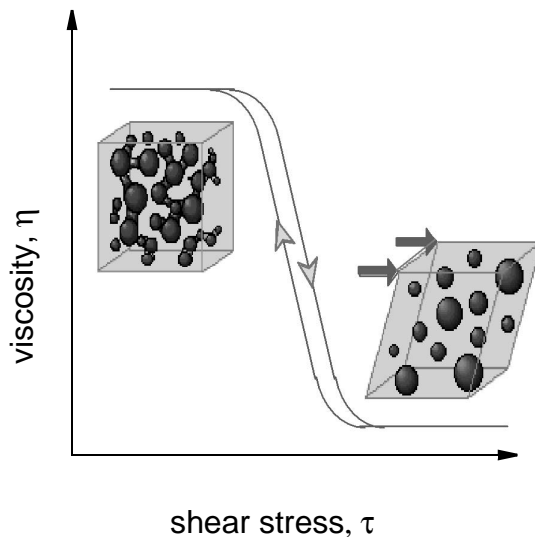
Figure 2.1: Schematic breakup of solid skeleton when sheared [UGG00a].
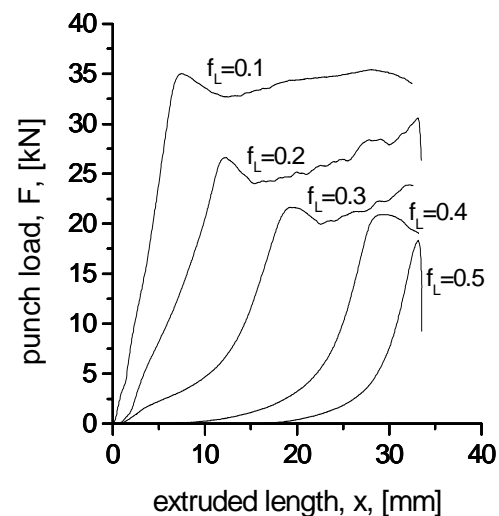
Figure 2.2: Thixotropic behaviour of Al 7075 by backward extrusion [OGR01].

The interconnected solid skeleton breaks up resulting in a suspension containing α-grains and liquid. A semi-solid backward extrusion experiment demonstrates the transition from solid behaviour to thixotropic behaviour (Fig. 2.2). Due to laminar filling of the cavity and lower process temperatures several specific advantages of thixoformed components in comparison to conventional forming techniques can be indicated (Table 2.1).

Table 2.1: Characteristics of SSM for future exploitation [FLE99].

Characteristic	**Potential benefit or application**
Lower heat content than liquid metal	- Higher speed part forming - Higher speed continuous casting - Lower mould erosion - Ferrous part forming - Forming of other high-melting-point materials - Forming of reactive materials
Solid present at time of mould filling	- Less shrinkage voids - Less feeding required - Less macrosegregation - Fine grain structure
Viscosity higher than in liquid metals and controllable	- Less entrapped mould gases - Reduced oxides - improved machinability - Less mould attack - Higher speed part forming - Improved surface finish - Automation - New processes
Flow stress lower than for solid metals	- Forming of intricate parts - High speed part forming - Lower cost part forming - High speed forming of continuous shapes (e.g. extrusion) - New processes
Ability to incorporate other materials	- Composites
Ability to separate liquid and solid	- Purification

2.1.1 TECHNOLOGIES FOR SSM PROCESSING [FAN02]

Technologies for SSM processing can be generally divided into two basic routes: the thixo-route and the rheo-route. The thixo route is basically a two step process, involving preparation of a feedstock material with thixotropic characteristics, then reheating the feedstock material to semi-solid temperature to produce the SSM slurry which is subsequently used for component shaping. The rheo-route involves preparation of a SSM slurry from liquid alloys by shearing during solidification and transferring the prepared SSM slurry directly to a die or mould for component shaping.

The objective of feedstock production is to provide a material with a characteristic thixotropic microstructure where a non-dendritic (or globular) primary phase with a fine grain size is uniformly distributed in a matrix of lower melting point. Thixotropic feedstock production can start either from a liquid alloy through controlled solidification under specific conditions, or from solid state through heavy plastic deformation and recrystallization. Currently, there is little choice in commercially available feedstock materials, and alloys are usually limited to aluminum based materials, mostly A356 and A357 type cast alloys with 3-6 inch billet diameter, produced by MHD stirring. However, there are a number of other production techniques which are at different stages of research and development.

2.1.1.1 TECHNOLOGIES FOR PRODUCTION OF NON-DENDRITIC FEEDSTOCK

Mechanical stirring

Melt agitation is commonly generated by means of augers, impellers, or multipaddle agitators mounted on a central rotating shaft. The shear offered by the stirrer during solidification promotes the formation of non-dendritic structure.

Magnetohydrodynamic (MHD) stirring

In this technique, local shear is generated by rotating electromagnetic fields within the continuous casting mould, and continuous billets of solidified non-dendritic alloy can be produced. The stirring is deep in the sump of the liquid, which has previously been filtered and degassed, so that contamination is virtually eliminated. At present, MHD stirring has established itself as the most widespread practice for feedstock production. Electromag-

netic stirring can be achieved through three different modes: vertical flow, horizontal flow, and helical flow, with the helical mode being ultimately a combination of the vertical and horizontal modes (Fig. 2.3).
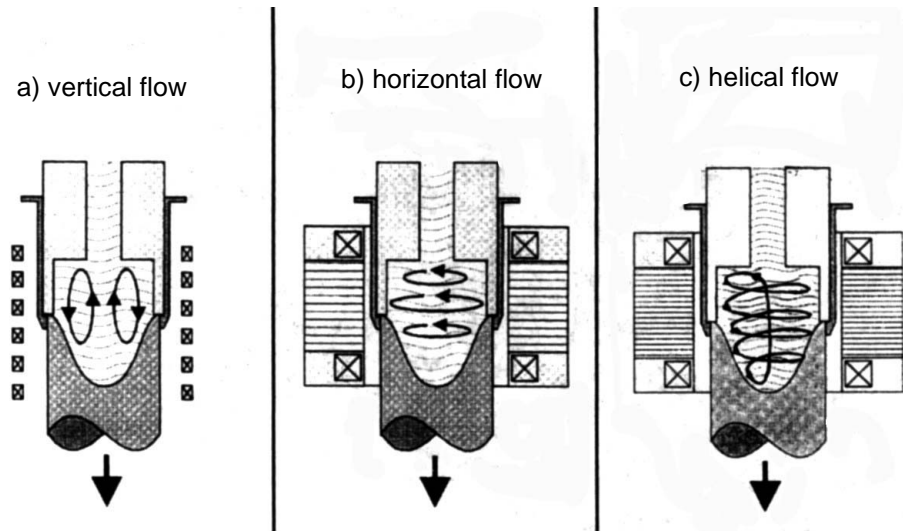
Figure 2.3: Different flow modes of electromagnetical stirring, a) veritcal flow, b) horizontal flow and c) helical flow [NIE00].

In the horizontal flow mode, the motion of the solid particles takes place in a quasi-isothermal plane probably the dominant mechanism for spheroidization. In the vertical flow mode, the dendrites located near the solidification front are recirculated to the hotter zone of the stirring chamber and partially remelted, and therefore thermal processing is dominant over mechanical shearing. The continuous casting is made through either a vertical or horizontal arrangement, depending on the casting direction in relation to the gravity direction.The major advantages of horizontal continuous casting include better economy, continuous production, and low investment costs, but the quality of the billet is influenced by the gravity.

Stress induced and melt activated (SIMA) process

An alternative to the liquid agitation route is the SIMA process. This process originally developed by Young et al. [YOU83] involves:

a) cold deformation of a hot extruded and quenched billet to induce residual plastic strain.

b) reheating the cold worked billet to a semisolid temperature to produce the globular structure.

c) thixoforming the billet in its semisolid state.

This process is based on the scientific understanding that high angle grain boundaries induced by plastic deformation and recrystallization will be wetted by liquid metal at the semisolid temperature, resulting in a fine and globular structure. The SIMA process produces high quality feedstock for thixoforming and has the potential for wrought alloys and high melting temperature alloys such as steel and superalloys. However, the SIMA process requires plastic deformation and recrystallization of conventionally cast dendritic materials by thermomechanical treatments that are energy and processing intensive making it cost approximately 3-5 times more than the MHD stirring process.

Spray casting

Spray casting (Osprey process) is another non-agitation process for feedstock production. In this process molten metal is directed through a nozzle to meet the high pressure inert gas (nitrogen or argon). The liquid metal stream is atomized by the high pressure gas into micrometer sized droplets that experience high cooling rate during their flight, the cooling rate being in the order of 10^3 K/s. While the large droplets remain fully liquid and the small droplets solidify during atomization, those of intermediate sizes become semi-solid. The droplets are collected on a moving substrate and consolidated to form a coherent preform.

Liquidus casting

Liquidus casting, also known as low superheat casting, has been developed recently as an alternative technique for production of thixotropic feedstock. In liquidus casting, melt with a uniform temperature just above its liquidus is poured into a mould for solidification. The resulting microstructures are usually fine and non-dendritic. Upon reheating, the liquidus cast microstructure spheroidizes rapidly to produce microstructural features suitable for thixoforming operations.

Ultrasonic treatment

Experimentally, it is well established that application of ultrasonic treatment to a cooling melt at a starting temperature just above its liquidus can produce effectively a fine and non-dendritic microstructure, which is suitable for subsequent reheating and thixoforming operations. Regarding the mechanism for the formation of such fine and non-dendritic structure, it is now generally believed that introduction of high power ultrasonic vibration

into a liquid alloy can lead to two basic physical phenomena: cavitation and acoustic streaming. Cavitation involves the formation, growth, pulsation, and collapsing of tiny bubbles in the melt. The compression rate of these unsteady bubbles can be so high that their collapsing generates hydraulic waves, thus producing artificial sources of nuclei. The propagation of a high intensity ultrasonic wave involves the initiation of steady state acoustic streaming in the melt. When ultrasonic vibration is coupled to the solidifying metal, the structural changes include grain refinement, suppression of the columnar grain structure, increased homogeneity, and reduced segregation.

Chemical grain refining

Chemical grain refinement is nowadays a common practice in continuous casting of aluminum alloys. This technique has also been considered for feedstock production. In most cases, a prealloyed wire is proportioned into the hot metal flow into the launder where it releases heterogeneous nucleation agents, usually titanium and boron based. Owing to the enhanced heterogeneous nucleation rate and suppression of dendritic growth, a fine and equiaxed structure can be achieved. With an appropriate grain refining, such a structure can also be suitable for subsequent reheating and thixoforming. However, chemical grain refilling is not used alone, but used in conjunction with other feedstock production methods, such as MHD stirring and liquidus casting. One disadvantage of the chemical grain refinement method is that nucleation agents are only effective to specific alloy systems, another is that in some cases these additives will remain present in the product as nonmetallic inclusions, which may impair both the processability of the semifinished stock and the mechanical properties of the final product.

2.1.1.2 TECHNOLOGIES FOR COMPONENT SHAPING

Thixoforming

Thixoforming is a general term coined to describe the near net shape forming processes from a partially melted non-dendritic alloy slug within a metal die. If the component shaping is performed in a closed die, it is referred to as thixocasting, while if the shaping is achieved in an open die, it is called thixoforging. There are two separate stages involved in the thixoforming process: reheating and forming. Reheating to the semisolid state is a particularly important phase in the thixoforming process. Currently, reheating is achieved

horizontal continuous casting
with MHD stirring facility

sawing into slugs

thixoforging   thixocasting

remelting + ladling
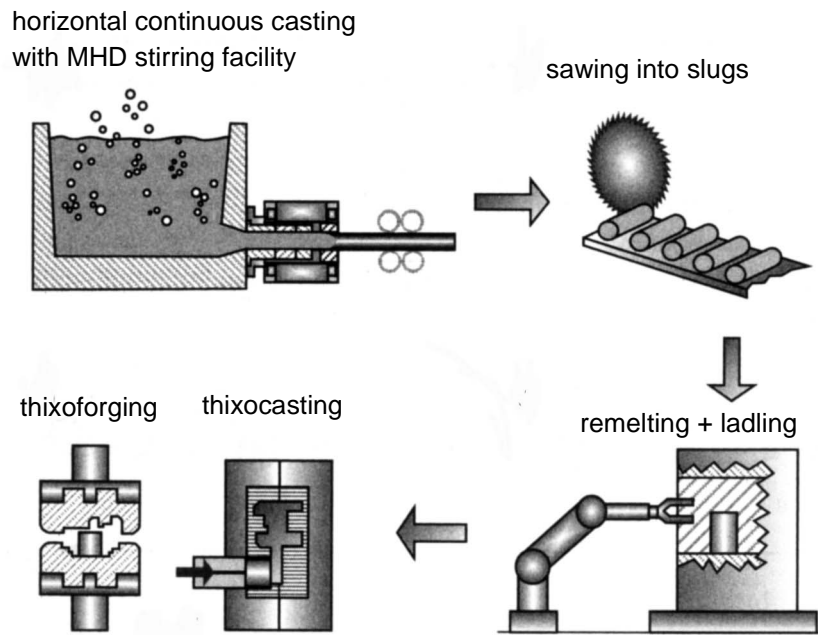
Figure 2.4: Process scheme of conventional thixoforming [GUL01].

mainly by induction heating, which ensures precise and fast heating, which is necessary for SSM processing. The forming process takes place either with casting (thixocasting) or with forging (thixoforging), as schematically illustrated in Figure 2.4. At present, thixocasting through horizontal cold chamber die casting is the dominant process. A robot arm transfers the semisolid slug into the shot chamber and the plunger injects the materials into the die cavity by a hydraulic ram. All the thixocasting machines are real-time controlled and thus permit a reaction to possible fluctuation during the forming process. At this stage, smooth laminar mould filling is the crucial step for the forming process. This can be achieved by an optimized shot profile tailored for specific alloys and their physical conditions. Another important aspect during the forming process concerns the design of the gating system and die cavity and the correct choice of die temperature.

Rheocasting

The process of production of non-dendritic semisolid slurry by shearing during solidification has been identified as rheocasting. Although rheocasting was identified as the production technology at the very beginning of semisolid processing research, it has not been commercialised to any great extent so far. This is possibly because of the poor quality of the semisolid slurry produced by stirring processes. However, component shaping

directly from SSM slurries is inherently attractive due to its characteristics, such as overall efficiency in production and energy management. One of the so called slurry-on-demand processes is the recently developed new rheocasting (NRC) process, which was patented by UBE Industries Ltd [UBE96]. In the NRC process, as shown schematically in Figure 2.5, a slightly overheated melt liquid metal is poured into specially designed steel crucibles, which are placed on a carousel next to a vertical SQC machine. In the crucible,
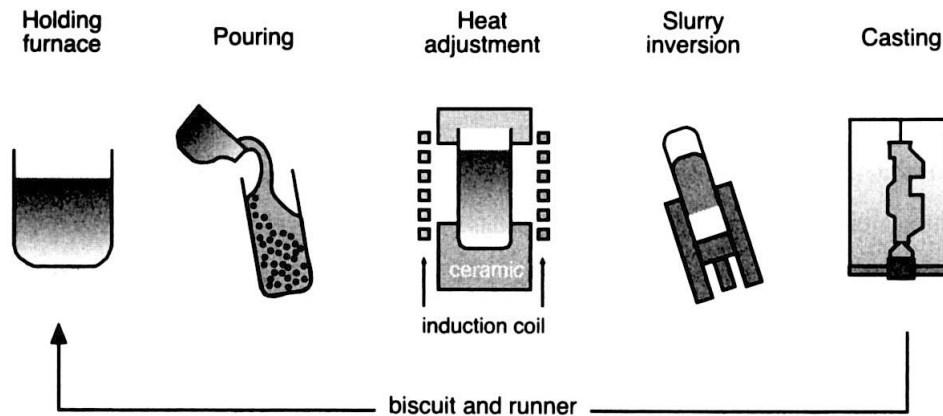
Figure 2.5: Process stages of the New Rheocast (NRC) Process, schematic [GUL01].

semisolid slurry is formed by controlled cooling through a mechanism similar to the case of liquidus casting described in Chapter 2.1.1.1. By controlling the slurry temperature (therefore solid fraction), a stable skeleton of the solid phase is formed within a few minutes after pouring. The solid-like slug of cylindrical shape is then heated by induction heating to homogenise the slug temperature before being transferred into the sleeve of the vertical SQC machine, where it is cast into its final shape. Since conventional alloys can be used, NRC offers a significant cost advantage over thixoforming and SQC processes. A detailed description of the NRC process can be found in [WAB01].

2.2 HEAT TREATMENT OF ALUMINUM ALLOYS

Controlled heat treatment of aluminum alloys can significantly influence properties such as strength, ductility, fracture toughness, thermal stability, residual stresses, dimensional stability, and resistance to corrosion and stress corrosion cracking. The main heat treatment procedures are homogenization, annealing, and precipitation hardening involving solution heat treatment, quenching, and ageing [DAH01]. A heat treatment and temper designation system has been developed by the Aluminum Association to describe the processing of wrought and cast aluminum alloys (Table 2.2).

Table 2.2: Heat treatment and temper designation system for aluminum alloys [DAH01].

Suffix		Treatment
F		As-fabricated
O		Annealed
H		Strain hardened by cold work
T		Heat treated to a stable condition, excluding annealing (O)
	T1	Cooled from an elevated temperature forming process (partial solution) followed by natural ageing
	T2	Cooled from an elevated temperature forming process, cold worked and naturally aged
	T3	Solution heat treated, quenched, cold worked and naturally aged
	T4	Solution heat treated, quenched and naturally aged
	T5	Rapidly cooled from elevated forming temperature and then artificially aged
	T6	Solution heat treated, quenched and then artificially aged
	T7	Solution heat treated, quenched and overaged
	T8	Solution heat treated, quenched, cold worked and then artificially aged (amount of cold work in % indicated by subsequent digit)
	T9	Solution heat treated, quenched, artificially aged and then cold worked
	T10	Cooled from an elevated temperature forming process, cold worked and then artificially aged
W		Unstable temper applied for alloys which age spontaneously at room temperature after solution heat treatment. Only specific if followed by the time of natural ageing.

2.2.1 HOMOGENIZATION

The as-cast microstructure of direct chill (DC) cast ingots normally displays significant segregation and supersaturation. Microsegregation in the cast ingots, i.e., segregation on a microstructural scale, is manifested by coring in the dendrites and also non-equilibrium eutectics and intermetallic phases at the grain boundaries. Coring describes the gradual change in composition from the center to the edge of dendrites and grains. Elements such as iron, chromium, zirconium, and manganese have a low solid-state diffusion rate and, therefore, exist in supersaturated solid solution in the aluminum dendrites owing to the high cooling rates during solidification. The main aim of homogenization is to improve workability and mechanical properties by dissolving the non-equilibrium brittle interdendritic constituents and by providing a more homogeneous structure throughout the ingot. Homogenization carried out at temperatures between the solvus and the solidus, ~450-600 °C, for extended periods of time, 2-10 h.

2.2.2 ANNEALING

Different types of annealing treatments with different objectives exist depending on the alloy system and prior processing. Full annealing (O temper) produces the softest, most ductile, and workable conditions for both heat-treatable and non-heat-treatable wrought alloys. Reduction or elimination of the strengthening from cold working is accomplished by heat treating at a temperature between ~250°C and 450°C for times ranging from a few seconds to several hours. The annealing temperature should not exceed 415 °C to avoid oxidation and grain growth. Heating and cooling rates must be controlled to avoid precipitation hardening or softening in heat-treatable alloys. Relatively slow cooling is recommended for all alloys to minimize distortion. However, for heat treatable alloys, a slow cooling rate will result in the formation of coarse precipitates. Annealing of castings is not common. However, it may be used to provide maximum dimensional stability for elevated temperature service and a high ductility. When used, the treatment involves 2-4h at 315-345°C to provide the optimum relief of residual stresses and precipitation of phases formed by any excess solute retained in solid solution in the as-cast state.

2.2.3 SOLUTION HEAT TREATMENT

Solution heat treatment to achieve the maximum concentration of solute in solid solution is carried out at a sufficiently high temperature for sufficiently long times to produce a nearly homogeneous solid solution. The temperature is determined based on the composition and maximum solid solubility, and is normally achieved by heat treating near, but below, the eutectic temperature. It is important to avoid local melting both during heating, i.e., heating sufficiently slowly to redissolve nonequilibrium precipitates, and at the solution heat treatment temperature. Normally, temperature variations within ± 6°C are allowed, but may be even stricter for some high-strength aluminum alloys. Underheating results in incomplete solution and reduces the strengthening potential of the alloy. solution heat treatment time depends on microstructure, section thickness, and furnace loading and can vary from less than a minute to 20h. Generally, the soak times for castings are longer than for wrought products due to coarser microstructures. Aluminum-silicon casting alloys in which the eutectic silicon is modified by the addition of elements such as strontium, sodium, or antimony, undergo rapid spheroidization of the silicon particles, while complete spheroidization is never achieved in unmodified alloys. solution heat treatment is normally performed in air, but molten salt baths or fluidized beds can be used to obtain more rapid heating. Distortion due to creep must be considered in designing the furnace loading equipment. High-temperature oxidation causing surface blistering and rounded pores within the material can result if the solution heat treatment is performed in an atmosphere with high moisture content and is aggravated by sulfur containing gases.

2.2.4 QUENCHING

Subsequent to solution heat treatment the material must be cooled at a sufficient rate to retain the solute in solid solution and to retain a high number of vacancies at room temperature. Precipitation during cooling could result in coarse particles that are detrimental to mechanical and corrosion properties. It also reduces the level of supersaturation and, therefore, the response to subsequent age hardening. Generally the highest attainable strength levels, the best combination of strength and toughness, and best corrosion resistance and resistance to stress corrosion cracking are, therefore, associated with the most rapid quenching rates. The sensitivity of alloys to quench rate and the allowable delay between solution heat treatment and quenching is determined from quench factor analysis

which is based on avoiding the tip of the nose of the Continuous Cooling Transformation (CCT) diagram. Precipitation kinetics is a compromise between degree of supersaturation and diffusion rate which depend on temperature in opposite ways, resulting in maximum nucleation and growth occurring over a critical temperature range which is between 290°C and 400°C for most alloys. Quench sensitivity is generally higher for higher solute levels and in alloys containing dispersoids which can act as nucleants for coarse precipitates. Water is normally used as the quenching agent. Components with complex shapes and with different thicknesses, such as castings and forgings, are often cooled at slower rates to avoid distortion and excessive residual stresses. This can be achieved by using water at 65-80°C, boiling water, polyalkylene glycol, forced air or mist.

2.2.5 AGEING

Ageing is the controlled decomposition of the supersaturated solid solution to form finely dispersed precipitates in heat-treatable alloys, usually by soaking for convenient times at one or sometimes two temperature levels. The decomposition is normally complicated and occurs through several precipitate stages. These finely dispersed precipitates have a dominant effect in raising yield and tensile strengths, and may also affect other properties such as corrosion resistance and dimensional stability. The age hardening response of some alloys is significantly improved by introducing a controlled amount of cold work prior to ageing. Some alloys retain a supersaturated solid solution and high vacancy concentration, without quenching, by rapidly cooling the material after mechanical working at elevated temperatures. In 1906 Alfred Wilm [WIL06] discovered that hardness and tensile properties of an Al-alloy with 3.5-5.5% Cu had increased after solution heat treatment, quenching and following two-day-ageing at room temperature. In 1939 Guiner and Preston discovered independently from each other copper-rich zones by means of X-rays small angle scattering which appeared precipitated in clusters and were named after them as GP-zones [GUI96]. In order to contribute substantially to an enhancement of strength three requirements had to be fulfilled in Orowan's theory of 1948:

1. a two-phase microstructure of the dispersoid type which impedes motion of dislocations in the matrix,

2. particle diameters and spacings not much larger than atomic size b: $S_p << 100b$,

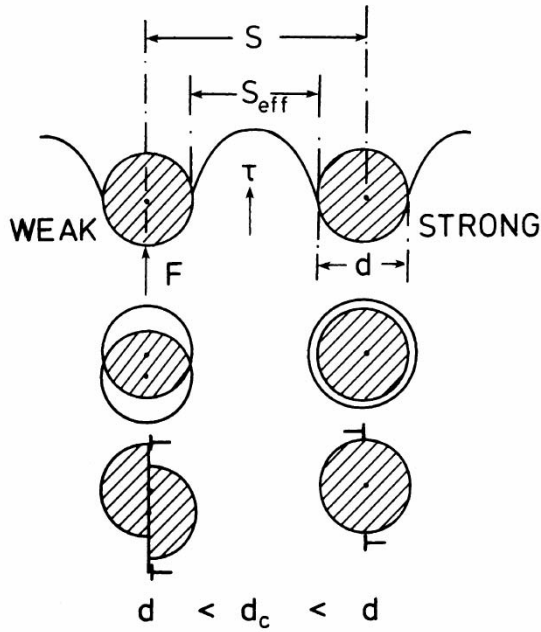3. particles strong enough to promote looping of dislocations without being sheared: $d_c < d_p$.

Figure 2.6: Force F exerted on particle by looping dislocation, schematic [HOR01].

The force *F* which a particle is able to sustain depends on its intrinsic strength and on the particle diameter (Fig. 2.6). Bypassing must take place for

$$F > G \cdot b^2 \qquad (2\text{-}1)$$

For coherent, ordered particles $F=C\cdot\gamma \cdot d_p$ (γ = energy of the antiphase domain boundaries) and consequently the critical particle diameter follows as:

$$d_c = C \cdot \frac{Gb^2}{\gamma_{APB}} \qquad (2\text{-}2)$$

C is a geometrical factor given by the shape of the particle. The other extreme case is a non-coherent particle with a high shear modulus G_β. A dislocation has to be recreated in order to shear the particle. Its critical diameter is consequently very small:

$$d_c = \frac{4\pi b G_\alpha}{G_\beta} \qquad (2\text{-}3)$$

The coherent case would be representative for a β" particle in Al-Si-Mg alloys. Hard non-coherent particles are Si or β-Mg$_2$Si equilibrium phase. The condition $d_p > d_c$ limits the applicability of Equation (2-4) which expresses the increase in yield stress due to dispersoid particles $\Delta\sigma_p$:

$$\Delta\sigma_p = \frac{Gb}{S_p} = \frac{Gb}{S - d_p} = \frac{Gb}{d_p} \cdot f_p^{\frac{1}{3}} \qquad (2\text{-}4)$$

where *S* is the spacing of the particle center. $S \approx S_p$ for small volume fractions $f \leq 1\%$, which are customary in Al-alloys [HOR01].

2.2.5.1 NATURAL AGEING

Natural ageing refers to the decomposition of the solid solution that occurs at room temperature. Most alloys age harden at room temperature and some alloys decompose over a few days to yield stable and adequate properties for many applications. Natural ageing is practised industrially with alloys that display the most significant changes in microstructure and properties over a period of a few days (< 4 days), while the subsequent changes are minor. Other alloys can continue to naturally age for many years. During natural ageing the high level of supersaturation and the high vacancy concentration causes rapid formation of clusters or coherent stable Guinier-Preston (GP) zones. In some alloys, notably the 2xxx series alloys, the ageing response is greatly improved by cold working the recently quenched material, i.e., T3 and T4 treatments are common for these alloys.

2.2.5.2 ARTIFICIAL AGEING

Artificial ageing involves decomposition at elevated temperature, normally in the range of 100-200°C, for times between 2h to 48h. Multiple ageing treatments can also be used. The artificial ageing treatment is designed to produce optimum size, distribution, constitution and morphology of precipitates and amount of solute in solid solution. Hardening is often obtained from partially coherent precipitates. Temperature control during artificial ageing is important while there are often large tolerances on treatment time. Paintbaking operations of many products are often performed in the artificial ageing temperature range and can result in significant hardening. The T6 temper normally yields the highest practical strength combined with useful engineering performance with respect to other specific requirements. Castings have the highest combination of strength, ductility, and toughness in the T6 temper. The T5 and T7 (overageing) treatments are more commonly used for castings than for wrought products. Overageing often involves heat treating at higher temperatures to carry the alloy beyond the maximum strength level. It results in lower strength and hardness than the T6 temper but yields improved dimensional stability during eleva-ted temperature service. The level of residual stress is reduced during artificial ageing, ranging from 10% to 35% for T6, while T7 provides even more substantial reductions. Although the alloys are suitable for age hardening, thermal treatments are normally not beneficial to the mechanical properties of high pressure die-castings, owing to problems such as blistering from entrapped air.

2.3 THE Al-Si EUTECTIC

The Al-Si system is a simple binary eutectic with limited solubility of aluminum in silicon and limited solubility of silicon in aluminum. The solubility of silicon in aluminum reaches a maximum 1.65 at.% at the eutectic temperature, and the solubility of silicon increases with temperature to 0.016% Si at 1190 °C [MAK01]. Figure 2.7 depicts the contemporary Al-Si phase diagram, calculated with Thermo-Calc.
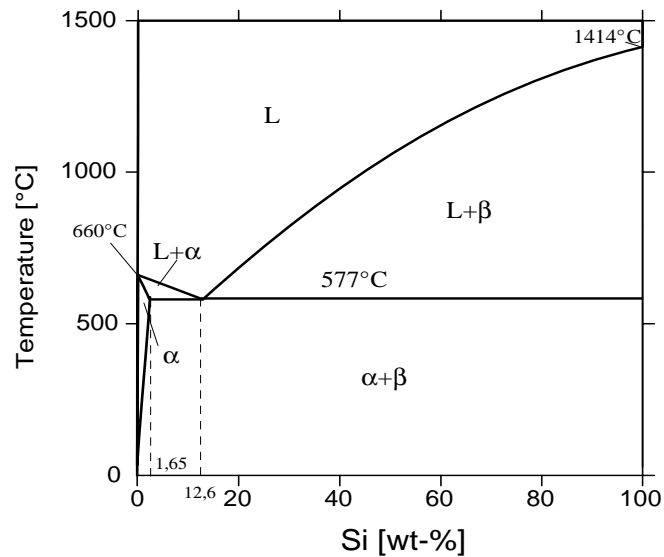

Figure 2.7: Simple binary phase diagram of Al-Si.

There is only one invariant reaction in this diagram, namely

$$L \rightarrow \alpha + \beta \tag{2-5}$$

In Equation (2-5), L is the liquid phase, α is predominantly aluminum, and β is predominantly silicon. It is now widely accepted that the eutectic reaction takes place at 577°C and at a silicon level of 12.6%. Fig. 2.7 shows that the Al-Si eutectic can form as follows:

1. directly from the liquid in the case of a silicon concentration of 12.6% (i.e., for eutectic Al-Si alloy),

2. in the presence of primary aluminum in the case of silicon contents <12.6% (i.e., for hypoeutectic Al-Si alloys), and

3. in the presence of primary silicon crystals in the case of silicon contents >12.6% (for hypereutectic Al-Si alloys).

Eutectic microstructures can be fibrous or lamellar, regular or irregular (Fig. 2.8). The condition is that one phase must always have a low entropy of fusion, so that $\Delta S_{f,\,\alpha} < 2R$. At high volume fractions of both phases ($f \cong 0{,}5$), a situation which is encouraged by a symmetrical phase diagram, there is a marked preference for the formation of lamellar structures (e.g. Pb-Sn). On the other hand, if one phase is present in a small volume fraction, there is a tendency to the formation of fibres of that phase (e.g. Cr in NiAl-Cr). As a rule of thumb, one can suppose that when the volume fraction of one phase is between zero and 0.25, the eutectic will probably be fibrous, especially if both phases are of non-faceted type. If it is between 0.25 and 0.5, the eutectic will tend to be lamellar. If both phases possess a low entropy of fusion, their growth is easy on all crystallographic planes and the resultant structures are regular (non-faceted/non-faceted eutectic). Fibres will become faceted if one phase has a high entropy of fusion or when interfaces having a minimum energy exist between the two phases. When the low volume fraction phase possesses a high entropy of melting, as do Fe-C and Al-Si, the eutectics are of non-faceted/faceted
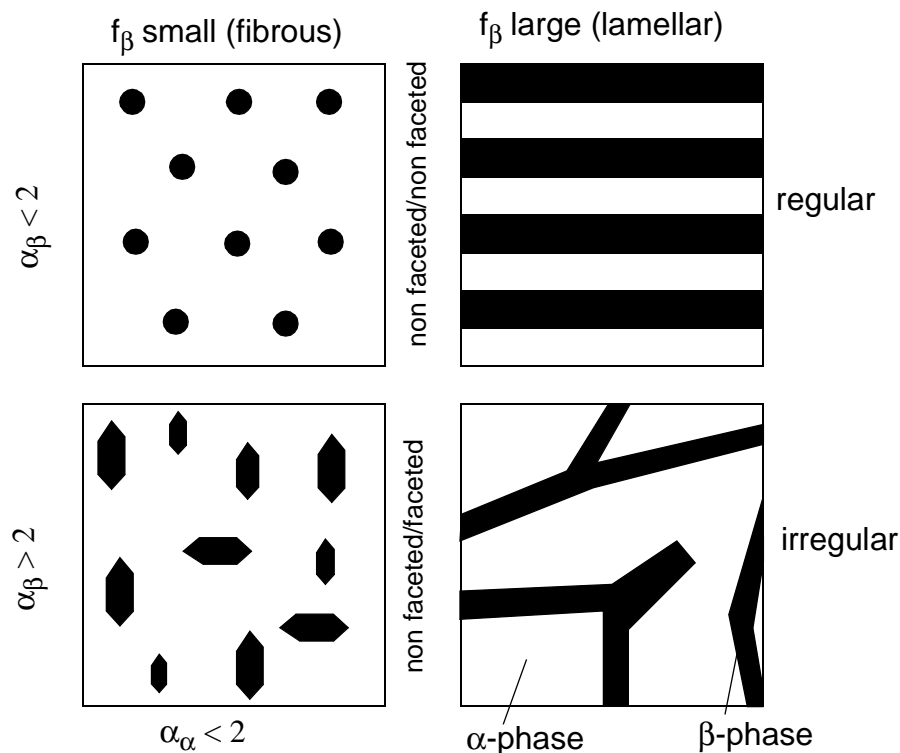

Figure 2.8: Types of binary eutectic morphology, seen in transverse cross-section [KUR86]. $\alpha = \Delta S_f / R$, where ΔS_f denotes the entropy of fusion and R the universal gas constant.

type and the microstructure is usually irregular. Even though the volume fraction of silicon in the Al-Si binary is less than 0.25, the typical Al-Si eutectic is closer to a lamellar structure than to a fibrous one. This is usually attributed to the strong anisotropy of growth of silicon and to the relatively low interfacial energy between silicon and aluminum [KUR86].

2.3.1 MODIFICATION OF THE Al-Si EUTECTIC

Aladar Pacz discovered in 1921 that: "When normal Al-Si alloys are treated after simple melting with an alkali fluoride or with sodium or potassium, so-called ‚modified' alloys result. In the case of the normal alloys, the silicon occurs as relatively large plates and needles, while in the modified ones the silicon is in a state of high dispersion". The preparation of both normal and modified has been patented by Pacz and by the Aluminum Company of America (ALCOA) [PAC21]. Now it is well established that the Al-Si eutectic can exhibit either of two morphologies an unmodified and a modified morphology. The unmodified morphology is typically coarse and flaky and is usually observed in slowly cooled foundry alloys when no chemical modifiers are added. The microstructure of an unmodified Al-Si eutectic is shown in Figure 2.9.
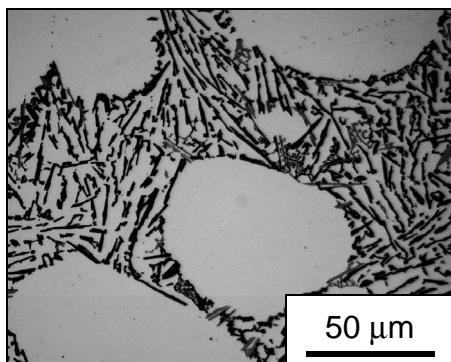
Figure 2.9: Unmodified Al-Si eutectic.
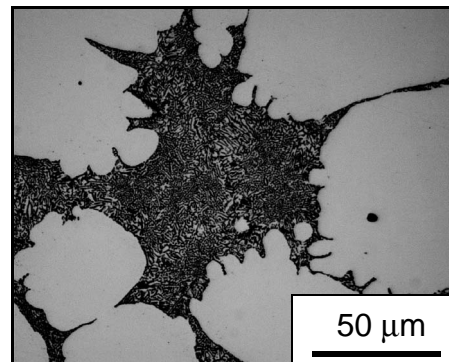
Figure 2.10: Sr-modified Al-Si eutectic.

In chemically modified alloys or at relatively fast cooling rates, such as in chill casting, the Al-Si eutectic is much finer and the silicon assumes fibrous morphology as shown in Figure 2.10. It should be noted however that the growth mechanism of silicon in the chemically modified alloy is quite different from that in the chill cast alloy.

In 1987 Lu and Hellawell conducted detailed TEM studies on impurity modified silicon fibres in order to document their growth mechanism. Lu and Hellawell [LU85] observed significant twinning in the flake morphology and the impurity modified fibres, but not in the quench modified fibres. Moreover, they observed that twinning in the impurity modified fibres was more frequent than in the silicon fibre with flake morphology. Based on these observations they concluded that silicon in the flake morphology grows predominantly by the layer mechanism illustrated in Figure 2.11. According to the impurity in-
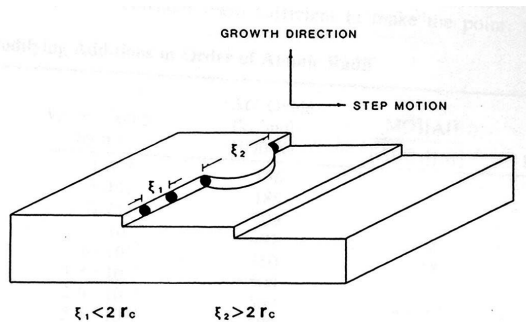

Figure 2.11: Schematic representation for adsorbing of impurity atoms at monolayer steps on a growth interface, r_c is some critical dimension for layer extension [LU87].
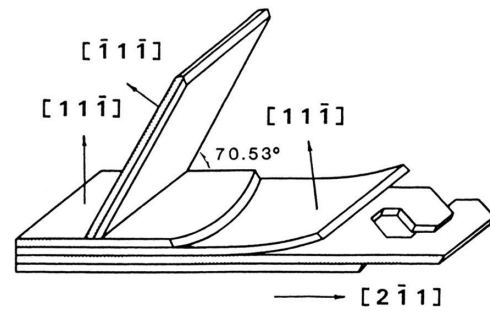

Figure 2.12: Schematic branching in silicon flakes [LU87].

duced twinning theory [LU87], chemical modifiers are impurities that poison already growing atomic silicon layers by becoming adsorbed onto surface steps and kinks thus preventing the attachment of silicon atoms to the crystal. Furthermore, the adsorbed impurity atoms induce twinning by altering the stacking sequence of atomic layers as the newly added layers seek to grow around the adsorbed impurity atom. Thus, during growth of the fibrous eutectic the fibres branch frequently (Fig. 2.12), with a wide range of branching angles, in order to maintain optimum interphase diffusion distances at the solid liquid interphase [HOG87]. Lu and Hellawell assumed a face centered cubic structure and calculated the ratio of impurity atom radius (r_i) to matrix atom radius (r) that is required for impurity induced twinning and found it to be $r_i/r = 1.6457$. Analysis for sodium in modified Al-Si alloys via Auger electron spectroscopy and via electron microprobe measurements show that sodium segregates in the silicon fibres and in the aluminum matrix, which seems to validate the impurity induced twinning theory. It is interesting to note that sodium, which has less than the ideal radius ratio for eutectic modification as predicted

by the impurity induced twinning theory, is a better modifier than ytterbium and calcium, which are very close to the ideal radius ratio. Moreover, lithium, which is much smaller than the ideal radius ratio modifies the silicon morphology when added in large concentrations to Al-Si alloys [MAK01]. Figure 2.13 illustrates the ratio of atomic radii for various elements and their reported effect on the Al-Si eutectic.
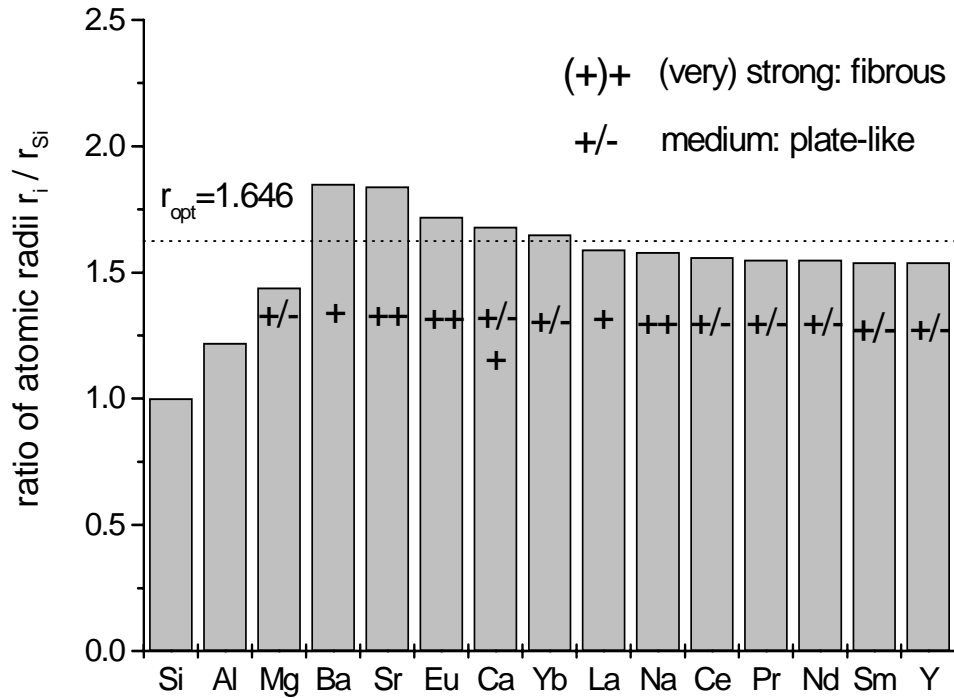

Figure 2.13: Optimal ratio of atomic radii for impurity induced twinning after the model of Lu and Hellawell [LU87] and reported modification level for different elements. (References: Mg [JOE91], Ba, Yb, Y [KNU01], Sr [CLO81, CLO82, VEN91, HAQ94, SHI98], Eu, Pr, Nd, Sm [QIY81], Ce [QIY81, ROB98], Na [PAC21, KIM63, VEN91], La [KIM63, BAC83], Sb [MEY74, KNU01], Ca (+) [KNU01], Ca (+/-) [KIM63, ABD98]).

2.4 MICRO- AND MACROSEGREGATION

Segregation terms the demixing of elements as a result of non-equilibrium states during solidification. It occurs as a consequence of the different solubility of these elements in the solid and the liquid phase, respectively. These segregations remain for the most part present even after complete solidification. Furthermore, segregation is highly influenced by mass transport phenomena (e.g. diffusion) in the solid phase and in the liquid phase. Segregation can be seen as short range (micro) segregation and long range (macro) segregation. Concentration differences of the latter are in the order of the component and remain unchanged even after long-term heat treatment. Short range segregations are in the order of the grains and can mostly be eliminated by a homogenization heat treatment. Different models have been developed for long and short range segregation [SAH99], respectively, of which the following is a relevant abstract.

2.4.1 EQUILIBRIUM SOLIDIFICATION (LEVER RULE)

As the solidification proceeds under the equilibrium condition, the solute compositions in the solid, c_S, and the liquid, c_L, vary along the solidus and liquidus lines, respectively (Fig. 2.14). The ratio c_S / c_L is referred to as the equilibrium partition or distribution coefficient, k [ASM88].
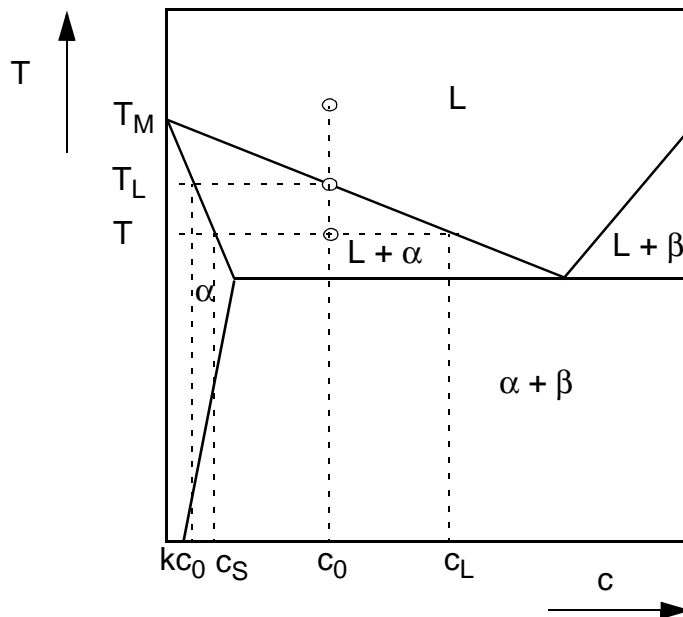

Figure 2.14: Simplified phase diagram of a binary eutectic system, $k = c_S / c_L$.

In the equilibrium condition, there is ideal diffusion in the solid and complete mixing in the liquid ($D_S = \infty$, $D_L = \infty$). A liquid with a initial concentration, c_0, solidifies at $T=T_L$ with a solid fraction of $k \cdot c_0$. The mass balance which remains effective during the whole solidification process can be written to

$$c_S \cdot f_S + c_L \cdot f_L = c_0 \tag{2-6}$$

where f_S and f_L denote the fraction of solid and liquid phase, respectively. With $f_S = 1 - f_L$ for the considered one-dimensional solidification and $k = c_S / c_L$ Equation (2-6) yields

$$c_S = \frac{kc_0}{1 - (1\text{-}k)f_S} \tag{2-7}$$

also known as the law of lever. On the basis of the simplified phase diagram in Figure 2.14, a relationship between the liquid fraction, f_L, and the temperature, T, can be written to

$$f_L = 1 - f_S = 1 - \frac{c_L - c_0}{(1 - k)c_L} = 1 - \frac{T_L - T}{(1 - k)(T_M - T)} \tag{2-8}$$

2.4.2 NON-EQUILIBRIUM SOLIDIFICATION (SCHEIL-MODEL)

The boundary conditions for this model are no diffusion in the solid and complete mixing in the liquid ($D_S = 0$, $D_L = \infty$). The solidification starts again at $T=T_L$ with a solid fraction of $c_S = k \cdot c_0$. However, no diffusion in the solid effectuates that c_S remains constant in a discrete area during solidification. Solely at the solid/liquid interface a local equilibrium of $c_S^* = k \cdot c_L^*$ is formed. With a change of the solid fraction df_S the difference ($c_L^* - c_S^*$) leads to a uniform increase of the concentration dc_L in the remaining melt ($1 - f_S$). The mass balance therefore is

$$(c_L^* - c_S^*)df_S = dc_L(1 - f_S) \tag{2-9}$$

Integration of Equation (2-9)

$$\int_{c_0}^{c_L} \frac{dc_L}{(1-k)c_L} = \int_0^{f_S} \frac{df_S}{1-f_S} \tag{2-10}$$

with the boundary condition $c_L = c_0$ at $f_S = 0$ yields Equation (2-11), commonly known as Scheil's equation:

$$c_S^* = kc_0 \cdot (1-f_S)^{(k-1)} \tag{2-11}$$

Rearrangement of Equation (2-11) with the aid of relationships illustrated in Figure 2.14, a dependence of liquid fraction, f_L, from temperature, T, can be indicated as follows:

$$f_L = 1 - f_S = \left(\frac{c_L}{c_0}\right)^{\frac{1}{k-1}} = \left(\frac{T_M - T}{T_M - T_L}\right)^{\frac{1}{k-1}} \tag{2-12}$$

2.4.3 SOLIFICATION FROM SEMI-SOLID STATE

New boundary conditions for Equation (2-9) must be set if the liquid solidifies from the semi-solid state. Assuming equilibrium condition at $f_S = 0.5$, the new boundary condition are $c_0 = (c_L + c_S)/2$ at $f_S = 0.5$ [UGG00b]. Integrating Equation (2-9) with the boundary conditions for semi-solid solidification gives:

$$f_S^{0,5\,Scheil} = 1 - 0.5 \cdot \left(\frac{(T_M - T)(k+1)}{2m_L c_0}\right)^{\frac{1}{k-1}} \tag{2-13}$$

This model can be used to estimate the amount of unexpected eutectic due to non-equilibrioum solidification from the semi-solid state. However, the model only works properly under the assumption of linear solidus and liquidus lines, respectively.

2.5 MULTIPARTICLE DIFFUSION - OSTWALD RIPENING [GLI00]

Almost a century ago the chemist W. Ostwald observed that the solubility of a substance introduced as particles into an otherwise saturated solution was slightly greater for fine particles than coarse ones. The enhanced solubility of fine particles or droplets in a second continuous phase leads to the growth of the larger particles at the expense of the smaller - a process generically termed *Ostwald ripening* (Fig. 2.15). The phase separation result-
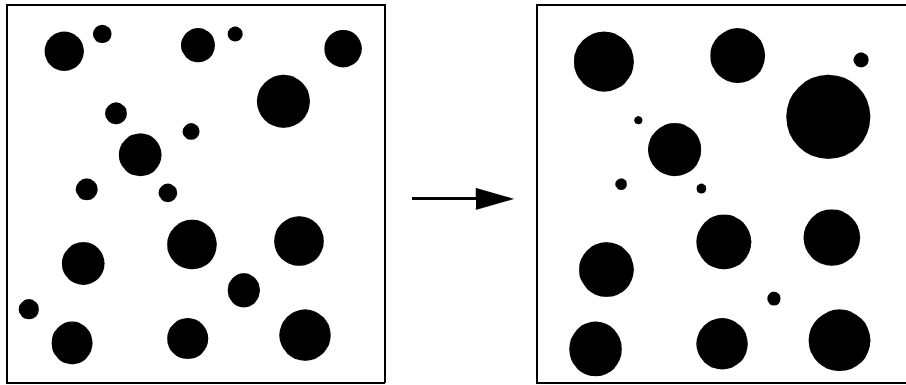

Figure 2.15: Ostwald ripening (schemtaic): Larger particles grow at th expense of the smaller particles [MAS95].

ing from curvature-induced solubility changes and the competitive multiparticle diffusion in solid and liquids is termes *microstructural phase coarsening*. The diffusive transport is driven by the chemical gradients surrounding each particle. Multiparticle diffusion requires both the enhancement of solubility with curvature, and the transport of species through the host matrix between the particles. The basic theory of coarsening was developed by Lifshitz, Slyozov and Wagner, which is known as the *LSW theory* [KUC72]. The main result from the *LSW theory* is that the mean volume of particles grows proportional to time:

$$\overline{R^3} - \overline{R_0^3} = \frac{8D\sigma\Omega c_\infty}{9k_BT} \cdot t = K_{LSW} \cdot t \qquad (2\text{-}14)$$

where R_0 denotes the radius R at $t = 0$, D is the diffusion coefficient, σ the specific interfacial energy, Ω the mean atomic volume, c_∞ the equilibrium concentration in the matrix, and k_B Boltzmann's constant [SAH99].

2.5.1 INFLUENCE OF CURVATURE ON SOLUBILITY

The chemical potential of a solute μ_B at a curved interface relative to the chemical potential at a planar interface, μ_B^0, is given by

$$\mu_B(H) = \mu_B^0 + R_g T \cdot \ln a_B(H) \, , \tag{2-15}$$

with H as the mean curvature. Chemical potential changes at curved interfaces induce slight shifts in the phase equilibria in the free energy-composition diagram, Figure 2.16. These shifts cause corresponding changes in the activity $a(H)$ or equilibrium solubility. The solubility change resulting from the curvature is known as the Thomson-Freundlich effect. For the small changes in the concentration caused by phase curvature, the ratios of the activity and the composition are approximately equal:

$$\frac{a_B(H)}{a_B^0} \cong \frac{c(H)}{c_{planar}} \tag{2-16}$$

The Thomson-Freundlich effect shows that local concentration differences arise in any polydisperse collection of particles in local equilibrium with a matrix phase. The solubility of B atoms saturation the matrix of α-phase surrounding a spherical particle of β-phase with a mean curvature much smaller than the reciprocal capillary length, $H \ll l_c^{-1} = (2\gamma\Omega/R_g T)^{-1}$, may be linearized as

$$c_B(H) = c_B \cdot e^{\left(\frac{2\gamma\Omega}{R_g T} \cdot H\right)} \cong c_B\left(1 + \frac{2\gamma\Omega}{R_g T} \cdot H\right) \tag{2-17}$$

where c_B denotes the bulk solubility in the α-phase at a planar α–β interface (H=0). The small solubility increase depicted for the curved particle (dashed curve in Fig. 2.16) is found from Equation (2-17) as

$$\frac{c_B(H) - c_B}{c_B} = \frac{2\Omega\gamma}{R_g T}H = \vartheta(R) \tag{2-18}$$

where γ is the α-β interfacial energy and Ω the mean atomic volume. The capillary diffusion potential, $\vartheta(R)$, represents the equilibrium interfacial values of the dimensionless
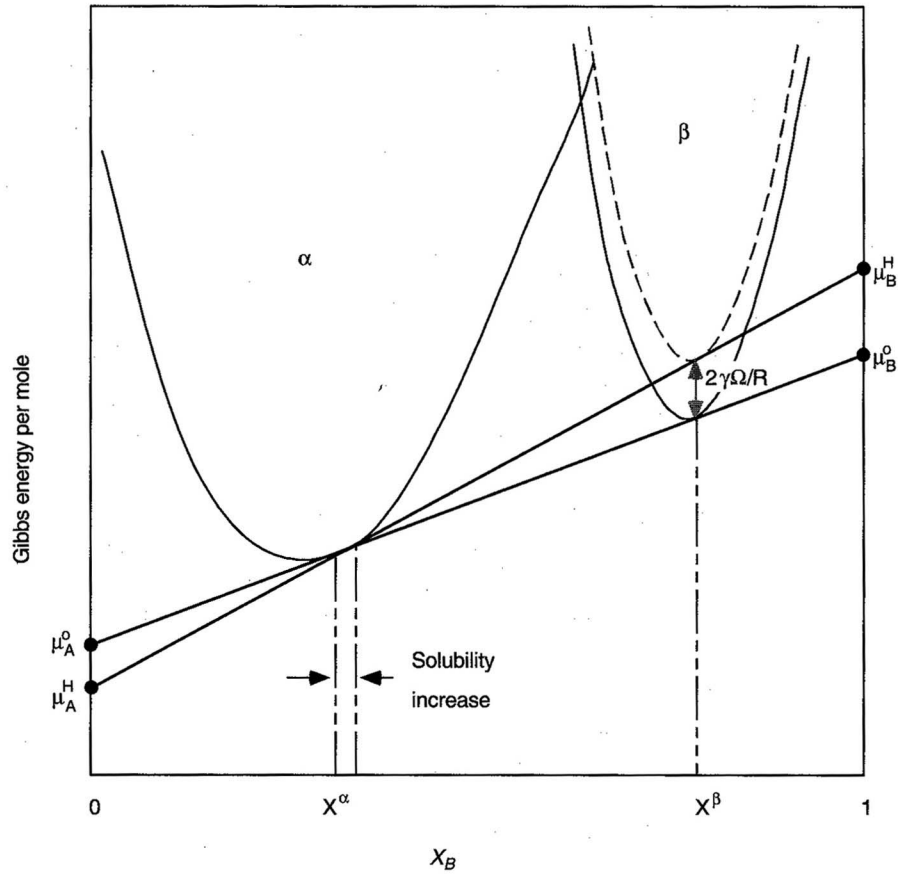
Figure 2.16: Free energy versus composition for planar (solid curves) and curved inter-faces (dashed curve). (Not to scale) [GLI00].

potential in the matrix at the α-β interphase of a spherical β particle of radius R. Because of the complexities of the diffusion field, the diffusion problem is reduced to that of a single, isolated spherical grain, which imposes the following boundary conditions on the diffusion potential in the surrounding α matrix:

$$\vartheta(r)\big|_R = \frac{1}{R} \tag{2-19}$$

$$\vartheta(r)_{lim \ r \to \infty} = \frac{1}{\langle R \rangle} \tag{2-20}$$

The boundary conditions shown in Equation (2-19) and Equation (2-20) are consistent with the assumption that each particle interacts with the average diffusion potential $1/\langle R \rangle$, established by the total population of spherical particles dispersed throughout the

matrix. This assumption, known as the *mean-field approximation*, precludes direct inter-actions among the individual particles. Figure 2.17 depicts the mean-field boundary con-dition schematically. The average diffusion potential sensed far away from each „isolated" particle is that of the average particle, with the average curvature $1 / \langle R \rangle$.
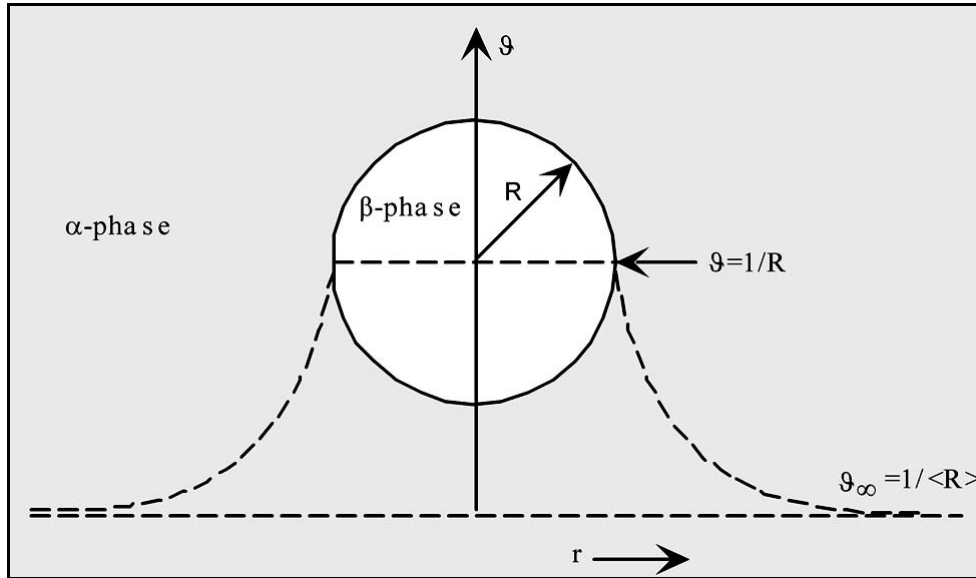

Figure 2.17: Diffusion potential surrounding an isolated spherical particle embedded in a matrix containing a population of particles with an average radius $\langle R \rangle$ [GLI00].

The solution to the quasi-static diffusion equation

$$\nabla^2 \vartheta(r) = 0 \tag{2-21}$$

for a given particle with the boundary conditions specified in Equation (2-19) and Equa-tion (2-20) is given by the spherically symmetric solution

$$\vartheta(r) = \frac{1}{r}\left(1 - \frac{R}{\langle R \rangle}\right) + \frac{1}{\langle R \rangle} \ . \tag{2-22}$$

A normalized graph of the diffusion potential for particles with various radii is shown plotted in Figure 2.18. Note that the average-sized particle has a normalized radius equal to unity; the gradient surrounding this particle is, on average, zero. This condition is con-sistent with the mean-field approximation. The instantaneous average particle neither grows nor shrinks, because it is in momentary local equilibrium with the matrix phase dif-
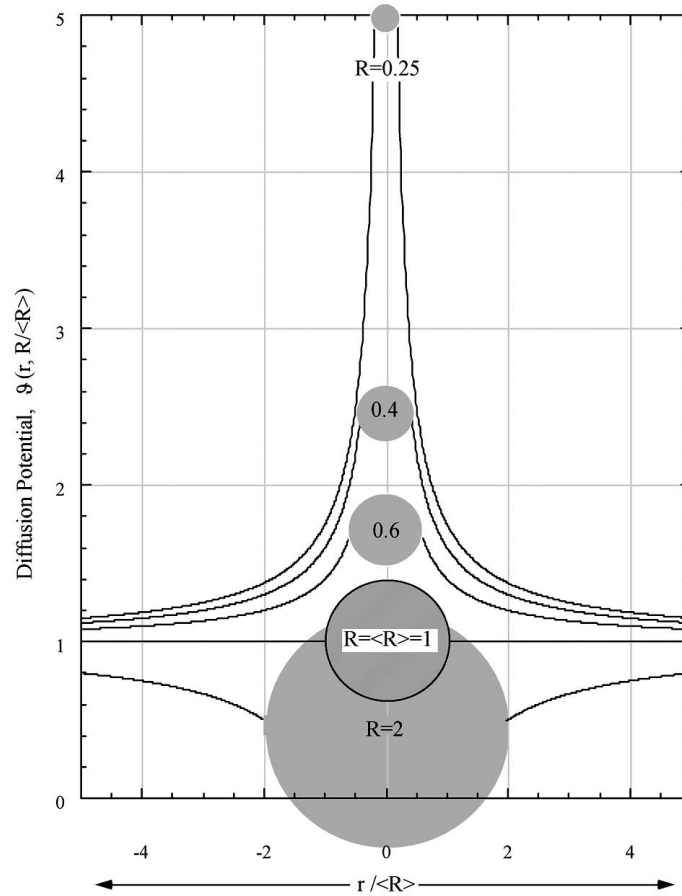
Figure 2.18: Diffusion potential $\vartheta(r)$ for spherical particles with various radii versus normalized radial distance. Radii and distances are expressed in units of the average radius $\langle R \rangle$. The critical particle $R = \langle R \rangle$ separates the population of smaller shrinking particles, surrounded by negative gradients, and larger growing particles, surrounded by positive gradients [GLI00].

fusion potential. The rate of growth (or shrinkage) of the particle is related to the diffusion potential gradient at the interphase:

$$\left. \frac{d\vartheta}{dr} \right|_{r=R} = \frac{1}{R^2}\left(\frac{R}{\langle R \rangle} - 1 \right). \tag{2-23}$$

If R is the dimensionless particle radius, defined in the boundary condition of Equation (2-19), the expected growth or shrinkage rate is given by the mean-field kinetic equation

$$\frac{dR}{d\tau} = \left(\frac{d\vartheta}{dr}\right)_{r\,=\,R} = \frac{1}{R^2}\left(\frac{R}{\langle R\rangle} - 1\right) \tag{2-24}$$

Equation (2-24) is the main result obtained from mean-field theory. It shows that particles larger than the average are expected to grow, whereas particles smaller than the average are expected to shrink.

3
ALLOY DESIGN

Alternative processes like thixoforming mostly evoke a certain need for new materials. The thixoforming process occurs in the semi-solid range, i.e. at totally different temperatures than conventional forming techniques like forging or casting. Thus, diffusion and solubility of significant elements are different. This might open a new process window for alloys specifically developed for semi-solid processing.

3.1 EXPERIMENTAL PROCEDURE

3.1.1 THERMODYNAMIC CALCULATIONS

Thermo-Calc Version M was used for thermodynamic calculations. Thermo-Calc is a databank for inorganic chemistry and metallurgy developed at the Division of Material Science & Engineering of the Royal Institute of Technology in Stockholm. It is restricted to equilibrium calculations but it is possible to use Thermo-Calc as a subroutine for simple simulations of for example non-equilibrium Scheil-Gulliver solidification which was used in this work. For equilibrium calculations the POLY3 modulus with a special Al-database was used. With POLY3 it is possible to calculate many different kinds of equilibria and diagrams, in particular multicomponent phase diagrams. Special databases have been fed by a large quantity of data for thermochemical quantities and chemical equilibria which has been determined experimentally. These databases contain the expressions relating the Gibb's energy of each phase to the temperature, pressure and constitution of the phase [SUN97].

3.1.2 CHEMICAL ANALYSIS

The chemical composition was determined at AluLend GmbH with a spark spectrometer Spectro - Lab M8 of Spectro-Analytical Instruments. The values are mean values of three measurements.

3.2 THE SYSTEM Al-Si$_X$-Mg$_Y$

Among commercial aluminum casting alloys those with silicon as the major alloying element are the most important, mainly because of their excellent casting characteristics. Additions of Si to pure aluminum impart high fluidity, good feeding characteristics, low shrinkage and good hot cracking resistance. The properties of aluminum-silicon alloys make them very popular in various applications including the automotive, aerospace and defence industries. The high strength to weight ratio is one of their most interesting characteristics. As the density of Si is 2.3 g/cm^3, it is one of the few elements which may be added to aluminum (2.7 g/cm^3) without loss of weight advantage [PAR00]. Aluminum-silicon alloys that do not contain copper additions are used when good castability and good corrosion resistance are needed [DAV93]. Magnesium can act as a substitute for copper. Magnesium and silicon can form the intermetallic hardening phase Mg$_2$Si which precipitates in the α-aluminum matrix and increases the yield strength.
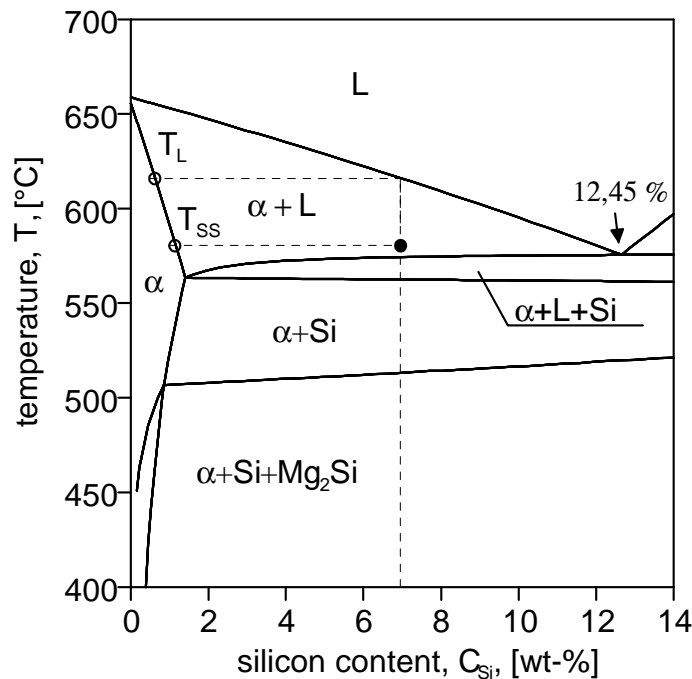

Figure 3.1: Pseudo-binary section of the system AlSiMg0.3.

Due to their excellent castability and good strength-ductility ratio, AlSi7Mg(0.3-0.4) (A356, EN-42100, THIXALLOY®630) and AlSi7Mg(0,45-0.7) (A357, EN-42200,

THIXALLOY®650) are both standard alloys for light metal cast components. Figure 3.1 illustrates a pseudo-binary section through the system AlSiMg0.3. The temperature interval of solidification is about 60 °C and the semi-solid forming temperature, T_{SS}, at a liquid and solid fraction of ca. 50% can be detected to ~580°C.

3.2.1 INCREASING OF Mg CONTENT

It is a well known fact that the yield strength can be increased by an increase of alloyed Mg [WIL11], [RAV98], [CAC99]. The maximum amount of Magnesium which can be dissolved in α-aluminum at simultaneous presence of Si and Mg_2Si is between 0.45 wt% (Fig. 3.3) and 0,75 wt% (Fig. 3.4) at 555°C. Magnesium which cannot be dissolved in the
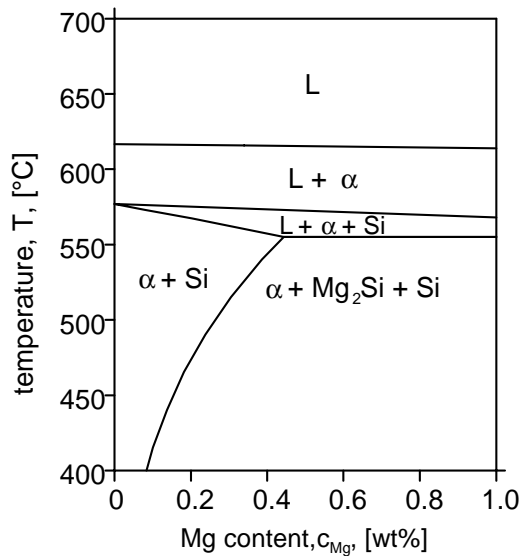
Figure 3.3: Pseudo-binary section of the system AlSi7Mg.
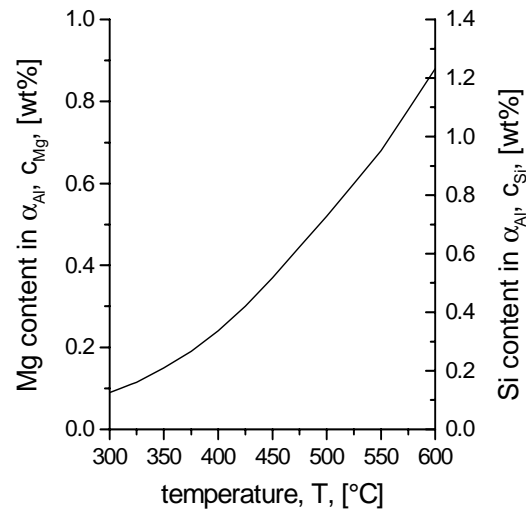
Figure 3.4: Solubility of Mg and Si in α_{Al} with concurrent presence of Mg_2Si and Si in equilibrium [APE90].

matrix is available for the formation of undesired intermetallic compounds. Impurities like iron, which is the most deleterious impurity for AlSiMg alloys, form various intermetallic compounds with Si and Mg such as α(Fe_2SiAl_8), β($FeSiAl_5$) and π($FeMg_3Si_6Al_8$). Among these compounds, the formation of plate shaped β compounds reduces the mechanical properties, particularly ductility and fracture toughness. The size and the volume fraction of the β plates depend strongly on the Fe content, solidification rate [RAV98] and level of modification [PEN98]. The β-phase - π-phase transformation is dependant of the

Mg content. As long as β-FeSiAl$_5$ is the Fe bearing phase all the Mg will be in solid solution. Further additions of Mg will first lead to transformation of the β-AlFeSi into π-FeMg$_3$Si$_6$Al$_8$, while the concentration of Mg in solid solution stays constant. When all the β-FeSiAl$_5$ has been transformed, additions of Mg will give increased Mg in solid solution, with π-FeMg$_3$Si$_6$Al$_8$ as the only Fe-bearing phase [DON00]. Taylor et al. report a transformation of π-phase to β-phase in low Mg alloys (0.3-0.4%). In alloys with higher Mg content (0.7wt%) the larger π-phase particles are more dominant [TAY00]. While sharp edges of β-FeSiAl$_5$ plates act as stress raisers with detrimental consequences for the ductility, the π-FeMg$_3$Si$_6$Al$_8$ phase has less negative effect on the ductility, because larger amounts of Mg are consumed in forming these constituents and therefore the amount of Mg available for forming Mg$_2$Si precipitates is reduced, resulting in softening of the matrix [RAV98].

Recent semi-solid light-metal research activity has focused on increasing strength without any high temperature heat treatment (T5) [GAR99]. Components in T5 are artificially aged directly after fabrication without any solution heat treatment. It is important to note that T5 hardening can only be obtained by Mg and Si that is already in solid solution in the as-cast condition. While silicon is abundant in Al-Si cast alloys, magnesium is the crucial element for optimal precipitation of Mg$_2$Si. As depicted in Figure 3.5, the Mg concentration in α-aluminum, c_{Mg}, at semi-solid forming temperature, T_{SS}, of conventional A356 alloy is low. However, increasing the Mg content of the alloy up to 0.8 wt% leads to a significant improvement of Mg concentration in α-aluminum.
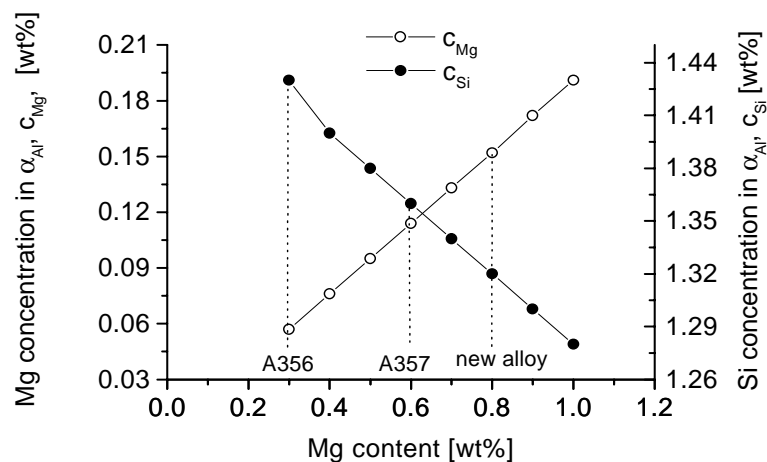

Figure 3.5: Change of Si- and Mg-concentration in α-Aluminum of AlSi7Mg at 580 °C with increasing Mg content, calculated with Thermo-Calc (equilibrium).

Scheil simulations of AlSi7 alloy with 0.3, 0.6 and 0.8 wt% Mg show that the eutectic temperature is slightly lowered with increasing Mg content (Fig. 3.6). At semi-solid forming temperature of 580°C each alloy consists of approximately 55% liquid and 45% solid phase.
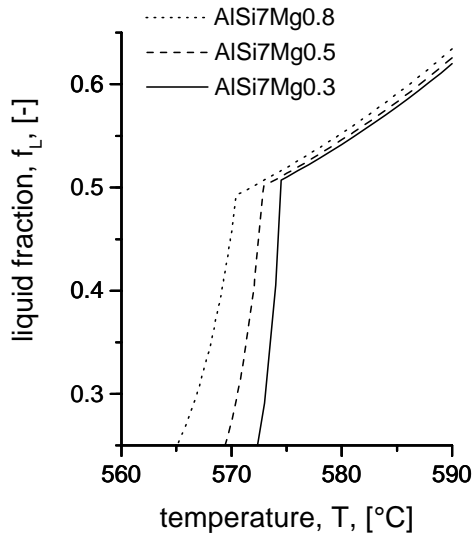

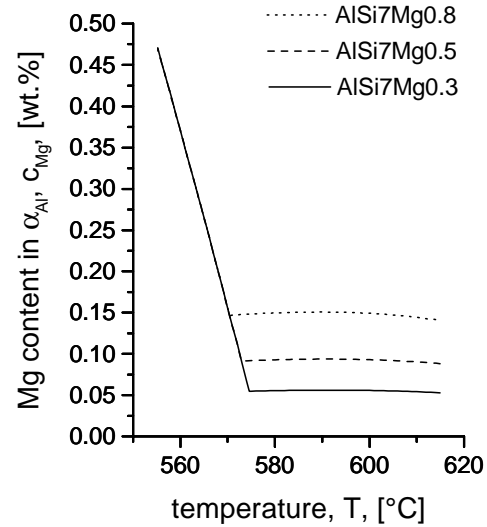*Figure 3.6: Scheil simulation of AlSi7 with various Mg contents.*

Figure 3.7: Temperature dependence of Mg-concentration in α-Aluminum of AlSi7 with various Mg contents.

The result of equilibrium calculations of Mg content in α-aluminum with respect to the temperature shows Figure 3.7. During reheating of the slugs to the semi-solid temperature of 580°C AlSi7Mg0.8 can dissolve much more Mg in the α-aluminum matrix than the standard alloys A356 and A357, respectively.

From Fick's law the diffusion path is given by

$$x = \sqrt{D \cdot t} \tag{3-1}$$

where D denotes the diffusion coefficient and t the diffusion time. Considering 5 min homogenization time of the slugs at semi-solid temperature level of 580°C, it can be seen in Figure 3.8, that the diffusion path at 580°C for Mg yields about 70 µm. Assuming a mean
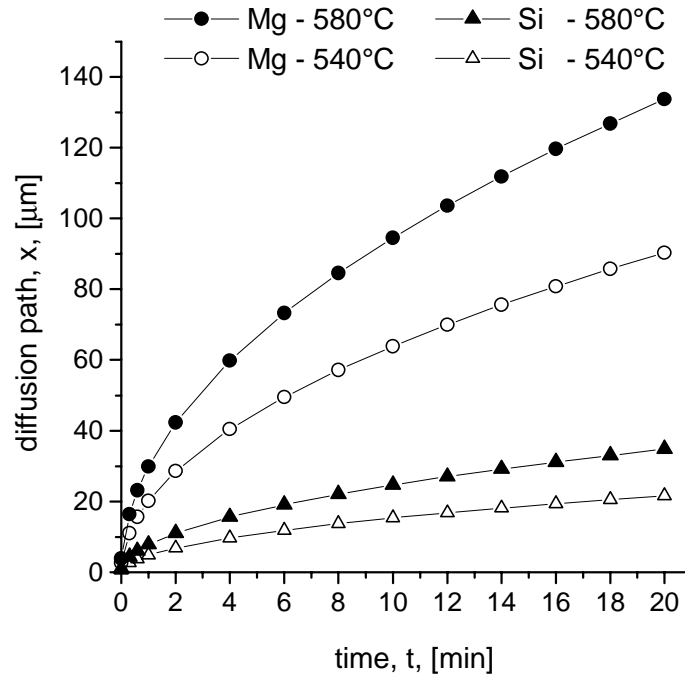
Figure 3.8: Mean diffusion path of Mg and Si in α-aluminum at 540°C and 580°C.
D calculated from $D_{0,Si}$ = 2.48 [cm²/s], $E_{A,Si}$ = 137 [kJ/mol], $D_{0,Mg}$=1.24 [cm²/s],
$E_{A,Mg}$ = 113 [kJ/mol].

grain size of ~100 μm it becomes clear that the reheating stage of the thixocating process seems to be suitable to bring Mg in solid solution. Hence the alloy with 0.8 wt% Mg should be able to precipitate more of the hardening phase Mg_2Si in α-aluminum when artificially aged directly after fabrication than A356 or A357, respectively.

The chemical composition of alloys with increased Mg content is given in Table 3.1.

Table 3.1: Chemical composition of A356 and A357 and AlSi7Mg0.8 in wt%.

Alloy	Si	Mg	Fe	Mn	Cu	Ti	Be	Sr	Al
AlSi7**Mg0.3**	7.15	**0.32**	0.15	0.017	0.004	0.086	0.002	0.031	bal.
AlSi7**Mg0.5**	6.88	**0.53**	0.16	0.009	0.005	0.064	0.002	0.031	bal.
AlSi7**Mg0.8**	7.1	**0.79**	0.15	0.010	0.005	0.08	0.001	0.028	bal.

3.2.2 LOWERING OF Si CONTENT

Scheil simulations in Figure 3.9 clearly illustrate that by reducing the Si content from 7% to 5% the amount of eutectic phase can be lowered. While AlSi7Mg0.8 contents ~50% eutectic phase, its amount can be decreased to ~42% (AlSi7Mg0.8) and ~33% (AlSi5Mg0.8). Concurrently the amount of ductile α-aluminum phase is increased which might lead to the assumption that the total ductility of the alloy will be increased. The concentration of Mg in α-aluminum at semi-solid temperature, $T_{SS, (fL=fS=0.5)}$, is slightly increased with decreasing Si content (Fig. 3.10).
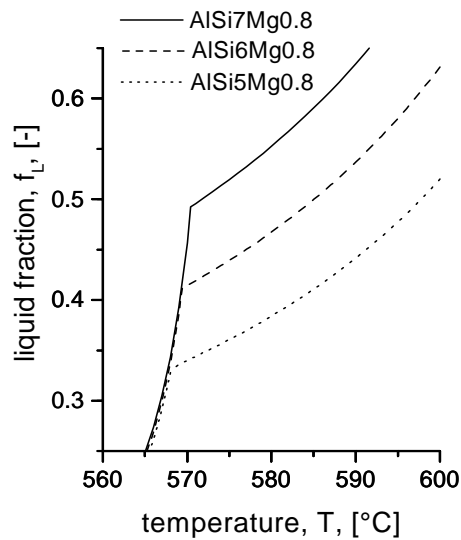
.

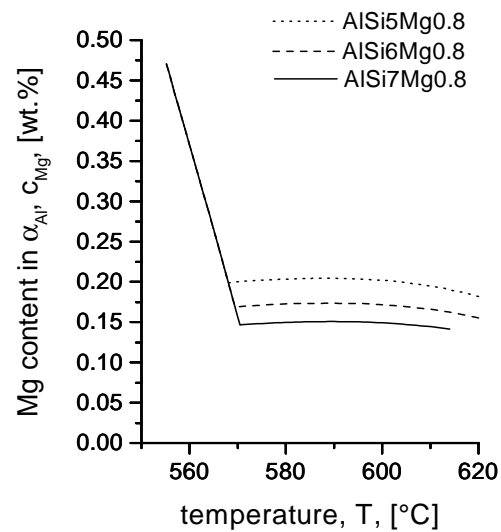*Figure 3.9: Scheil simulation of AlMg0.8 with various Si contents.*

Figure 3.10: Temperature dependence of Mg-concentration in α-Aluminum of AlMg0.8 with various Si contents.

3.2.3 Mn ADDITION

Manganese is used by the foundry industry to impede the sticking of the alloy to the mould. Addition of 0.6% Mn is also reported to improve the fracture toughness of AlSi7Mg alloys [VOJ01]. In order to investigate the influence of different Mn additions AlSi5Mg0.8 with either 0.4 wt% and 0.8 wt% Mn was produced. The chemical composition of alloys with reduced Si content can bee seen in Table 3.2.

Table 3.2: Chemical composition of alloys with reduced Si content and Mn addition in wt%.

Alloy	Si	Mg	Fe	Mn	Cu	Ti	Be	Sr	Al
Al**Si7**Mg0.8	**7.1**	0.79	0.15	0.010	0.005	0.08	0.001	0.028	bal.
Al**Si6**Mg0.8	**6.01**	0.80	0.13	0.008	0.005	0.07	0.001	0.031	bal.
Al**Si5**Mg0.8	**4.86**	0.79	0.11	0.007	0.004	0.06	0.001	0.028	bal.
AlSi5Mg0.8**Mn0.4**	5.33	0.79	0.14	**0.39**	0.004	0.06	0.002	0.029	bal.
AlSi5Mg0.8**Mn0.8**	5.29	0.82	0.16	**0.78**	0.004	0.06	0.002	0.027	bal.

3.3 THE SYSTEM Al-Mg$_X$-Si$_Y$

Die cast components are net-shape components with a complex geometry and thin wall thickness. During solution heat treatment and especially during quenching distortion cannot completely be avoided. A few years ago a new die casting alloy was invented which fulfilled the desired strength and especially ductility requirements for many components without any heat treatment [KOC98]. The alloy *Magsimal59* with the chemical composition AlMg5.5Si2Mn is reported to reach 185 MPa yield strength and 18% fracture elongation in the F state [FRA98].

Figure 3.11 shows a pseudo-binary section through the system AlSi2Mg. The hatched area covers the tolerance of Mg content of *Magsimal59*. The liquid alloy solidifies directly into the α+Mg$_2$Si area. The result is a very fine eutectic containing predominantly Mg$_2$Si and Al$_6$Mn phases which ensures a high ductility. The isothermal section of the system AlSiMg at 587°C (Fig. 3.12) which is just below the eutectic temperature, T_E = 599°C, makes clear that the chemical composition of *Magsimal59* must deviate from the quasi-binary composition in order to avoid the three phase area L+α+Mg$_2$Si area during solidification. In fact the point where the solidification range of α_{Al}-Mg$_2$Si eutectic equals zero does not lie on the quasi-binary line of α_{Al}-Mg$_2$Si with strict stoichiometric composition ratio (w_{Mg}/w_{Si} = 1.71), but it shifts to the Mg-rich side [LI 97].
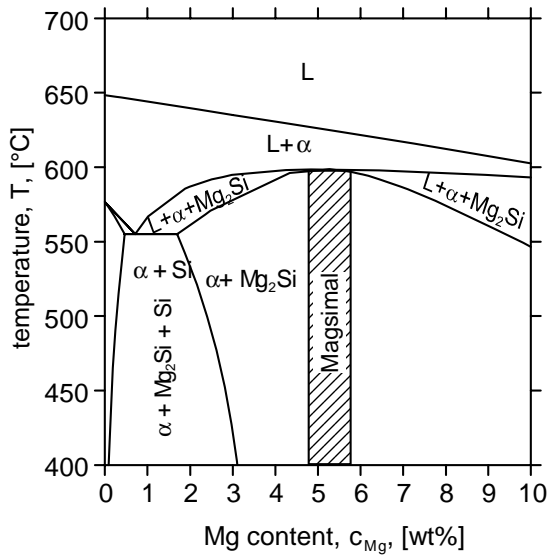
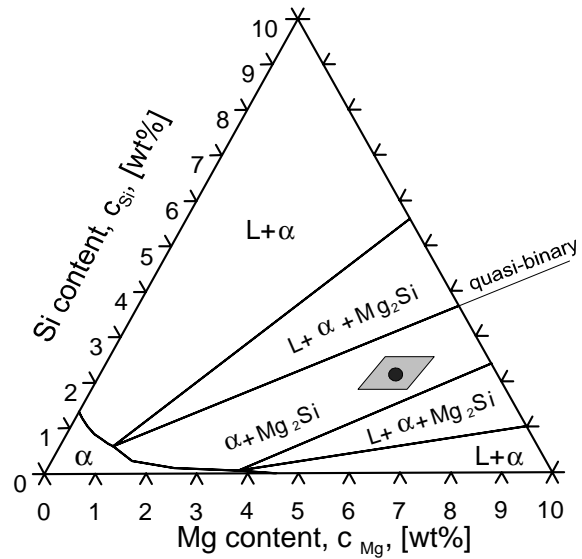*Figure 3.11: Pseudo-binary section through the system AlSi2Mg.*

Figure 3.12:Position of Magsimal59 in the isothermal section of system AlSiMg at 587°C.

An aluminum alloy with 5 wt% Si and 1.75 wt% Mg shows a similar interesting solidification behaviour (Fig. 3.13). This alloy solidifies directly from the L+Si area into the α+Si+Mg$_2$Si area.
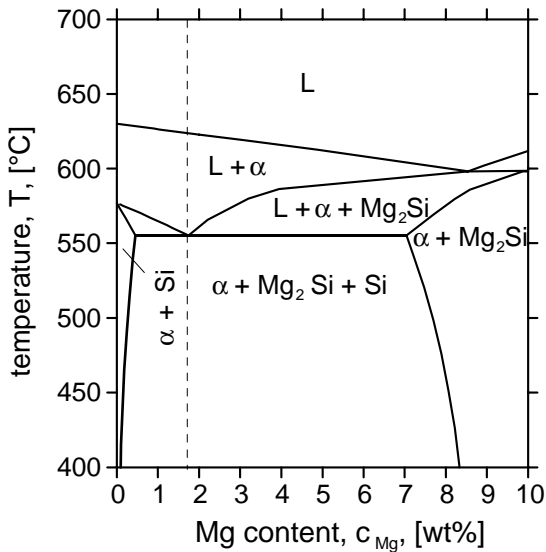

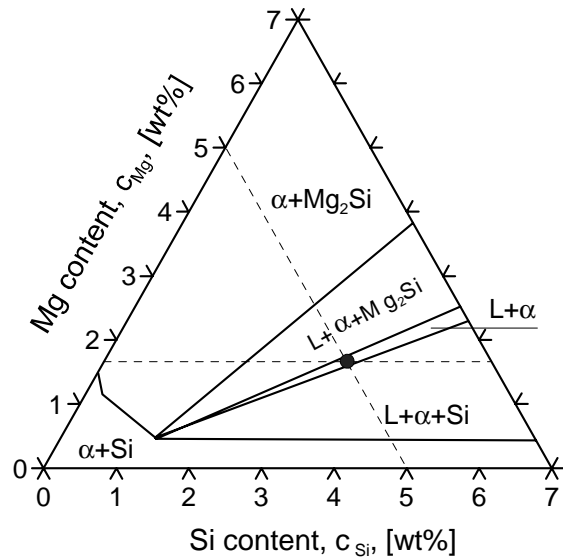*Figure 3.13: Pseudo-binary section through the system AlSi5Mg.*

Figure 3.14: Position of AlSi5Mg1.75 in the isothermal section of system AlSiMg at 556°C.

The temperature range of solidification of ~75°C is more than sufficient for semi-solid forming.The isothermal section in Figure 3.14 just above the eutectic temperature, T_E=555°C, illustrates the importance of exact chemical composition to avoid the three-phase-area L+α+Mg$_2$Si at higher and L+α+Si area at lower Mg content.

Scheil simulations of *Magsimal59* in comparison to AlSi5Mg1.75 are depicted in Figure 3.15. The semi-solid forming temperature, T_{SS}, at a liquid fraction of 0.5 is in the range of 600°C for both alloys. AlSi5Mg1.75, however, contains less eutectic phase (~30%) than *Magsimal59* (~50%).
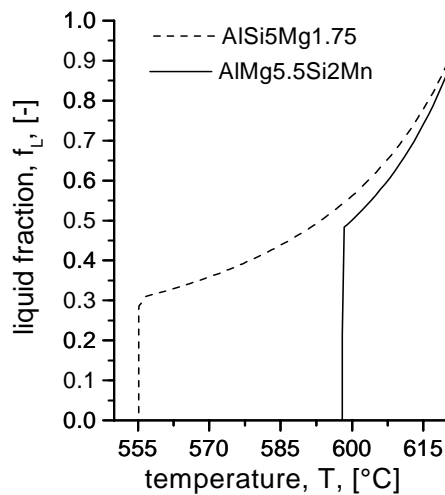
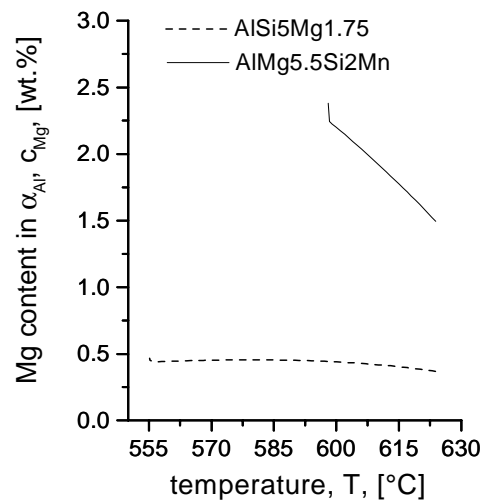

Figure 3.15:Scheil simulation of Magsimal59 (AlMg5.5Si2Mn) and AlSi5Mg1.75.

Figure 3.16:Temperature dependence of Mg-concentration in α-Aluminum of Magsimal59 (AlMg5.5Si2Mn) and AlSi5Mg1.75.

With a solubility of almost 2 wt% Mg in α-aluminum at the semi-solid forming temperature of 600°C (Fig. 3.16) *Magsimal59* can dissolve four times more Mg in α-aluminum than AlSi5Mg1.75. But since the solubility of Si at the same temperature is just 0.18 wt% the amount of possible Mg$_2$Si-formation is limited to ~0.3 wt%. Almost the same amount of possible Mg$_2$Si-formation can be found in AlSi5Mg1.75 with a Mg solubility of 0.44 wt% and Si solubility of 0.77 at the same semi-solid forming temperature.

Chemical compositions of produced alloys AlSi5Mg1.75 are given in Table 3.3. The modifying agent Ba, which was reported to evoke a well modified eutectic structure [KNU01], was used as a substitute for Sr in one of the following alloy modifications.

Table 3.3: Chemical composition of developed alloys in wt%.

Alloy	Si	Mg	Fe	Mn	Cu	Ti	Sr	Ba	Al
AlSi5Mg1.75	5.24	**1.71**	0.12	0.016	0.008	0.07	0.023	-	bal.
AlSi5Mg1.75 Mn0.6**Sr**	4.99	**1.69**	0.12	0.562	0.005	0.05	**0.024**	-	bal.
AlSi5Mg1.75 Mn0.6**Ba**	5.01	**1.68**	0.10	0.56	0.003	0.05	<0.001	**0.05**[*]	bal.

[*] alloyed, not analysed

3.4 SUMMARY OF PRODUCED ALLOYS

The main alloying elements of all alloys are summarized in Table 3.4.

Table 3.4: Summary of main alloying elements of developed alloys.

Alloy	Si	Mg	Mn	Fe	Sr	Ba	Al
AlSi7Mg0.3	7.15	0.32	0.017	0.15	0.031	-	bal.
AlSi7Mg0.6	6.88	0.53	0.009	0.16	0.031	-	bal.
AlSi7Mg0.8	7.1	0.79	0.010	0.15	0.028	-	bal.
AlSi6Mg0.8	6.01	0.80	0.008	0.13	0.031	-	bal.
AlSi5Mg0.8	4.86	0.79	0.007	0.11	0.028	-	bal.
AlSi5Mg0.8Mn0.4	5.33	0.79	0.39	0.14	0.029	-	bal.
AlSi5Mg0.8Mn0.8	5.29	0.82	0.78	0.16	0.027	-	bal.
AlSi5Mg1.75	5.24	1.71	0.016	0.12	0.023	-	bal.
AlSi5Mg1.75Mn0.6Sr	4.99	1.69	0.562	0.12	0.024	-	bal.
AlSi5Mg1.75Mn0.6Ba	5.01	1.68	0.56	0.10	<0.001	0.05[*]	bal.

[*] alloyed, not analysed

<div align="right">

4

</div>

MICROSTRUCTURE AND MECHANICAL PROPERTIES

4.1 EXPERIMENTAL PROCEDURE

4.1.1 FABRICATION OF THE PRECURSOR MATERIAL

All alloys were produced at Aluminium Lend GmbH & Co KG cast shop in Lend, Austria. The melt was modified with an AlSr10 master alloy, treated with argon for about 30 minutes and then horizontal continuously cast by applying electromagnetic stirring facility in order to provide globular α-grains. The rods were sawn into slugs of appropriate size for thixoforming.

4.1.2 THIXOFORMING OF COMPONENTS

The slugs were reheated to the semi-solid state (f_L=f_S=0.5) and formed at THIXALLOY$^®$ Components & Co KG in Lend, Austria. A mass-produced thixocomponent was chosen to be tested with the newly developed alloys. This side door pillar of the Audi A3 can be seen in Figure 4.1. The components were partly T5 and partly T6 heat treated. Heat treatment parameters are given in Table 4.1.

Table 4.1: Heat treatment parameters of thixoformed components.

T5	4h at 160°C
T6	12 h at 540°C, quenched in cold water, 4h at 160°C

Flat tensile specimens (Fig. 4.2) with a 6 x 2.5 mm^2 cross section area were cut out as illustrated in Figure 4.1.
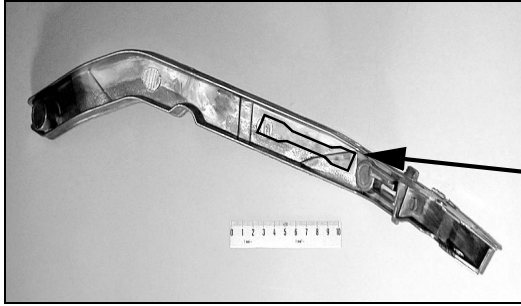
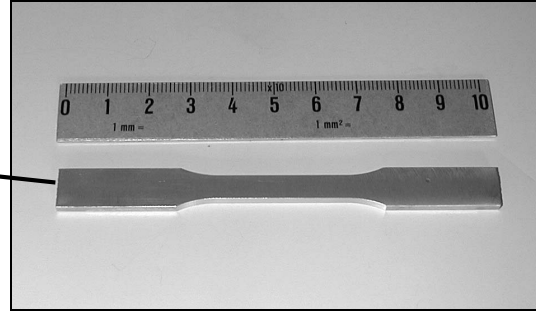*Figure 4.1: Thixoformed component of the Audi A3.*

Figure 4.2: Flat tensile specimen.

4.1.3 METALLOGRAPHY

Small specimens were embedded in raisin and then prepared by conventional metallographic preparation which includes grinding and mechanical polishing. For a better contrast the samples were etched with Keller's reagent (2ml HF, 3ml HCL, 5 ml HNO_3, 190 ml H_2O) for 30 seconds.

4.1.4 LIGHT MICROSCOPY

A Polyvar widefield photomicroscope of Reichert-Jung with an implemented digital camera (Leica) was used for optical examination of the microstructure.

4.1.5 ELECTRON MICROSCOPY

Scanning electron microscopy (SEM) pictures and energy dispersive X-rays (EDX) analysis was carried out on a Cam-Scan CS4 scanning electron microscope. For chemical identification of phases and intermetallic compounds spot measurements and mapping measurements were used for visualization of the element's distribution. Examinations were made with a voltage of 20 keV and a working distance of 35 mm for EDX analysis and 11 mm for SEM pictures.

4.1.6 TENSILE TESTING

The static mechanical properties were tested on a Schenck Trebel tensile testing maschine with a 100 kN force sensor.

4.2 MICROSTRUCTURE

4.2.1 AlSi7Mg(0.3-0.8)

The microstructure of the precursor material of AlSi7Mg(0.3-0.8) is shown in Figure 4.3 and Figure 4.5. The globulitic (bright) α-aluminum phase and the (dark) aluminum-silicon eutectic can be identified.
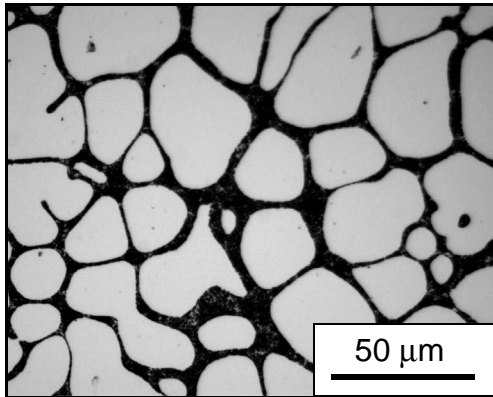

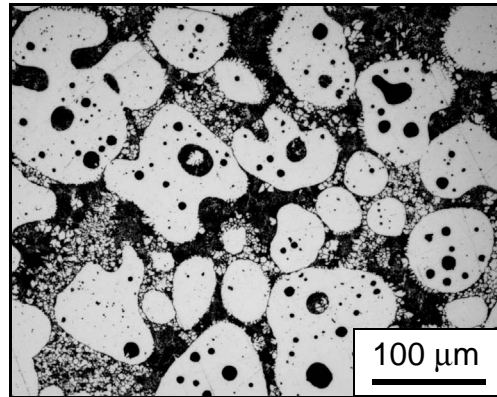*Figure 4.3: Microstructure of the precursor material of AlSi7Mg0.3.*

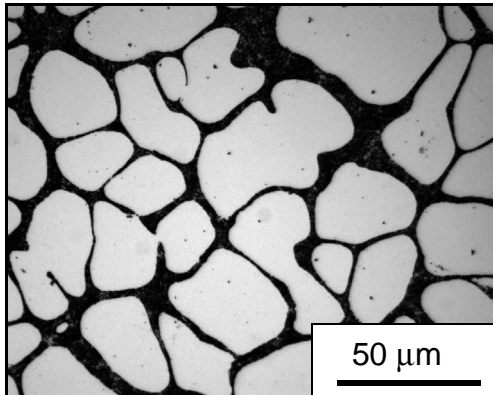*Figure 4.4: Microstructure of the thixoformed material AlSi7Mg0.3 (F).*

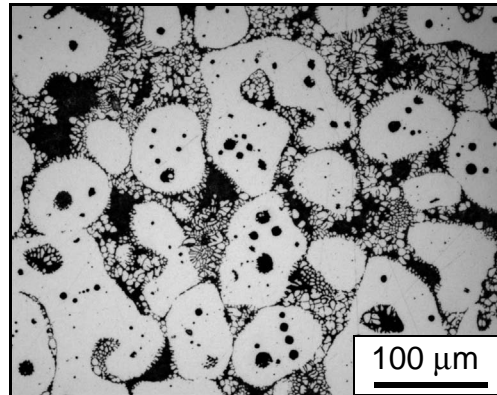*Figure 4.5: Microstructure of the precursor material of AlSi7Mg0.5.*

Figure 4.6: Microstructure of the thixoformed material AlSi7Mg0.5 (F).

The α-aluminum to eutectic ratio does not significantly change when the amount of Mg is increased from 0.3 wt% to 0.8 wt%, which is in good accordance to the Thermo-Calc results in Figure 3.6. While the precursor slugs are reheated, some eutectic is entrapped within the α-globules during ripening. The outcome is a microstructure which is typical for conventional thixocasting and can be seen in Figure 4.4 and Figure 4.6.

4.2.2 AlSi(7-5)Mg0.8

By lowering the Si content the amount of the brittle Al-Si eutectic can be reduced (see Fig. 3.9). The microstructure of the precursor material is depicted in Figure 4.7, Figure 4.9 and Figure 4.11, where the reduction of the (dark) eutectic is evident. The increase of
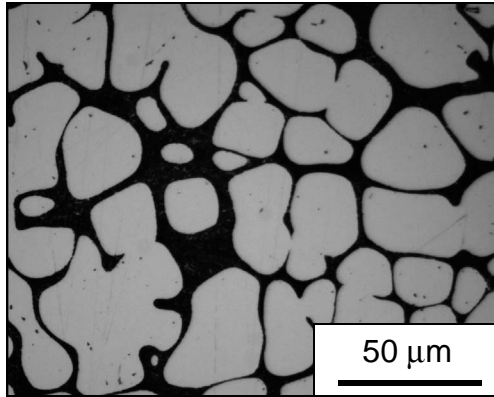

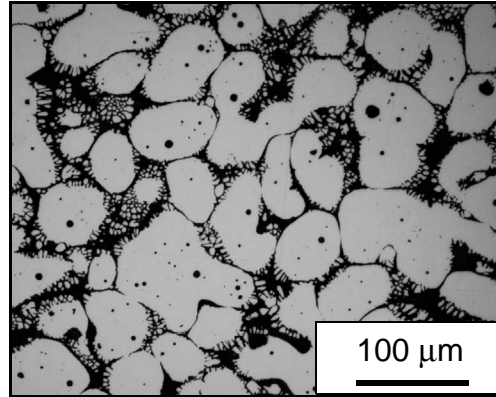*Figure 4.7: Microstructure of the precursor material of AlSi7Mg0.8.*

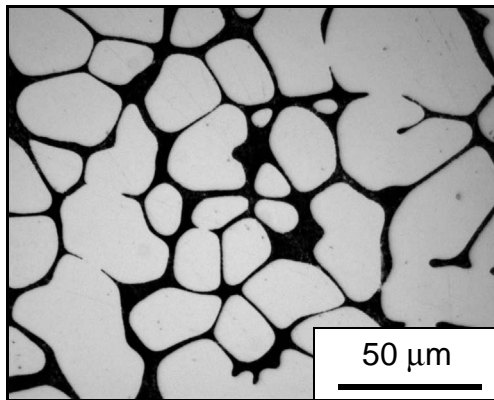*Figure 4.8: Microstructure of the thixoformed material AlSi7Mg0.8 (F).*

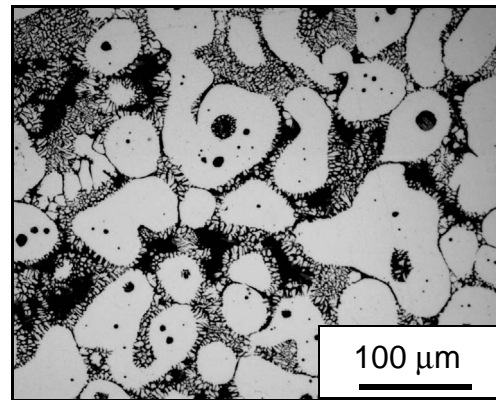*Figure 4.9: Microstructure of the precursor material of AlSi6Mg0.8.*

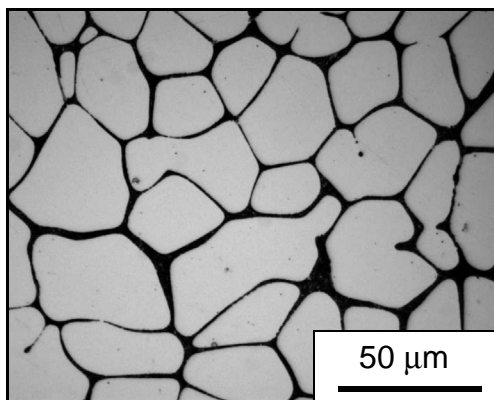*Figure 4.10: Microstructure of the thixoformed material AlSi6Mg0.8 (F).*

Figure 4.11: Microstructure of the precursor material of AlSi5Mg0.8.
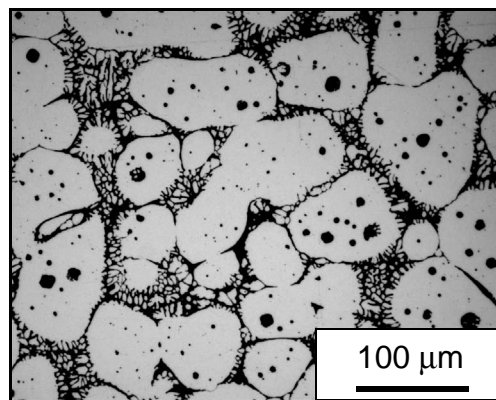
Figure 4.12: Microstructure of the thixoformed material AlSi5Mg0.8 (F).

secondary aluminum is evident as well in the microstructure of the thixoformed material (Fig. 4.8, Fig. 4.10 and Fig. 4.12).

The iron containing intermetallic compounds Al_5SiFe (β-phase), Figure 4.13, and $Al_8Si_6Mg_3Fe$ (π-phase), Figure 4.14, could be detected by EDX. The latter was predominantly found in the alloy with 0.8 wt% Mg content.
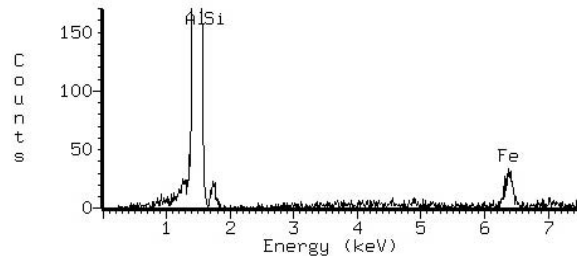
Figure 4.13: SEM picture and chemical composition of the β-phase Al_5SiFe in AlSi7Mg0.8.
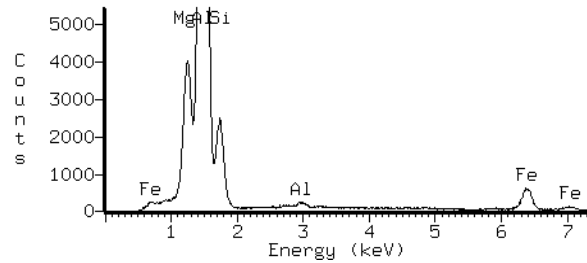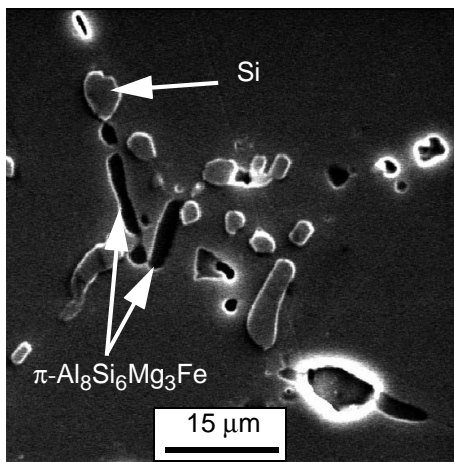
Figure 4.14: SEM picture and chemical composition of the π-phase $Al_8Si_6Mg_3Fe$ in AlSi7Mg0.8.

4.2.3 AlSi5Mn(0.4 - 0.8)

With increasing Mn content intermetallic compounds containing Al, Si, Mn and Fe could be identified. The chemical composition of the phases was detected via EDX spot measurement to approximately 70.5 at% Al, 13 at% Si, 11.5 at% Mn and 5 at% Fe. Microstructures of as-cast condition, Figure 4.15 and Figure 4.17, and T6 condition, Figure 4.16 and Figure 4.18, show size and distribution of those intermetallic compounds.
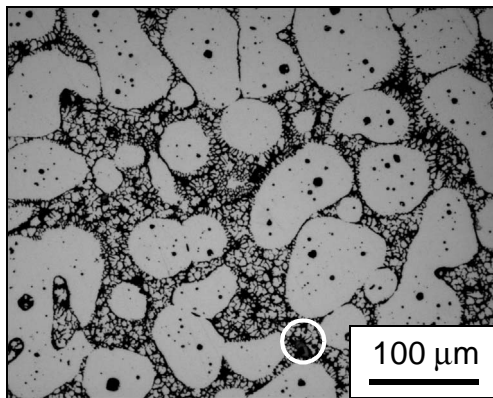
Figure 4.15: Microstructure of thixo-formed AlSi5Mg0.8Mn0.4 (F).
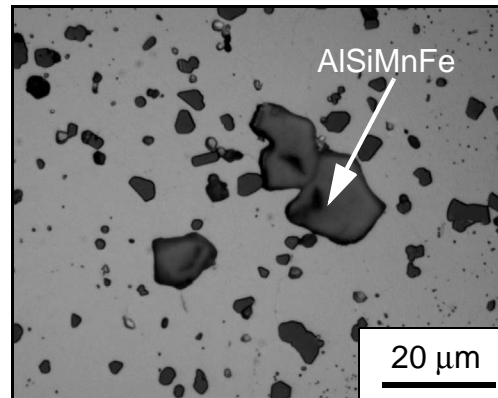
Figure 4.16: Microstructure of thixo-formed AlSi5Mg0.8Mn0.4 (T6).
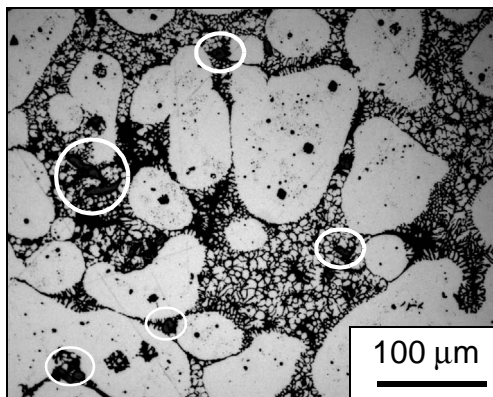
Figure 4.17: Microstructure of thixo-formed AlSi5Mg0.8Mn0.8 (F).
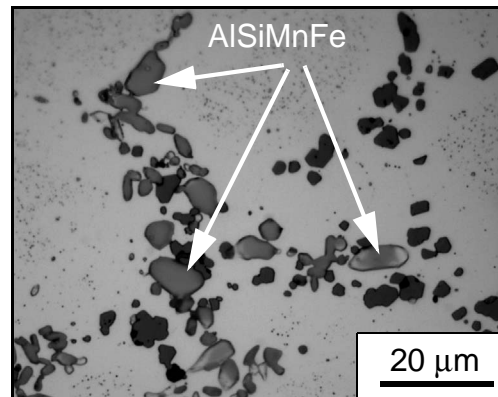
Figure 4.18: Microstructure of thixo-formed AlSi5Mg0.8Mn0.8 (T6).

4.2.4 AlSi5Mg1.75

Due to the special composition of AlSi5Mg1.75, a very fine Al-Si eutectic could be obtained. (Fig. 4.19). Mg_2Si in so called „chinese script" and $\pi(FeMg_3Si_6Al_8)$ phase were identified.Comparing this microstructure to that of *Magsimal59* (Fig. 4.20), it becomes
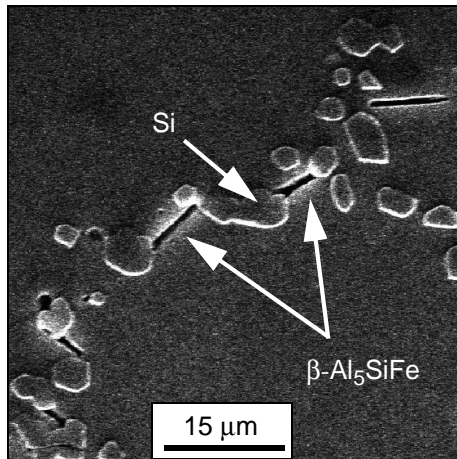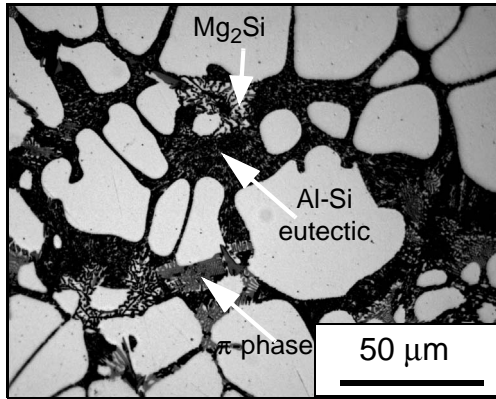

Figure 4.19: Microstructure of the precursor material of AlSi5Mg1.75.
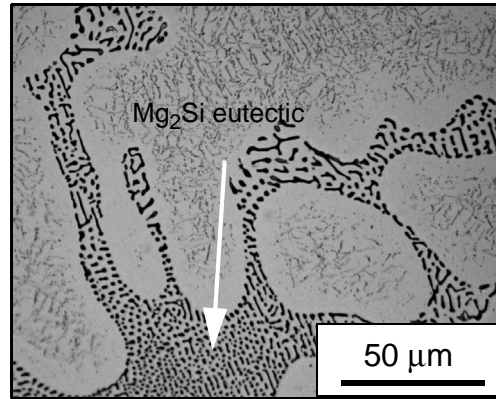
Figure 4.20: Microstructure of Magsimal59 (AlMg5.5Si2Mn).
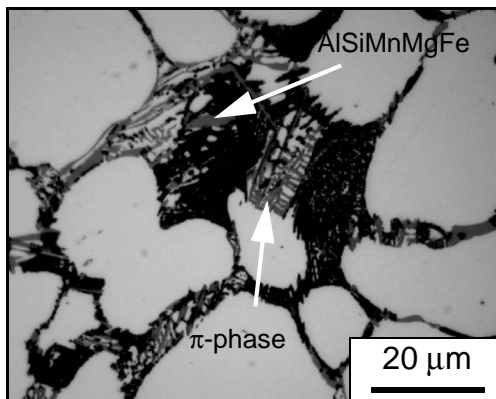
Figure 4.21: Microstructure of the precursor material of AlSi5Mg1.75Mn0.6Sr.
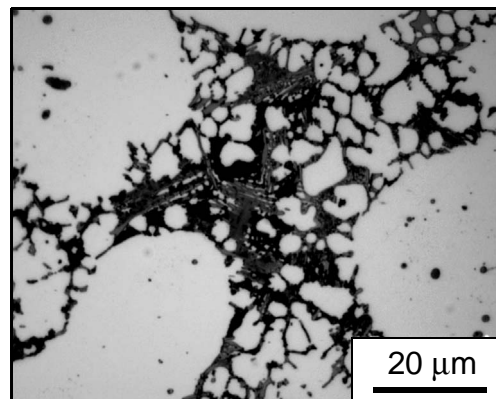
*Figure 4.22: Microstructure of the thixoformed material AlSi5Mg1.75Mn0.6Sr.*
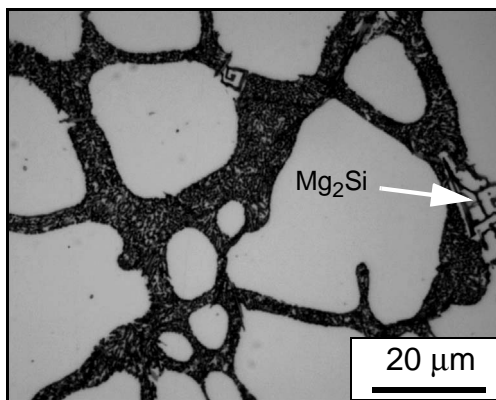
Figure 4.23: Microstructure of the precursor material of AlSi5Mg1.75Mn0.6Ba.
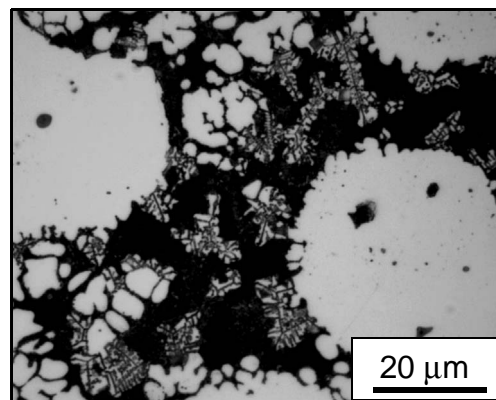
Figure 4.24: Microstructure of the thixoformed material AlSi5Mg1.75Mn0.6Ba.

visible that *Magsimal59* does not contain any undesired intermetallic compounds. AlSi5Mg1.75Mn0.6Sr contains intermetallic compounds which were detected to consist of approximately 73 at% Al, 13at% Si, 7 at% Mn, 4at% Mg and 3 at% Fe (Fig. 4.21, Fig. 4.22). At first sight the replacement of Sr with Ba (ca. 500 ppm) does not seem to have any influence on the modification behaviour (Fig. 4.21, Fig. 4.23). But SEM pictures of the eutectic structure of AlSi5Mg1.75Mn0.6 modified either with Sr and Ba reveal a significant difference. The eutectic modified with Sr shows a very rough lamella-like structure (Fig. 4.25). The Ba modified eutectic, though, consists of extremely fine silicon spines (Fig. 4.26).
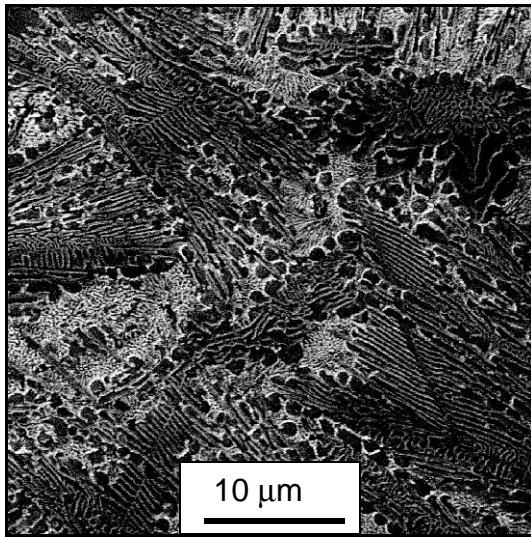
Figure 4.25: SEM picture of the eutectic of AlSi5Mg1.75Mn06Sr.
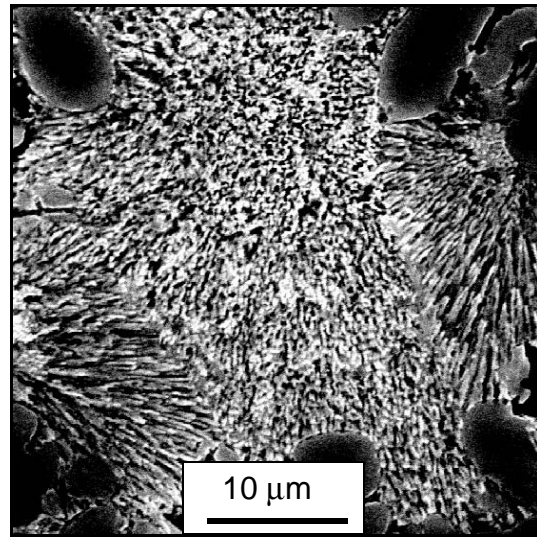
Figure 4.26: SEM picture of the eutectic of AlSi5Mg1.75Mn06Ba.

4.3 MECHANICAL PROPERTIES OF THIXOCOMPONENTS

4.3.1 INFLUENCE OF INCREASING Mg CONTENT

The influence of Mg on the static mechanical properties is illustrated in Figure 4.27. The yield strength can be raised with increasing Mg content in F, T5 and T6 state. The gain of strength goes along with a corresponding reduction of ductility.
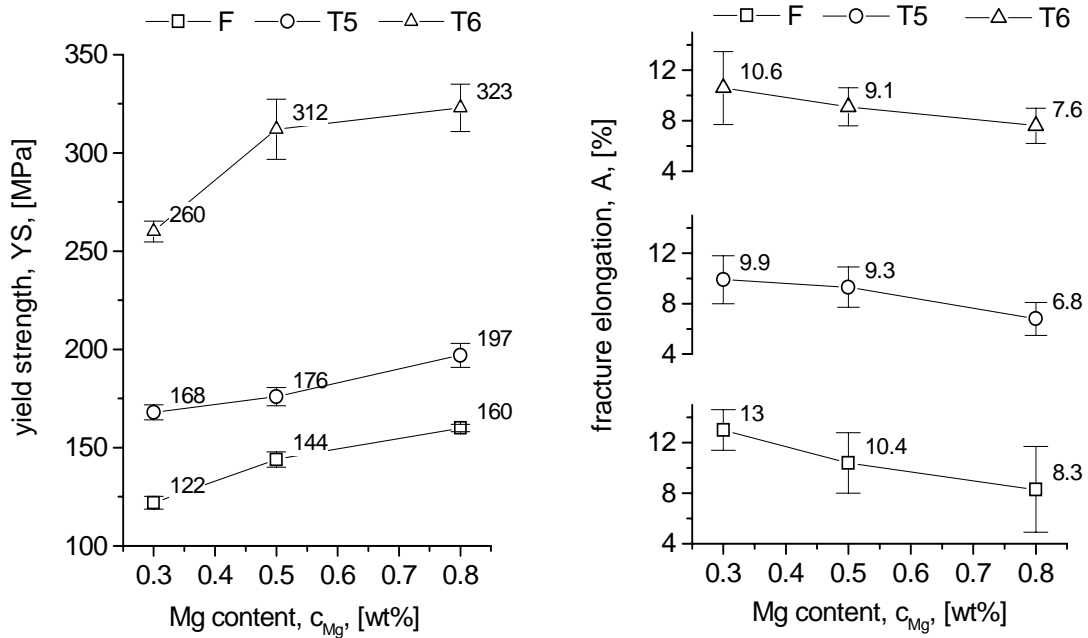
Figure 4.27: Influence of Mg content on thixoformed AlSi7 in F, T5 (4h/160°C) and T6 (12h/540°C + 4h/160°C).

4.3.2 INFLUENCE OF DECREASING Si CONTENT

When the silicon content of AlSi7Mg0.8 is reduced from 7 wt% to 5 wt% the yield strength remains more or less unaltered. There is a slight but by no means significant increase of fracture elongation at reduced silicon contents (Fig. 4.28). Especially the alloy AlSi6Mg0.8 with yield strength of 195 MPa and fracture elongation of 8% is an recommendable candidate for various applications without any high temperature heat treatment.
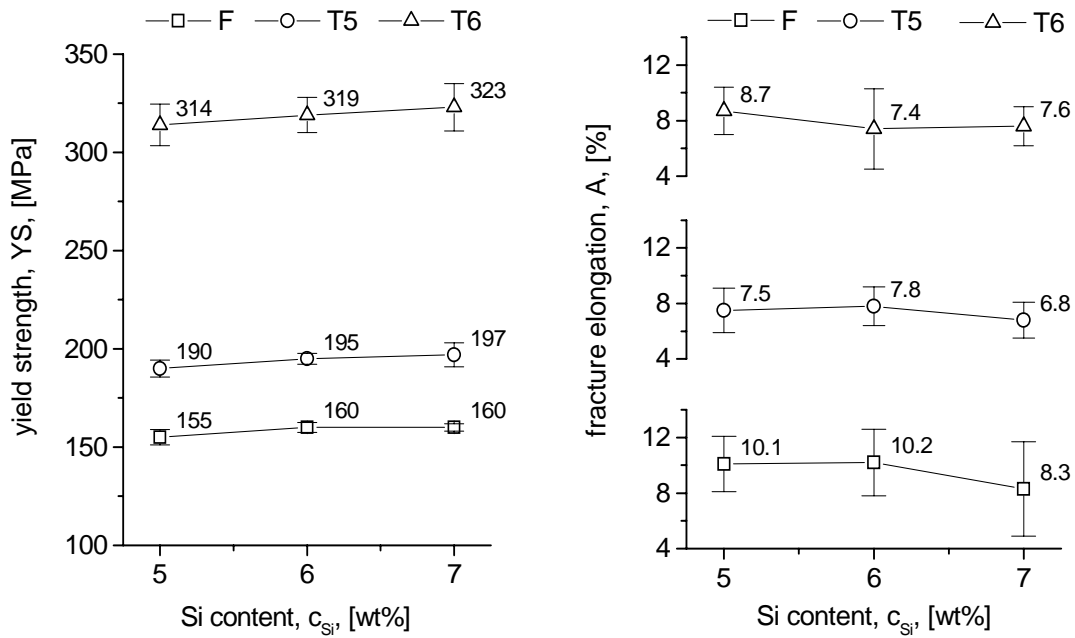
Figure 4.28: Influence of Si content on thixoformed AlSi7 in F, T5 (4h/160°C) and T6.

4.3.3 INFLUENCE OF Mn CONTENT

Except for T6, the addition of Mn neither has a significant influence on the yield strength nor on the elongation fracture of AlSi5Mg0.8.
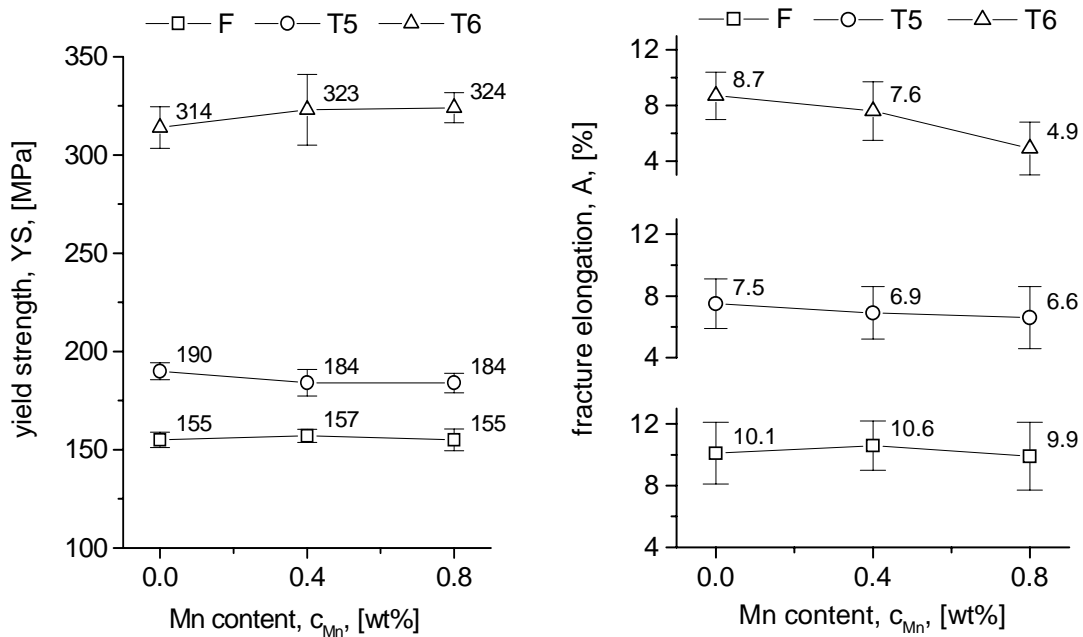
Figure 4.29: Influence of Mn content on thixoformed AlSi5 in F, T5 (4h/160°C) and T6 (12h/540°C + 4h/160°C).

4.3.4 AlSi5Mg1.75 WITH INFLUENCE OF Sr AND Ba

As depicted in Figure 4.30, AlSi5Mg1.75 shows a yield strength of YS > 200 MPa in the as-cast condition and YS > 250 MPa in T5. But the fracture elongation of A=3.5% (F) and A=2.5% (T5) is very poor. Addition of 0.6 wt% Mn and Sr as modifying agent does not show any improvements. However, substituting Sr with Ba almost doubles the value for fracture elongation in F, T5 and T6.
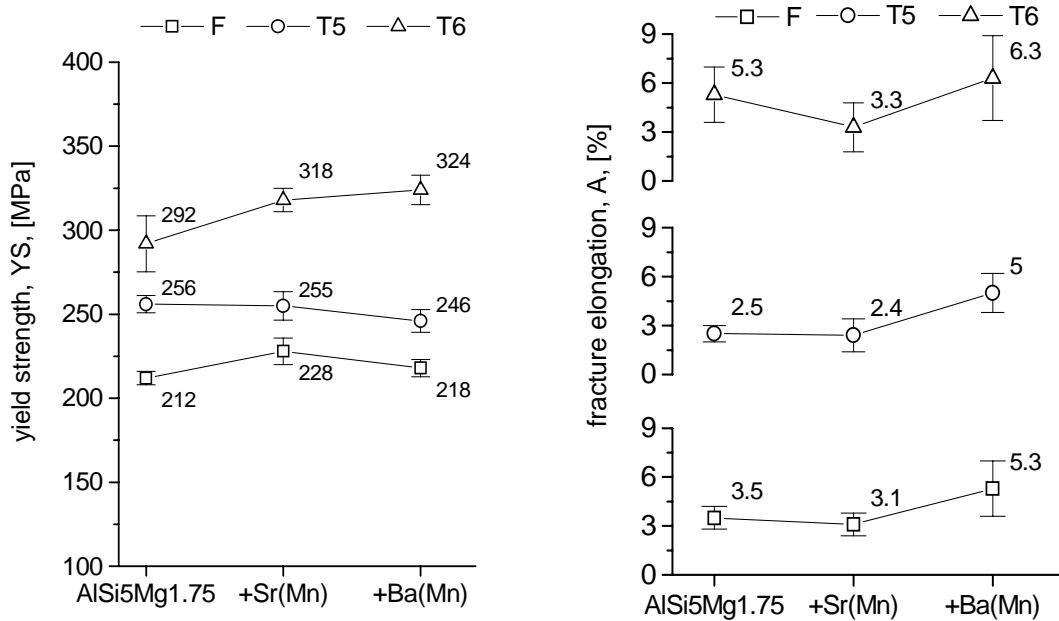
Figure 4.30: Influence of Mn on the modifiers Sr and Ba on thixoformed AlSi5Mg1.75 in F, T5 (4h/160°C) and T6 (12h/540°C + 4h/160°C).

4.4 CONCLUSIONS OF ALLOY DEVELOPMENT

The development of new alloys with reduced silicon content and increased Mg content, especially for SSM components in T5, has brought up some remarkable results. During reheating and processing of AlSi(5-7)Mg0,8 more Mg compared with A356 can be dissolved in the α-aluminum matrix. Thus, the F-yield strength of 160 MPa is much higher than the usual F level of A356 (ca. 120 MPa). The T5 yield strength reaches almost 200 MPa. Especially the alloy AlSi6Mg0.8 with yield strength of 195 MPa and fracture elongation of 8% is an recommendable candidate for various applications without any high temperature heat treatment. Alloying Mn up to 0.8 wt% does not significantly impair the

fracture elongation and yield strength in F and T5 condition of AlSi5Mg0.8. A deterioration of fracture elongation can only be observed with 0.8 wt% Mn in T6.

The alloy AlSi5Mg1.75 shows an relatively high yield strength of 212 MPa in the as-cast condition which can be increased to 256 MPa in T5. Due to coarsely precipitated Mg_2Si, the fracture elongation in F and T5 does not even reach 4%. The values in T6 (YS = 292 MPa and A = 5.5%) are comparable to values of thixoformed AlSi5Si2 (YS = 300 MPa and A = 4%) published in [NIE00].

The commonly used modifying elements Na (>600ppm) and Sr (>300ppm) are reported to form needle- and plate-like intermetallic compounds of the type $Al_x(Si)_y(Na/Sr)_z$ [WAL93]. Thus, alternative modifying agents might be of interest. The modification effect of elements which meet the requirements after the theory of Lu & Hellawell (see Fig. 2.13) as well, was reported to be very strong with Eu [QIY81], La [QIY81], [BAC83] or Ba [KNU01]. From the economic point of view, Ba seems to be the most recommendable one. Ba as a substitute for Sr shows a better modification of the Al-Si eutectic (see Fig. 4.26) which leads to a significant amelioration of ductility in AlSi5Mg1.75Mn06. As a consequence the values for fracture elongation are almost doubled in F, T5 and T6 condition.

5

DUCTILITY OF Al-Si ALLOYS

The discovery of eutectic Si modification in Al-Si alloys with Na by Aladar Pacz [PAC21], resulting in the extreme enhancement of ductility, had a major influence on the following extensive technical use of Al-Si alloys. Because ductility is the problem value for many safety components, the knowledge of possibilities to alter the morphology of brittle silicon crystals in the eutectic phase is very important. This morphology undergoes a significant modification from as-cast to T6 state. Figure 5.1 shows the evolution of the eutectic phase of A356 from F (as fabricated) to T6 and the corresponding qualitative course of strength and ductility. Due to Sr modification, changing the morphology of the eutectic silicon from long plates to acicular fibres, the ductility increases significantly. In T5
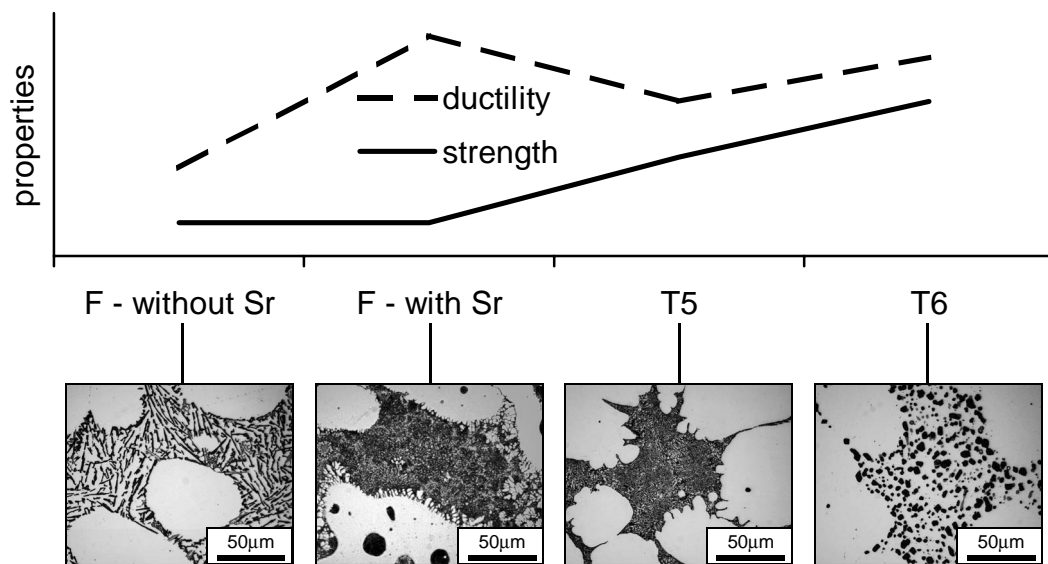
Figure 5.1: Qualitative course of strength, ductility and corresponding micro-structure of Al-Si alloys in different temper conditions.

(artificially aged without solution heat treatment) the α_{Al}-matrix is hardened by Mg_2Si precipitates while the eutectic silicon keeps its fibrous morphology. This results in increase of strength and decrease of ductility. The most effective mutation in the morphology of eutectic silicon is observed from T5 to T6. Due to T6 solution heat treatment, the small silicon platelets spheroidize and contribute substantially to good ductility properties in T6 state. The T6 solution heat treatment also supplies the α_{Al}-matrix with Mg and Si for maximal Mg_2Si precipitation. Thus, from T5 to T6, strength and ductility increases.

5.1 DUCTILITY OF Al-Si-Mg SEMI-SOLID STRUCTURES IN T5
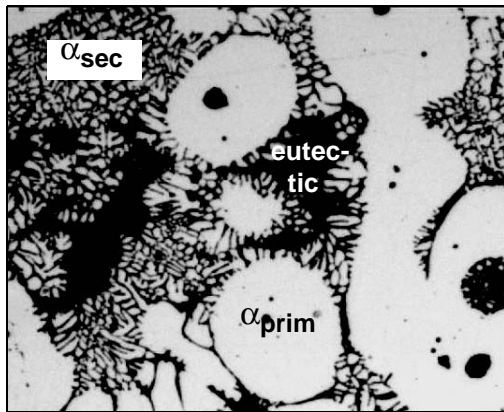
Figure 5.2: Microstructure of thixoformed AlSi6Mg0.8.

For safety components made from Al-Si alloys a minimum fracture elongation of 15% is desired. Concurrently the yield strength must not drop below 150 MPa. Due to economical reasons, this high ductile condition preferentially should be obtained without any high temperature heat treatment. Ductility of Al-Si alloys is predominantly influenced by the brittle eutectic. Thus, a reduction of its amount seems to be advisable. Scheil calculations of

Figure 3.9 show that the amount of eutectic can be reduced from $f_L = 0,5$ (7% Si) to $f_L = 0,33$ (5% Si). With less Si the semi-solid processing temperature, $T_{SS,(fL=fS=0,5)}$, shifts to a level which is significantly higher than the eutectic temperature. Thus, solidification of the liquid part of the semi-solid suspension results in the formation of eutectic and secondary α-aluminum (Fig. 5.2). The total ductility of a thixoformed component consists of both, ductility contributed by the eutectic and ductility contributed by primary and secondary α-aluminum phase. Thus, at first sight a decrease of the amount of eutectic, i.e. an increase of the volume fraction of secondary aluminum must lead to an increase of total ductility. But results in Figure 4.28 show almost no influence of reduced eutectic on the fracture elongation. In fact, however, the contiguity of the different phases, C, as a measure for their interconnection has to be taken into account (Fig. 5.3). In case of fully con-

nected α-aluminum its contiguity tends to equal 1, in case of fully isolated α-aluminum C_α is 0 [KAU00]. The contiguity value for the large globulitic primary α-aluminum, which remains solid during the whole forming process, is much higher than the contiguity value for the secondary α-aluminum. The latter solidifies into very small globules, which are totally surrounded by eutectic phase (Fig. 5.2). Thus, the contiguity of secondary α-aluminum is diminishing low. Consequently, there is no significant contribution of secondary α-aluminum to the total ductility. Regarding the analytical formulation of the total ductility, exemplarily expressed by the toughness J_{IC} (Equation (5-1)), it is clear that if the first term (α_{prim}) remains constant and the second term (α_{sec}) is negligible, it is the ductility of the eutectic that has to be improved.

$$J_{IC}^{total} = J_{IC}^{\alpha} \cdot C_{prim}^{\alpha} \cdot V_{prim}^{\alpha} + J_{IC}^{\alpha} \cdot C_{sec}^{\alpha} \cdot V_{sec}^{\alpha} + J_{IC}^{Eu} \cdot (1 - C_{ges}^{\alpha} \cdot V_{ges}^{\alpha}) \qquad (5\text{-}1)$$

Corresponding values of fracture toughness are given by

$$K_{IC} = [E \cdot J_{IC}]^{\frac{1}{2}} \qquad (5\text{-}2)$$

where *E* denotes Young's modulus.
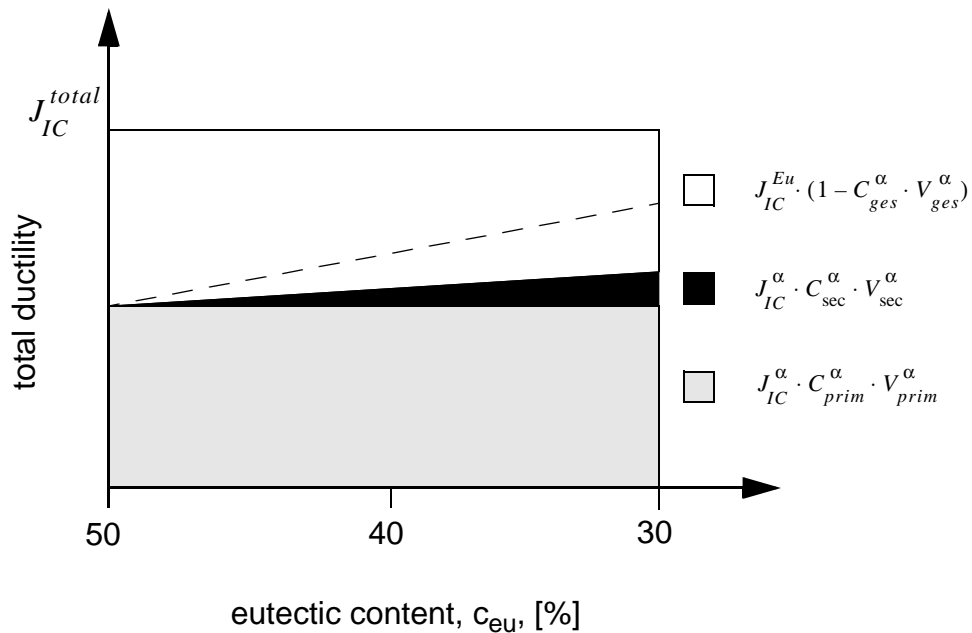
Figure 5.3: Schematic course of ductility when the amount of brittle eutectic is reduced. The dashed line symbolises the course without consideration of contiguity.

The lack of sufficient contiguity of secondary α-aluminum on one hand and the sharp-edged and fibrous rod-like eutectic silicon on the other hand prevent a high ductile (A>15%) state in T5. Thus, a high temperature heat treatment seems to be unavoidable. The ductility of the Al-Si eutectic can be improved either by means of modifying agents like Sr or Na or by spheroidization of silicon.

6
SILICON SPHEROIDIZATION

Eutectic silicon spheroidizes during a high temperature treatment, which is the main reason for enhanced ductility properties in T6 condition (see Fig. 5.1). The evolution of the change of eutectic silicon during high temperature treatment can be roughly divided into three steps:

1. Disintegration of the silicon
2. Spheroidization
3. Growth of Si particles in the matrix

The driving force of spheroidization is the same as is responsible for the disintegration of water jets, namely the minimization of surface energy under the effect of surface tension. Figure 6.1 shows the beginning of disintegration of a water jet, provoked by small fluctuations of its surface. Figure 6.2 illustrates the micrograph of A356 at the beginning of disintegration and spheroidization of eutectic silicon corals.
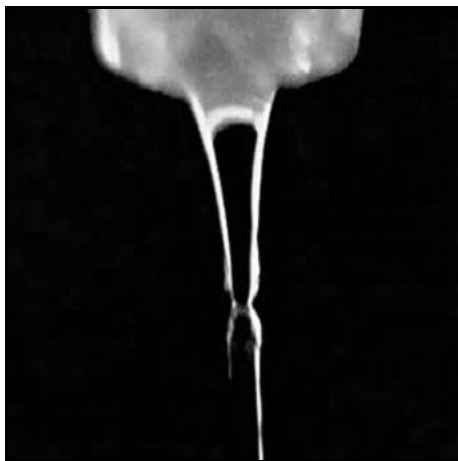
Figure 6.1: Rayleigh disintegration of a water jet.
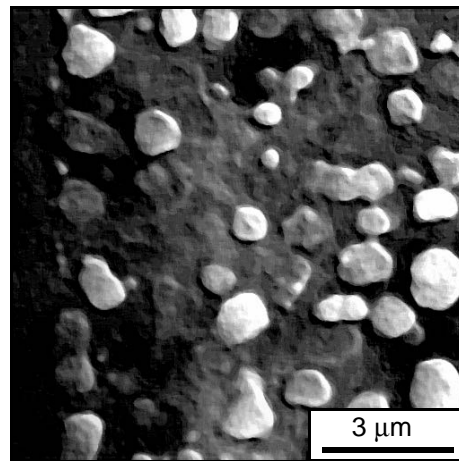
Figure 6.2:Disintegration of a silicon coral in A356 at 540°C.

6.1 STATE OF THE ART

About 60 years ago, Röhrig et al. already systematically investigated the mutations of the microstructure of different Al-Si alloys during annealing [RÖH41]. Unmodified and Na-modified Al-Si alloys (9-13% Si) were annealed at 300-550°C for 15 minutes to 38 days. First changes of the silicon's morphology were already observed after 15 minutes annealing time at 550°C. The edges of the silicon were rounded and the silicon spheroidized. Additionally they reported two important points: at higher temperatures the spheroidization started earlier and in modified alloys the silicon was much smaller and better spheroidized. Similar results were found by Paul et al. by investigating an eutectic aluminum alloy after 8h at 500°C. They pointed out that ductility is a function of the mean free path of the silicon particles in such way that ductility increases when the mean free path decreases [PAU82]. Meyers reports from silicon structures of solution treated A357 which were neither uniformly planar nor spherical. Most of them appeared to be oblate spheroids whose sizes varied vastly at each solution heat treatment time [MEY85]. Two stages of the spheroidization process were found from Zhu et al. who investigated an AlSi13 alloy at 540°C for 2h: the dissolution separation of eutectic Si branches and the spheroidization of these branches. The separation stage has the greatest effect on the time to complete spheroidization and is strongly affected by the morphology of the Si flake. The dissolution occurs at the branches, or the thin steps, which is accelerated by increasing number of branches and growth steps [ZHU85]. Apelian et al. observed spheroidization even after a short time of 10 min at 540°C [APE90]. Tensi et al. reported a coral-like structure from deep-etched eutectic silicon which became spherical after 0.5h of heat treatment at 500°C [TEN99]. Spheroidization of eutectic silicon in A319 at 470°C was reported to occur between 2h and 40h heat treatment in [PÁR00].

6.2 INFLUENCE OF MODIFICATION ON SILICON SPHEROIDIZATION

The morphology of eutectic silicon can be divided into a non-modified plate-like shape and a modified fine fibrous coral-like shape (Fig. 6.3 and Fig. 6.4). Thermal degradation of plates begins at local crystal defects, which begin to govern the break-up process. These defects are morphological faults like terminations, kinks and striations of the plates and holes and fissures in the plates [WER90a]. Silicon corals of a modified eutectic, however,

are the results of impurity induced twinning (see Chapter 2.3.1) which results in aniso-tropic multiple branching of silicon at the solid/liquid interface during solidification. As the original disturbances are responsible for the thermal instability of these structures a
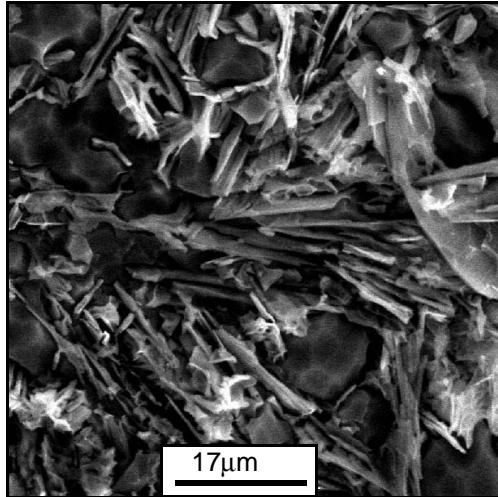
Figure 6.3: Silicon plates of an unmodified AlSi12 alloy.
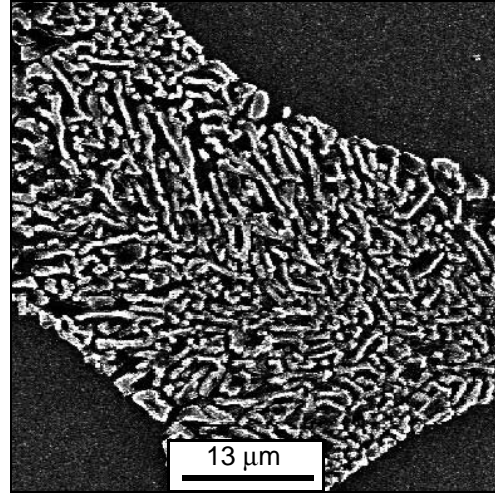
Figure 6.4: Silicon corals of a modified A356 alloy.

modified structure of Figure 6.4 will easier disintegrate and faster spheroidize than the un-modified plates of Figure 6.3. The positive effect of chemical   modifiers on the spheroidization rate of eutectic silicon has been documented by several studies [APE90, SHI90, PAR93].

6.3 MODEL OF SILICON SPHEROIDIZATION

Eutectic alloys frequently consist of rods of one phase embedded in the surrounding matrix of the other phase. These structures have a certain thermal instability. The first attempt to explain the shape instability of rods was made by Lord Rayleigh in 1878. Although his theory deals originally with the shape instability of jet fluids it also describes the spheroidization of the rod phase in an eutectic alloy [WER90]. Lord Rayleigh's perturbation theory has been successfully applied to describe the shape instability of chromium fibres in a NiAl-Cr eutectic [WAL73], of iron fibres in a Fe-FeS eutectic [MAR70], of $NiAl_3$ rods in a Ni Al_3-Al eutectic [NAK72], and of Ni fibres in a matrix of silver [MÜR80]. The analytic model, here used to describe the spheroidization of eutectic silicon, was originally

developed by Stüwe and Kolednik who calculated the disintegration time of potassium filled cylinders into spheres in tungsten [STÜ88]. The same model was later successfully used to calculate the disintegration time and spheroidization time of cementite plates in α-iron [WER89, WER90b]. In the following, an adapted version of the model is applied to the disintegration of eutectic silicon corals in Al-Si alloys. The deep-etched structure of a Sr modified eutectic silicon can be seen in Figure 6.5. If thermally activated, this structure disintegrates into small spheroids under the influence of surface tension. The branches of the silicon corals can be simplified seen as interconnected cylinders with radius ρ that transform into a row of equidistant spheres of radius R and spacing l (Fig. 6.6).
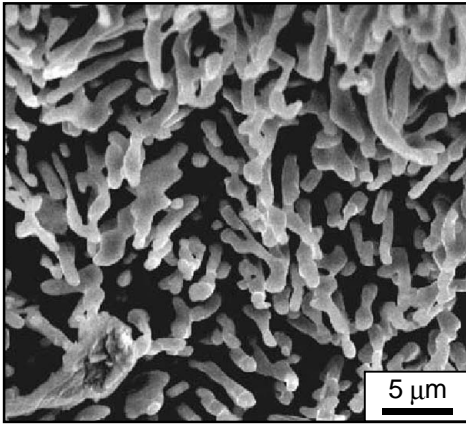
Figure 6.5: Deep etched silicon corals of a Sr modified Al-Si alloy [MAK01].
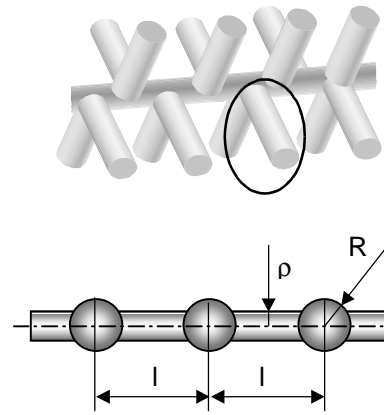
Figure 6.6: Model of a silicon branch which disintegrates into spheres.

The dimensionless variables

$$z = \frac{l}{\rho} \tag{6-1}$$

and

$$a = \frac{l}{R} \tag{6-2}$$

are used in the model. The constancy of volume during the shape transformation from a cylinder to a sphere yields the following relationship of the two variables:

$$a = \left(\frac{4}{3}\right)^{\frac{1}{3}} \cdot z^{\frac{2}{3}} \approx 1.1 \cdot z^{\frac{2}{3}}. \tag{6-3}$$

An obvious lower bound for a and z is provided by the condition that the surface of one

sphere must not be larger than the lateral surface of the cylinder which went into forming it:

$$2\pi\rho l \geq 4\pi R^2,$$ (6-4)

which leads to

$$z \geq \frac{3}{2} \quad \text{and} \quad a \geq 3$$ (6-5)

The cylinder must be unstable against fluctuations of its diameter. Let us consider a „near cylinder" having small fluctuations of its radius of the form

$$r = s + A \cdot \sin\frac{2\pi}{l} \cdot x$$ (6-6)

A is the amplitude of the original disturbance, l is its wavelength and s the mean radius of the body with

$$s = \rho\left(1 - \frac{A^2}{2\rho^2}\right)^{\frac{1}{2}}$$ (6-7)

The difference of surface between the disturbed and undisturbed cylinder was calculated by Stüwe and Kolednik to

$$S - S_0 \approx \frac{\pi}{2} \cdot A^2 \cdot \frac{4\pi^2 - z^2}{z}$$ (6-8)

where S_0 is the surface of the undisturbed cylinder. The cylinder will be unstable against a longitudinal fluctuation, if its wavelength is larger than the cylindrical circumference, or if $z \geq 2\pi$, which is a classical result, previously obtained by Lord Rayleigh for jets of fluids [RAY₁₈78].

The branches of the silicon corals, approximated by cylinders, may be weakly disturbed by a fluctuation with amplitude A and wavelength $l \geq 2\pi\rho$. If one layer of atoms, consisting of N atoms, diffuses from the adjoining necks to the bulge of the cylinder, the amplitude of the fluctuation will be increased by the atomic diameter, $\Delta A = \phi$, which is
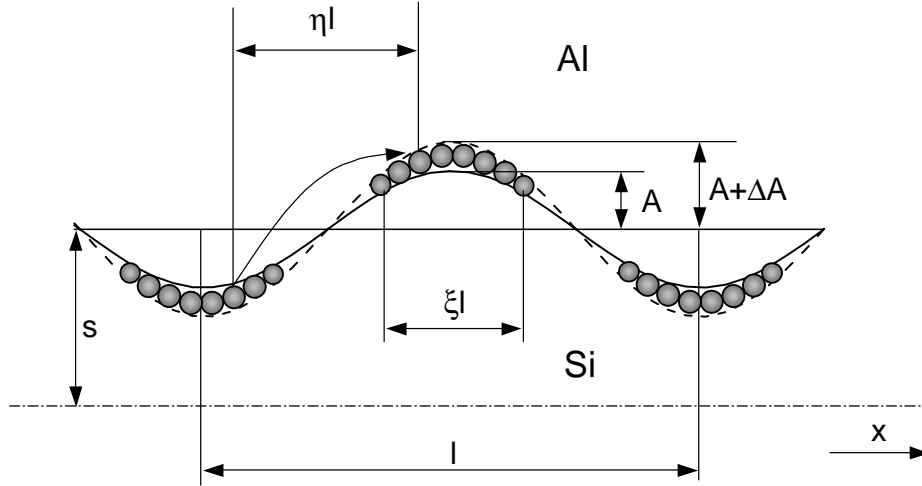
Figure 6.7: Dynamic model of a silicon coral branch. The fluctuation amplitude is increased by surface diffusion of the Si atoms at the Si-Al interface.

schematically illustrated in Figure 6.7.

The gain of surface energy will then be

$$\Delta U \ = \ \Delta S \gamma \ = \ \pi \frac{z^2 - 4\pi^2}{z} A \Delta A \gamma \tag{6-9}$$

with γ as the specific energy of interface of the Si-Al interface. Assuming a constant average driving force for the diffusion of one Si atom,

$$F \ = \ \frac{1}{N} \cdot \frac{\Delta U}{\eta l} \tag{6-10}$$

the mean velocity of the Si atoms (in x-direction) is given by the Nernst-Einstein relationship:

$$v_{Si} \ = \ F \cdot \frac{D_s}{kT} \tag{6-11}$$

T is the temperature, k Boltzmann's constant and D_s is the coefficient of surface diffusion at the Si-Al interface. If ηl denotes the mean diffusion path in x-direction, the growth rate, v_A, of the fluctuation amplitude will be

$$v_A = \frac{dA}{dt} = \frac{\phi}{\eta l} \cdot v_{Si} \tag{6-12}$$

Assuming a cylinder fraction of length ξl, the total number of diffusing atoms, N, is estimated as the number of atoms covering the surface shell of the cylinder fraction:

$$N = \frac{2\pi\rho}{\phi} \cdot \frac{\xi l}{\phi} \tag{6-13}$$

Equation (6-12) can be transformed to

$$\frac{dA}{dt} \approx \frac{1}{2\eta\xi} \cdot \frac{D_s\gamma}{kT} \cdot \left(\frac{\phi}{\rho}\right)^4 \cdot Z \cdot A \quad \text{with} \quad Z = \frac{z^2 - 4\pi^2}{z^4} \tag{6-14}$$

Integration of Equation (6-14) yields the size of fluctuation amplitude at a given annealing time t to be

$$A(t) = A_0 \cdot \exp\left[\frac{1}{2\eta\xi} \cdot \frac{D_s\gamma}{kT} \cdot \frac{\phi^4}{\rho} \cdot Z \cdot t\right] , \tag{6-15}$$

assuming an amplitude A_0 of the original disturbance. The condition $A(\tau) = \rho$ provides a simple estimate of the disintegration time, τ, of the cylinder

$$\tau = 2\eta\xi \cdot \frac{kT}{D_s\gamma} \cdot \left(\frac{\rho}{\phi}\right)^4 \cdot \frac{1}{Z} \cdot \ln\frac{\rho}{A_0} \tag{6-16}$$

The function Z of Equation (6-14) is a measure for the driving force for the break-up of the disturbed cylinder. It only depends on the geometry of the cylinder and is not influenced by mass transport mechanism. It describes the growth rate of the fluctuation amplitude (Fig. 6.8), which is positive for $z > 2\pi$ and runs through a maximum value at

$$z_{max} = 2\pi\sqrt{2} \approx 8{,}8 \quad \text{and} \quad Z_{max} = \frac{1}{16\pi^2} \approx 0{,}006 . \tag{6-17}$$
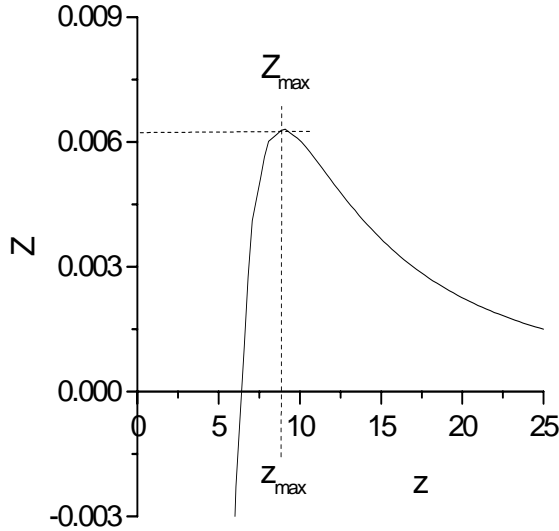
Figure 6.8: Function Z which determines the growth rate of the fluctuation amplitude.

Wavelengths smaller than $l = 2\pi\rho$ will be smoothed down very quickly because Z is then negative and large. All fluctuations with larger wavelengths grow. It seems reasonable that those original disturbances are selected for disintegration whose driving force for disintegration is large. Thus, the original disturbance is assumed to have a wavelength of $l = z_{max} \cdot \rho$, and the smallest possible amplitude is $A_0 = \phi$, where ϕ denotes the atomic diameter of silicon. From Figure 6.7 the factors η and ξ, determining the mean diffusion path and the number of the diffusing atoms are roughly estimated as 1/3. Substituting into Equation (6-16) leads to the disintegration time, τ_{max}, of a cylinder having a maximal growing fluctuation amplitude.

$$\tau_{max} = \frac{32\pi^2}{9} \cdot \frac{kT}{D_s\gamma} \cdot \left(\frac{\rho}{\phi}\right)^4 \cdot \ln\frac{\rho}{\phi} \qquad (6\text{-}18)$$

From Equation (6-18) it is evident, that the disintegration time is highly influenced by the radius, ρ, of the original cylinder and by the diffusion coefficient D_s. Very little diffusion data were found to describe the specific diffusion problem at the Si-Al interphase at temperatures between 400°C and 540°C. However, the following approach should give a clue how the diffusion process at the Si-Al interface might occur.

6.3.1 DIFFUSION OF Si AT THE Si-Al INTERFACE

Basically, there are two possibilities for a Si atom to migrate at the Si-Al interface: firstly, it can change its position by surface self diffusion, which means that the silicon changes its atomic position by diffusing on the Si-surface. Secondly, the silicon can leave the silicon lattice by interdiffusion and migrate through aluminum at the Al-Si interface favoured by lattice defects in the phase boundary. Regarding the activation energies either for surface self diffusion of ~2.3 eV [KEE94] and for Al-Si interdiffusion of ~1.4 eV [FUJ78] the interdiffusion is the more probable mechanism. The interdiffusion coefficient can be written as follows:

$$D_{inter} = D_{0, inter} \cdot \exp\left(-\frac{E_{A, inter}}{R \cdot T}\right) . \tag{6-19}$$
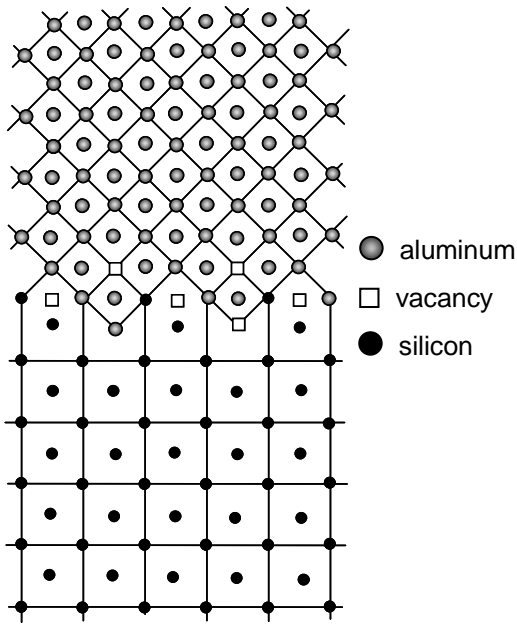
Figure 6.9: Phase boundary of aluminum and silicon (schematically).

$D_{0,inter}$ is the frequency factor and $E_{A,inter}$ the activation energy for interdiffusion. However, the activation energy for interdiffusion, $E_{A,inter}$, can be divided into the activation energy for the atom's migration, $E_{A,m}$, and the activation energy for vacancy formation, $E_{A,v}$. The change of volume during solidification is compensated by formation of vacancies in aluminum at the Al-Si interface [BEN00]. Hence, the vacancy probability at the Si-Al interface equals almost 1 (Fig. 6.9). Thus, the activation energy of vacancy formation can be neglected. The diffusion coefficient, D_s, for silicon at the Si-Al interface can now be written to

$$D_s = D_0 \cdot \exp\left(-\frac{E_{A, inter} - E_{A, v}}{R \cdot T}\right) \tag{6-20}$$

where, $E_{A,inter}$ denotes the activation energy for interdiffusion of Si in Al and $E_{A,v}$ is the activation energy of vacancy formation in Al.

6.3.2 RESULTS OF MODELLING SILICON SPHEROIDIZATION

The numerical values inserted in Equation (6-18) and Equation (6-20) can be seen in Table 6.1.

Table 6.1: Numerical values for the silicon spheroidization model.

Boltzmann's constant	k	1.38×10^{-23}	[J/K]
Universal gas constant	R	8.314	[J/mol·K]
Interfacial energy of Al-Si interface	γ	~ 1	[J/m^2]
Covalent atomic diameter of Si	ϕ	2.22×10^{-10}	[m]
Frequency factor [FUJ78][a]	D_0	2.29×10^{-4}	[m^2/s]
Activation energy for Si-Al interdiffusion [FUJ78][a]	$E_{A,inter}$	148.6	[kJ/mol]
Activation energy for vacancy formation in Al [VOL89]	$E_{A,v}$	74.3	[kJ/mol]

a.)The frequency factor and the activation energy for Si-Al interdiffusion are each mean values from four representative values published in [FUJ78].

Results of the disintegration model for different temperatures are depicted in Figure 6.10. The annealing temperature as well as the original radius of the silicon coral branches have
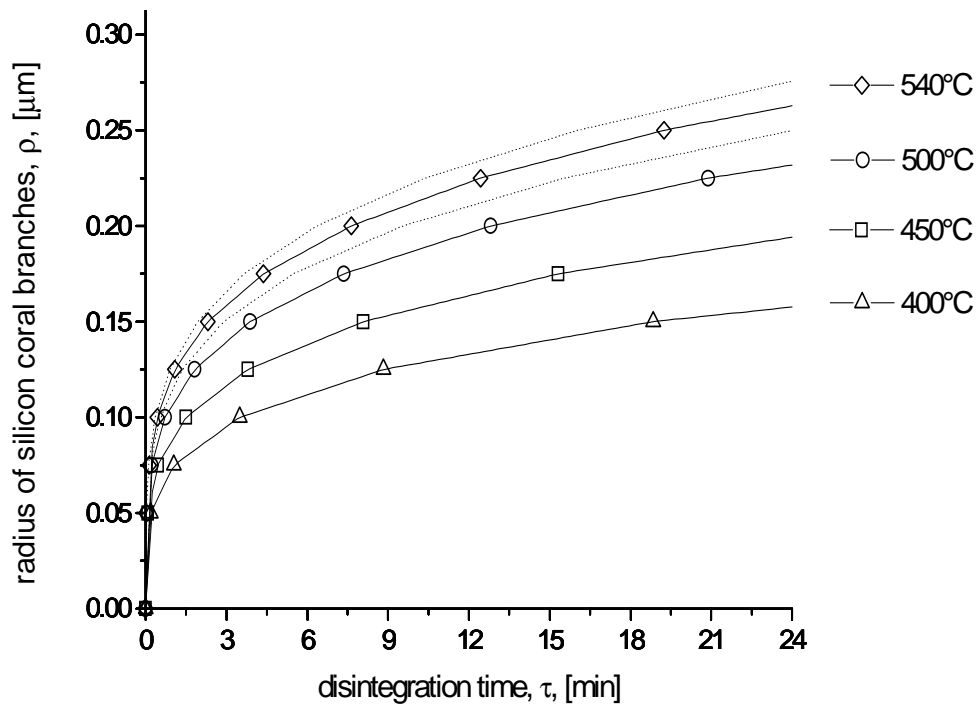
Figure 6.10: Results of the silicon spheroidization model. Disintegration time, τ, in dependence of the radius, ρ, of the silicon coral branches for various temperatures. Dotted lines indicate an error for the diffusion coefficient of +/- 20%.

a strong influence on the disintegration time. From quantitative metallurgy a mean radius of the silicon coral branches can be detected to $\rho_0 = 0.15$ +/- 0.05 µm. The model predicts that at 540°C disintegration and spheroidization of eutectic silicon corals are finished after a few minutes (ca. 2 minutes for $\rho_0 = 0.15$ µm and ca. 5 minutes for $\rho_0 = 0.20$ µm). Lowering the temperature will naturally prolong the disintegration time for the same ρ_0. The calculated values for the disintegration time will not even change significantly if an error of the diffusion coefficient of 20% is assumed.

6.4 EXPERIMENTAL INVESTIGATION ON SILICON SPHEROIDIZATION

An IR-furnace with implemented quenching facility was used to investigate high temperature silicon spheroidization. Small cubes of ~5 mm side length equipped with a thermocouple were placed in the IR-furnace, heated up to 400°C, 450°C, 500°C and 540°C, respectively, isothermally held for various times and finally quenched in cold water. The specimens were ground, polished and etched in a solution of 99,5% H_2O and 0,5% HF for 30 seconds. Best results for deep-etched pictures were obtained after an etching time of 2h with 5% NaOH and 95% H_2O. SEM pictures were taken and analysed by Leica QWin V2.2 software. Illustrated values are mean values of three measured pictures with about 300 silicon particles each.

6.4.1 STRUCTURAL PARAMETERS

The following parameters are used for quantitative microstructural analysis of the silicon particles in the eutectic region [HÖG96]:

- Mean area of silicon particles,

$$\bar{A}_{Si} = \frac{1}{n} \sum_{k=1}^{n} A_{Si} \quad , \tag{6-21}$$

where A_{Si} denotes the mean area of silicon particles of one measured picture with n as number of measured pictures

- Mean equivalent diameter of silicon particles,

$$D_{Si} = \frac{1}{n} \sum_{k=1}^{n} \sqrt{\frac{4A_{Si}}{\pi}} \quad , \tag{6-22}$$

which is the diameter of a circle with equivalent area, where A_{Si} is the area and n the number of measured silicon particles.

- <u>Mean interparticle spacing</u>,

$$\lambda_{Si} = \frac{1}{n} \sum_{k=1}^{n} \sqrt{\frac{A_{square}}{N_{Si}}} \quad , \tag{6-23}$$

with A_{square} as a squared measure area in the eutectic phase and n as number of measured pictures.

- <u>Mean spheroidization density</u>,

$$\xi_{Si} = \frac{1}{n} \sum_{k=1}^{n} \frac{N_{Si}}{A} \times 100 \ , \tag{6-24}$$

which describes the number, N_{Si}, of silicon particles counted in a reference area, A. The number of measured pictures is n. The values of ξ_{Si} are standardized for an area of $100 \ \mu m^2$.

- <u>Shape factor</u>,

$$F_{Si} = \frac{1}{n} \sum_{k=1}^{n} \frac{P_{Si}^2}{4\pi A_{Si}} \quad , \tag{6-25}$$

which can be used as a measure for the degree of spheroidization. P_{Si} symbolizes the perimeter of measured Si particles. The shape factor will yield unity, if the particle's cross-section area is a circle and > 1 if it deviates from a circle's shape.

6.4.2 MICROSTRUCTURE

The morphology's change of eutectic silicon with time at a temperature of 540°C can be seen in Figure 6.11. The spheroidization of the silicon corals is totally finished after 3 minutes of soaking time. After the spheroidization is completed the silicon particles grow in the α_{Al}-matrix. Deep-etched micrographs of Figure 6.12 reveal that the silicon corals are also three dimensionally separated after 3 minutes. During further annealing at 540°C, the silicon agglomerates again and forms large interconnected silicon crystals.
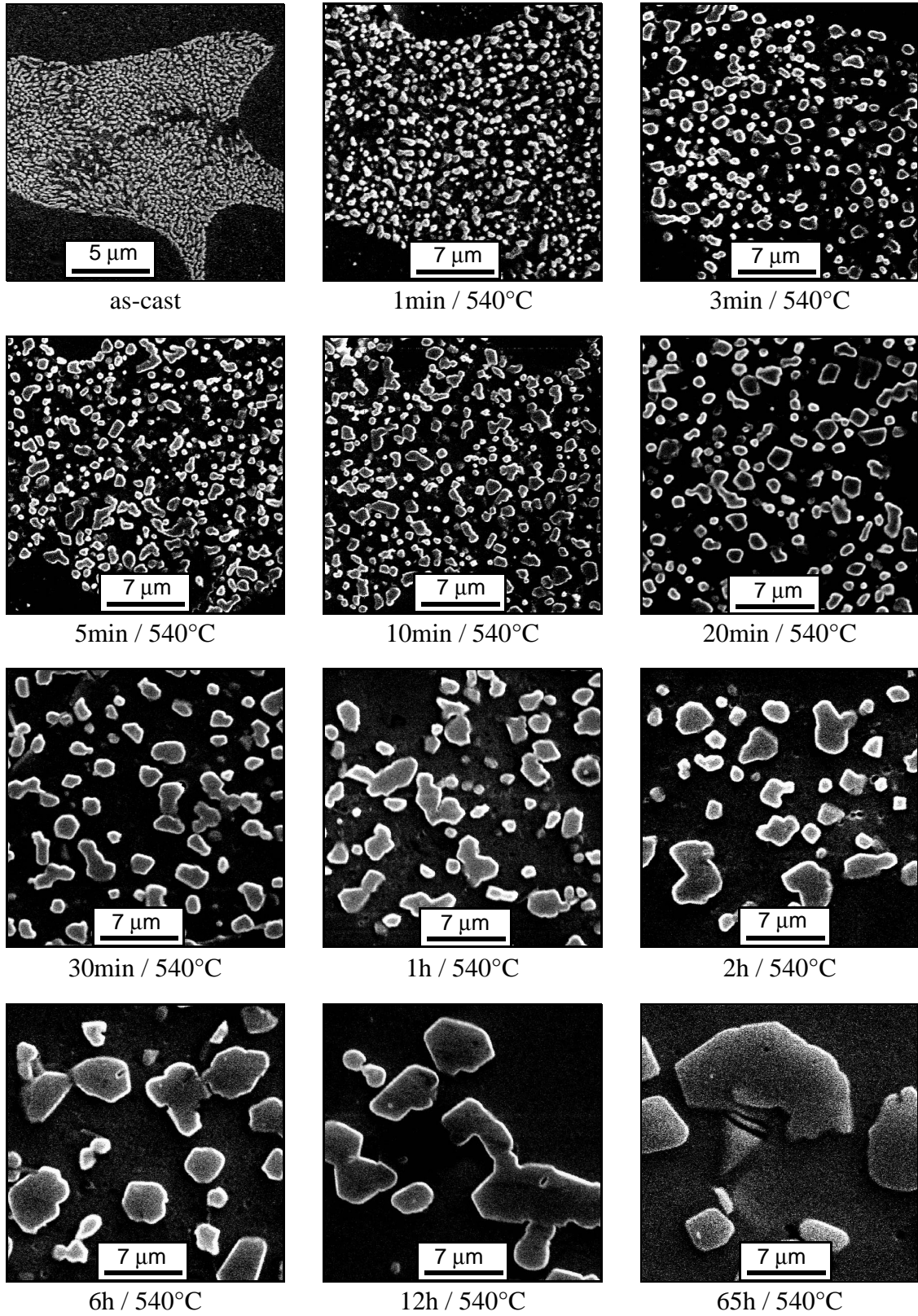
Figure 6.11: Chronology of silicon spheroidization of Sr-modified A356 at 540°C.
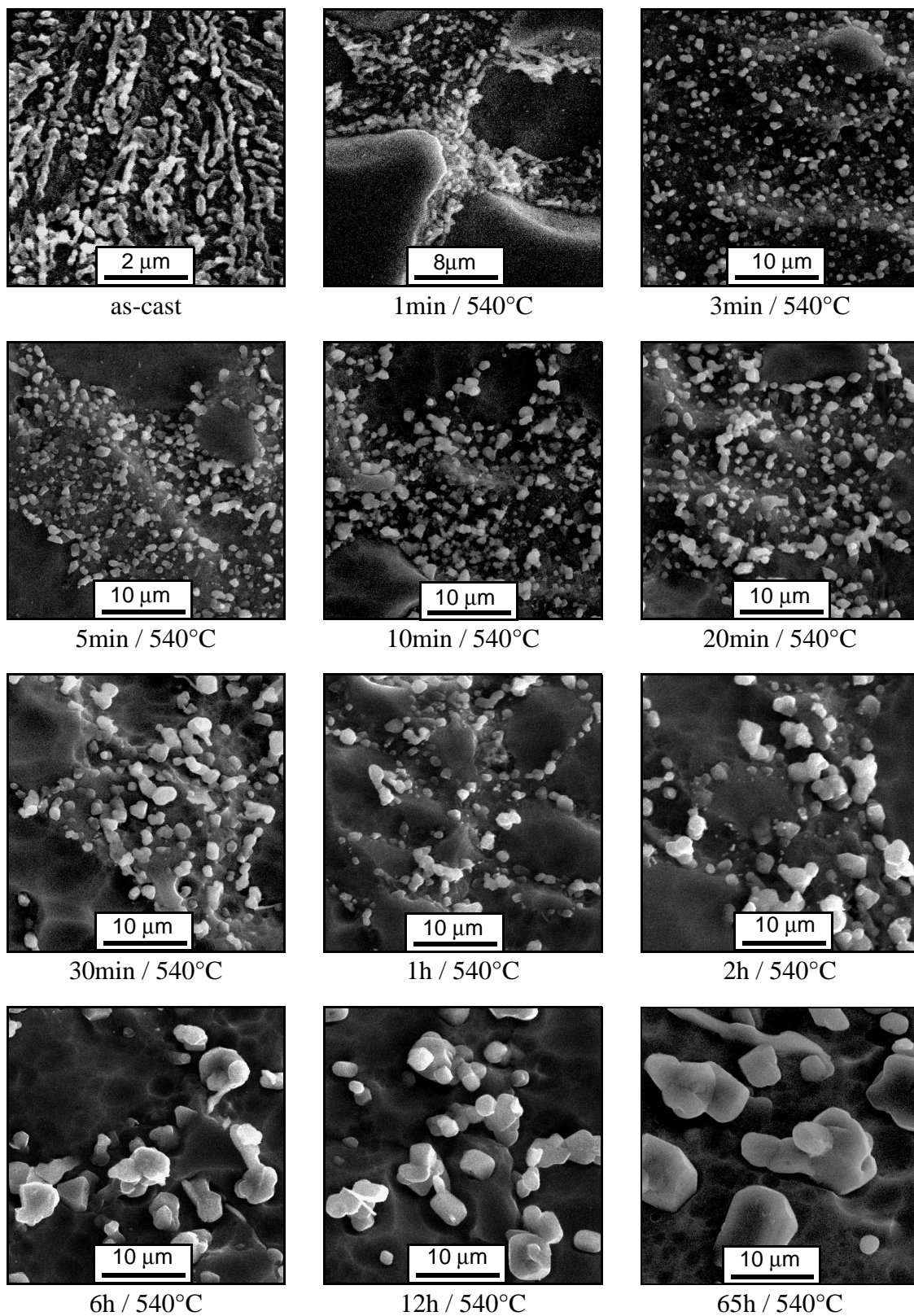
Figure 6.12: Deep-etched chronology of Si spheroidization of Sr-modified A356 at 540°C.

6.4.3 RESULTS OF MICROSTRUCTURAL ANALYSIS

The course of $\bar{A}_{Si}$ shows a linear behaviour from 1 minute to 65h soaking time at double logarithmic scale (Fig. 6.13).
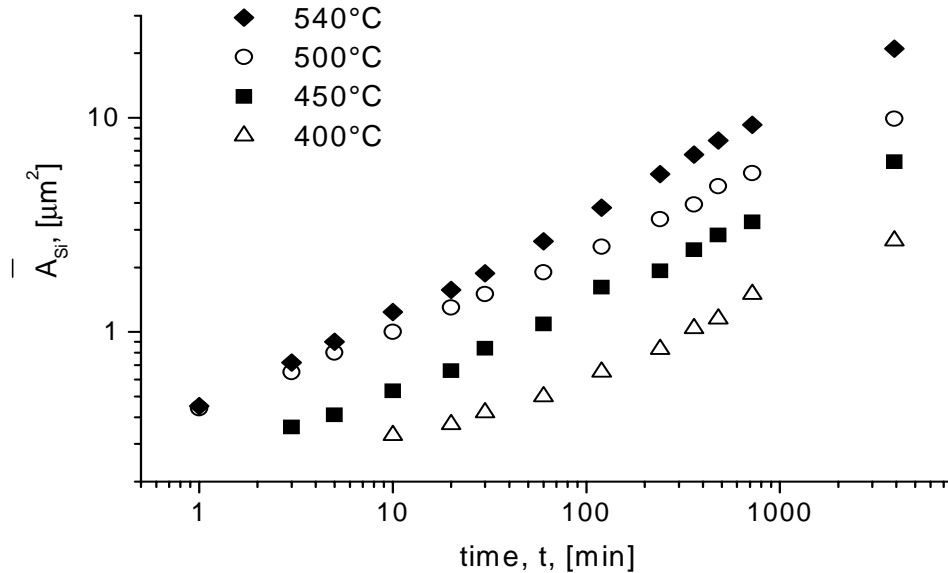
Figure 6.13: Growth of mean area of eutectic silicon particles, $\bar{A}_{Si}$, with time for various temperatures.

The growth of equivalent diameter of Si particles, D_{Si}, shows a linear behaviour when plotted against $t^{1/3}$, which indicates that the growth follows Ostwald ripening (Fig. 6.14)
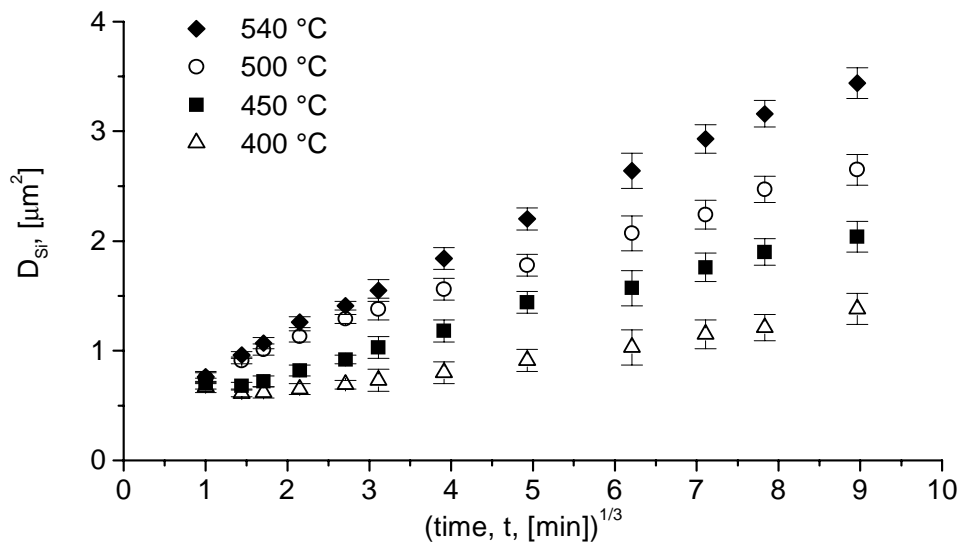
Figure 6.14: Growth of equivalent diameter of Si particles, D_{Si}, with time at various temperatures.

The mean interparticle spacing of euetctic silicon particles, λ_{Si}, also increases linearly with $t^{1/3}$(Fig. 6.15).
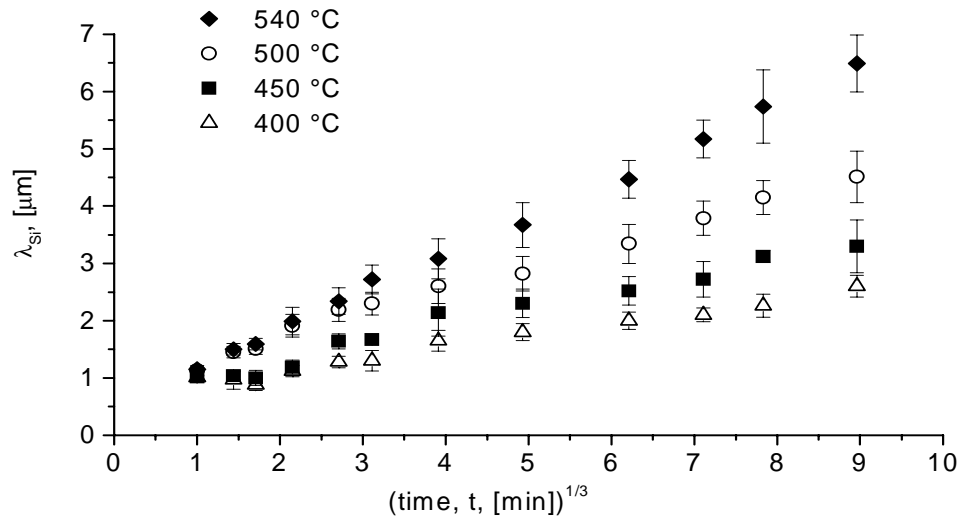
Figure 6.15: Course of the mean interparticle spacing of eutectic silicon particles, λ_{Si}, with time for various temperatures.

The shape factor, F_{Si}, shows a minimum after 3 minutes of holding time at 500°C and 540°C (Fig. 6.16). The minimum for 400°C and 450°C is not reached until 20 min soaking time.
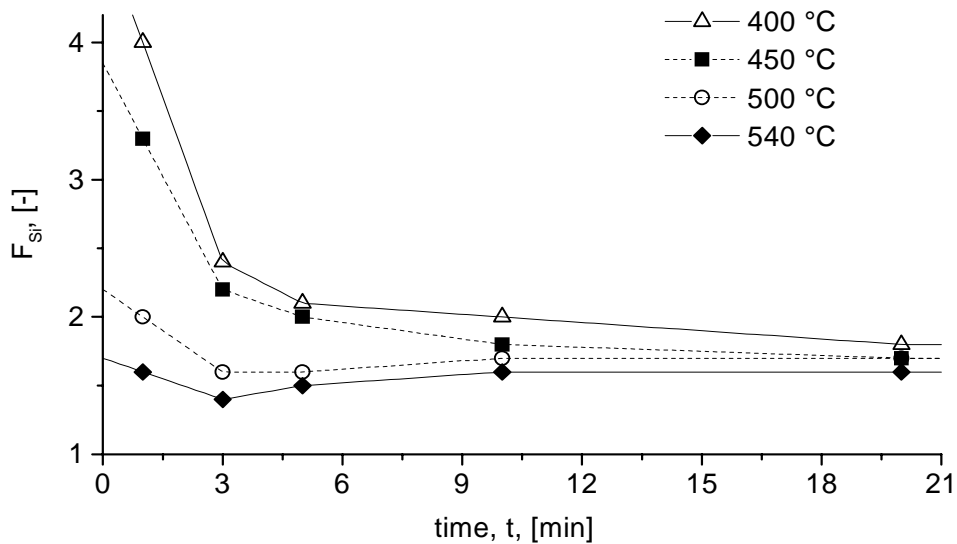
Figure 6.16: Course of the mean shape factor of eutectic silicon particles, F_{Si}, with time for various temperatures.

The mean spheroidization density, ξ_{Si}, in Figure 6.17 indicates that disintegration and growth of Si particles at temperatures between 500°C and 540°C do not differ significantly.
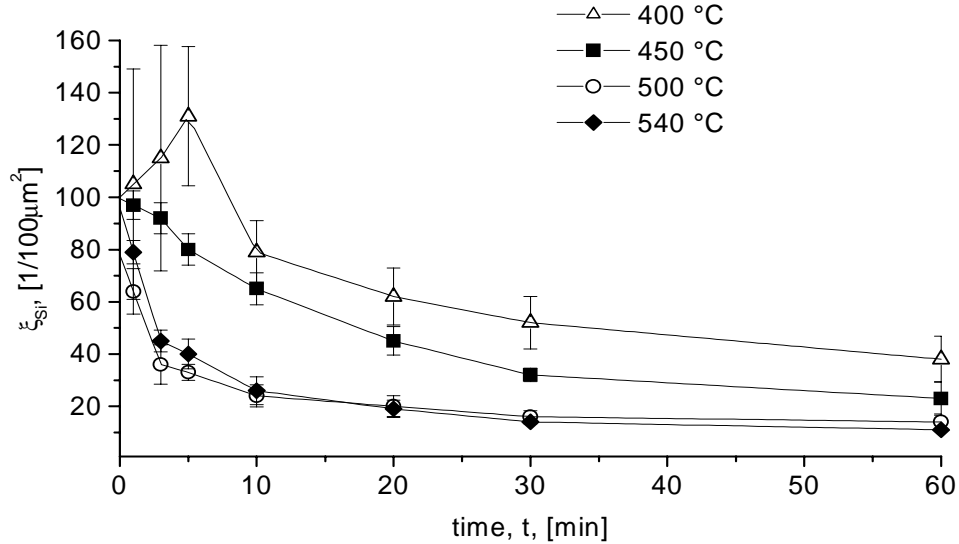
Figure 6.17: Course of the mean spheroidization density of eutectic silicon particles, ξ_{Si}, with time for various temperatures.

6.4.4 DISCUSSION OF SILICON SPHEROIDIZATION

The analytic model for silicon disintegration and spheroidization yields a disintegration time of ~2 min for 540°C (Fig. 6.10) which is in good accordance with experimental results. The micrographs from Figure 6.11 and Figure 6.12 clearly demonstrate the rapid spheroidization of Sr-modified silicon particles at 540°C. The shape factor, F_{Si}, as a measure for the grade of spheroidization shows a minimum after 3 minutes of holding time for 500°C and 540°C (Fig. 6.16). This indicates that at this temperature level the eutectic silicon corals disintegrate and spheroidize within about 3 minutes. At lower temperatures (400°C and 450°C) the minimum is not reached before 20 minutes, a result which can also be validated by the model. However, the values obtained from the model are highly dependant on the radius of the silicon branches, ρ, which can be influenced by chemical modifiers and cooling conditions. Hence, modified alloys exhibit a higher spheroidization rate than unmodified alloys, a result which was also previously obtained by other research studies [SHI89, APE90].

The mean equivalent diameter, D_{Si} (Fig. 6.14), and the mean interparticle spacing, λ_{Si} (Fig. 6.15), as measures for the growth rate is in direct proportion to time$^{1/3}$. Hence, the growth process of the silicon particles can be well described by the Ostwald ripening of precipitates, which states the following correlation between diameter of a growing phase and annealing time: $D_{Si} \sim t^{1/3}$. Pure Ostwald ripening means that bigger particles increase at the expense of smaller particles [SAH99] (see Chapter 2.5). Similar results have been obtained by Rhines et al. who found that Si particle growth, as measured by the increase in volume of the particles of average volume, is a linear of time at constant temperature [RHI86]. Taking the Ostwald ripening into account, the slight increase of the shape factor in Figure 6.16 from 3 to 10 minutes at 500°C and 540°C can be explained with the aniso-tropic growth (see deep-etched micrographs in Figure 6.12) of the silicon particles having a small detrimental influence on the shape factor.

The course of the mean spheroidization density as a measure, ξ_{Si}, in Figure 6.17 illus-trates that between 500°C and 540°C coarsening of Si particles starts at the very beginning of heat treatment. That also indicates that the disintegration process of the silicon corals is finished within minutes at these temperatures. At lower temperatures, especially at 400°C, the spheroidization density even increases within the first minutes. A possible ex-planation for this might be that most parts of the eutectic have not yet been properly dis-integrated.

6.4.5 SUMMARY OF SILICON SPHEROIDIZATION

Detailed investigations on silicon spheroidization in Sr-modified A356 have shown that the disintegration and spheroidization of the silicon coral branches is finished within 3 minutes of soaking time between 500°C and 540°C. Ostwald ripening of the sphe-roidized silicon particles were observed by quantitative microstructural analysis. An ana-lytic model which was originally developed by Stüwe and Kolednik for the disintegration of potassium filled cylinders into spheres in tungsten was successfully adapted to the spe-cific problem of Si spheroidization. The observed spheroidization times for various tem-peratures were in good accordance with calculated values.

7

SILICON SPHEROIDIZATION TREATMENT (SST)

7.1 INTRODUCTION

The need of lighter and safer cars is the driving force behind research in the area of high strength light metal safety part applications. Following the demands of the automotive industry, safety parts should have a minimum fracture elongation of 15% and a minimum yield strength of 180 MPa. The huge hurdle is the 15% fracture elongation which can not be reached by sand, die or permanent mould casting. The most promising candidate to fulfil these requirements eventually is thixocasting (Fig. 7.1).
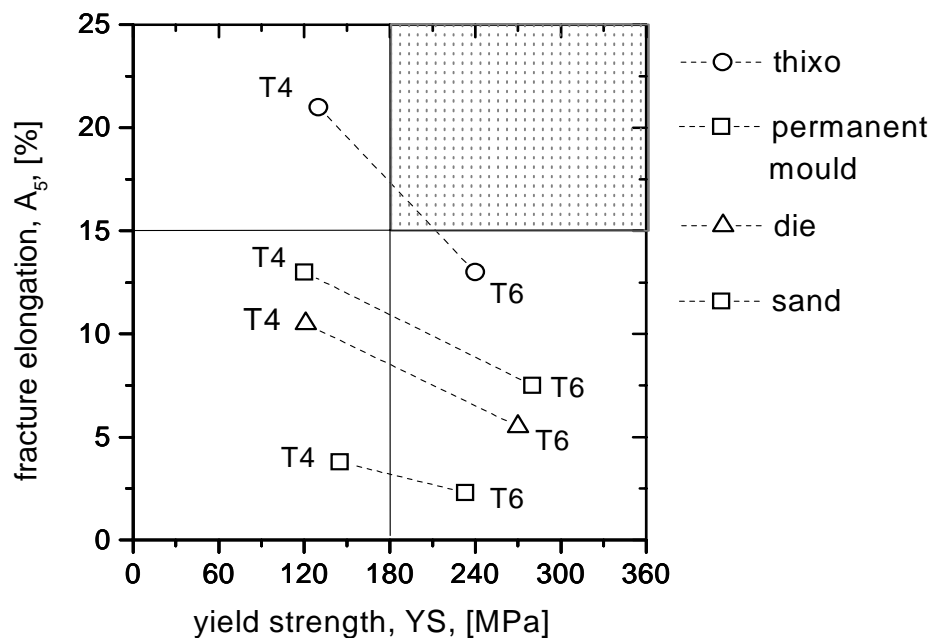
Figure 7.1: Fracture elongation to yield strength for A356 and various forming processes [GAB93]. Note that the dotted area of A>15% and YS>180 MPa cannot be reached by conventional heat treatment T4 or T6, respectively.

The spheroidized silicon is responsible for the good ductility values in T6 condition which is applied to many high strength aluminum safety parts. T6 treatment includes a solution heat treatment, continued by quenching in water followed by artificial ageing at slightly elevated temperature level. A recommended time range for T6 solution heat treatment is given from 2-12h at a temperature level very close to the solidus temperature [ALU95]. However, heat treatment standards for Al-Si alloys currently being used in the cast shops were developed several decades ago and need to be revised to suit current foundry practise. Due to the influence of modification on the spheroidization rate, long solution times used in most foundries may not be necessary when the alloy is properly modified [APE90]. Although the spheroidization of eutectic silicon in Al-Si alloys has been well documented (see Chapter 6.1), the effect of these spheroidized silicon particles on mechanical properties has not yet been studied [KAS93]. On the contrary it was reported that there is almost no influence of modification on the fracture elongation after a heat treatment of 2h at 540°C with specimens from permanent mould cast [PAR96].

Results of silicon spheroidization experiments of Chapter 6.4 clearly illustrate that silicon in a modified Al-Si alloys completely spheroidizes within minutes at $500°C < T < 540°C$. The effect of sole spheroidization on mechanical properties is subject of the following and termed Silicon Spheroidization Treatment or abbreviated SST.

7.2 DEVELOPMENT OF SST

Flat tensile specimens of thixoformed components, as described in Chapter 4.1.2, were placed in a furnace at 540°C, soaked until the metal temperature reached 500°C and then treated for one, three and five minutes, respectively. The specimens were then quenched in cold water and instantly artificially aged for 4 hours at 160°C.

The results for the alloy A356 and A357, respectively, which are depicted in Figure 7.2 and Figure 7.3., are mean values of three tested specimens where T6x1 implies 1 minute, T6x3 3 minutes and T6x5 5 minutes of SST annealing.
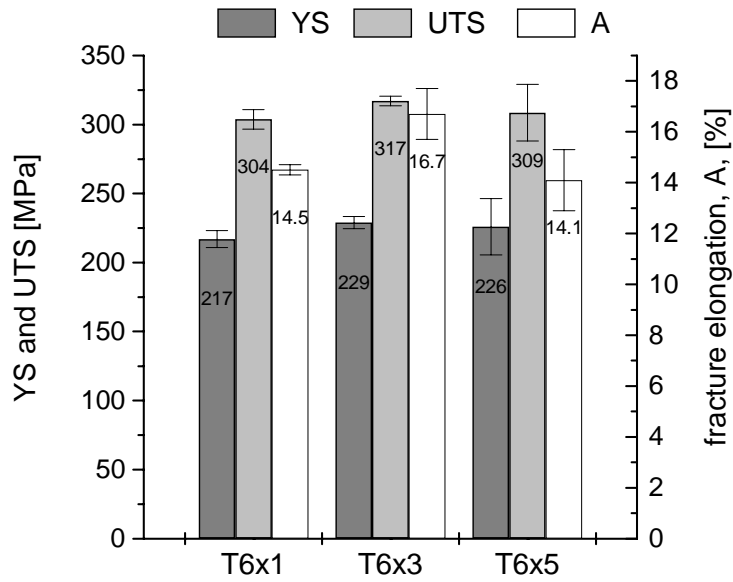
Figure 7.2: Mechanical properties of A356 after 1 min (T6x1), 3 min (T6x3) and 5 min (T6x5) of SST at 540°C, plus water quenching and artificial ageing for 4h at 160°C.

Both alloys show a maximum value of the fracture elongation after a 3-minute heat treatment at 540°C. Remembering the course of the shape factor of the silicon particles in Figure 6.16, it becomes evident that the elongation fracture yields a maximum when the shape factor yields a minimum.
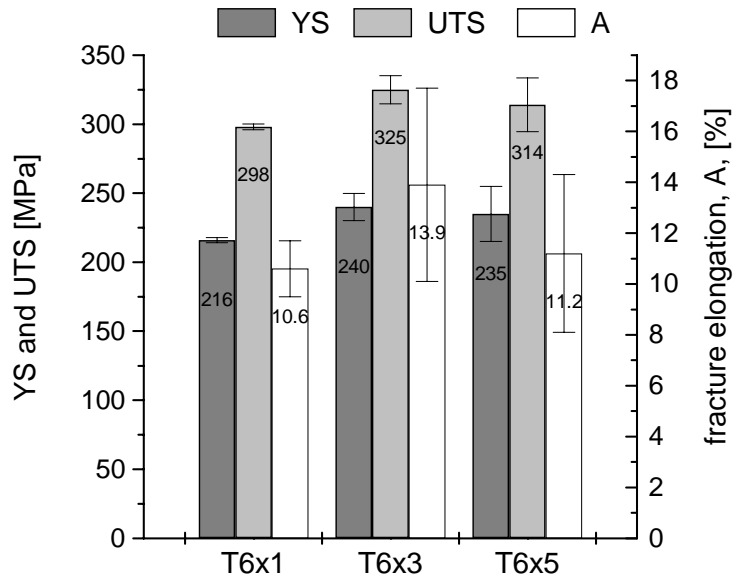
Figure 7.3: Mechanical properties of A357 after 1 min (T6x1), 3 min (T6x3) and 5 min (T6x5) of SST at 540°C, plus water quenching and artificial ageing for 4h at 160°C.

7.3 MECHANICAL PROPERTIES AND MICROSTRUCTURE OF SST

The heat treatment parameters of the newly developed temper conditions T4x3 and T6x3, respectively, in comparison to conventional temper conditions F, T4, T5 and T6 are summarized in Table 7.1. It is important to note that indicated temperatures are metal temperatures.

Table 7.1: Conventional and SST heat treatment parameters of thixoformed components.

conventional	F	as-fabricated
	T5	4h at 160°C
	T4	12 h at 540°C, quenched in cold water, aged at RT
	T6	12 h at 540°C, quenched in cold water, 4h at 160°C
SST	T4x3	3 min at 540°C, quenched in cold water, aged at RT
	T6x3	3 min at 540°C, quenched in cold water, 4h at 160°C

7.3.1 STATIC MECHANICAL PROPERTIES OF A356 AND A357

The mechanical properties of SST conditions T4x3 and T6x3 in comparison with F, T4, T5 and T6 are summarized for A356 in Figure 7.4.

Figure 7.4: Static mechanical properties of SST (T4x3 and T6x3) in comparison to F, T4, T5 and T6 conditions of thixoformed A356.

Although the yield strength from T4x3 to T6x3 is doubled, the elongation fracture value remains almost at the same high level. The difference between T5 and T6x3 is the 3 minute SST annealing. Due to SST, the eutectic silicon in T6x3 is spheroidized, and this results in a mean elongation fracture value which is 70% higher than the value of T5 with fibrous eutectic silicon. The yield strength increases significantly from T5 to T6x3. The small difference (15%) of T6 and T6x3 yield strength indicates that the diffusion of Si and Mg in the α_{Al}-matrix is almost finished within the first minutes of SST.

Comparable results are obtained when SST is applied to thixoformed A357 (Fig. 7.5). From T5 to T6x3 both the yield strength and the fracture elongation are increased. The gain of fracture elongation from T6 to T6x3 is 67%. The yield strength level of T6x3 cannot reach the T6 level after 3 minutes of annealing time. It is, however, significantly higher than the T5 level. While in T4 condition iron containing β–phases and π-phases are dissolved or spheroidized, it is observed that they cannot be spheroidized by short SST. This might be a possible explanation for the difference of fracture elongation between T4x3 and T4.

.

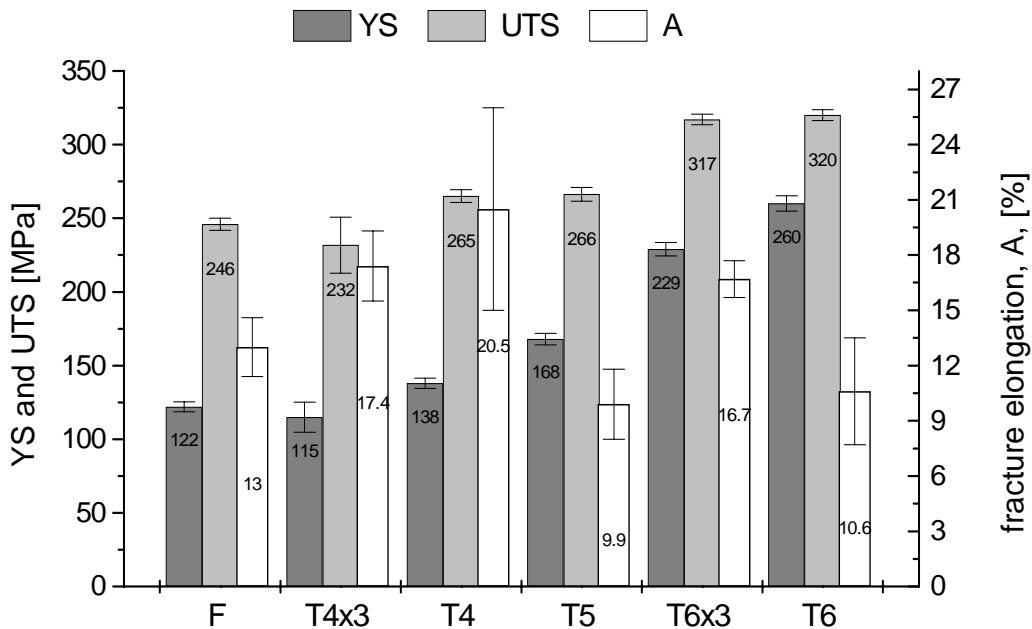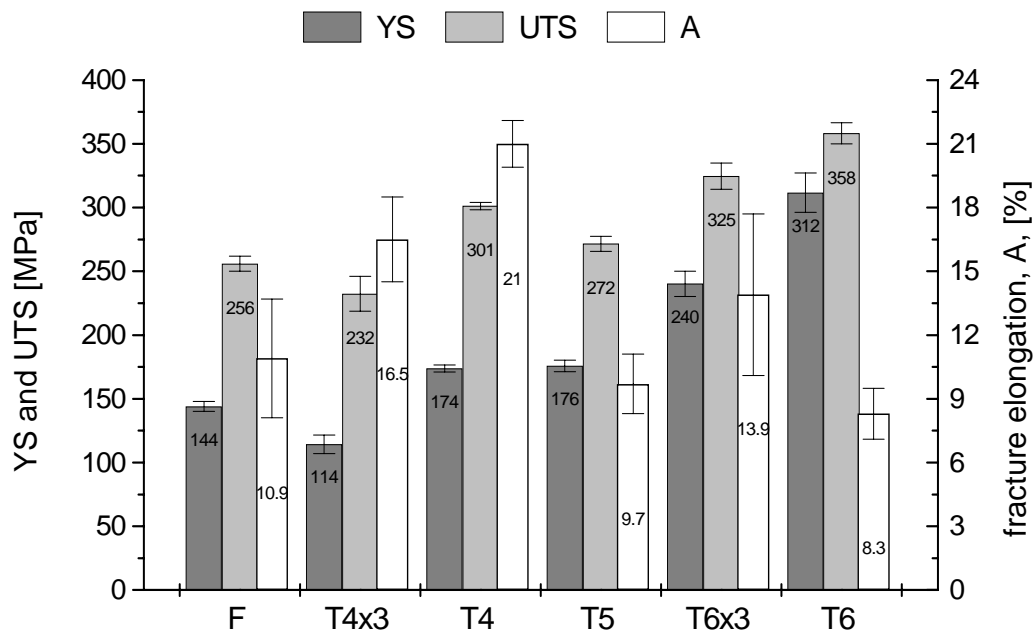*Figure 7.5: Static mechanical properties of SST (T4x3 and T6x3) in comparison to F, T4, T5 and T6 conditions of thixoformed A357.*

7.3.1.1 MICROSTRUCTURE OF SST TENSILE SPECIMENS

The microstructure of a T6 (Fig. 7.6) and T6x3 (Fig. 7.7) tensile specimen shows that the silicon particles in T6x3 are completely spheroidized and much smaller than the particles of the T6 specimen. Deep-etched micrographs reveal that silicon in T6 is agglomerated (Fig. 7.8) whereas silicon in T6x3 is almost completely separated (Fig. 7.9).
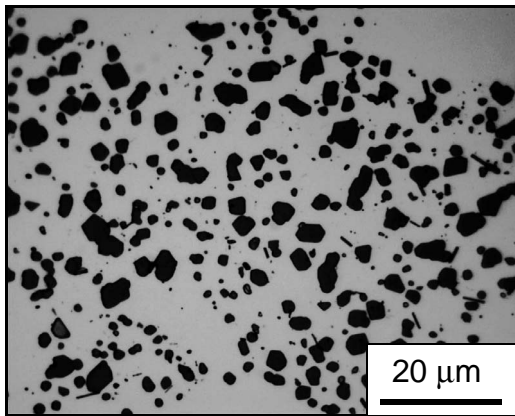
Figure 7.6: Microstructure of T6 tensile specimen(12h/540°C) with A =10 %.
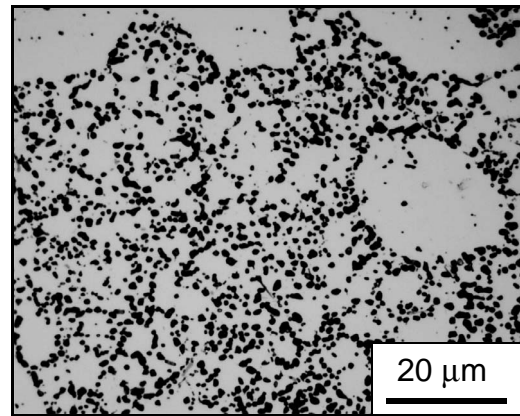
Figure 7.7: Microstructure of T6x3 tensile specimen(3 min/540°C) with A=18 %.
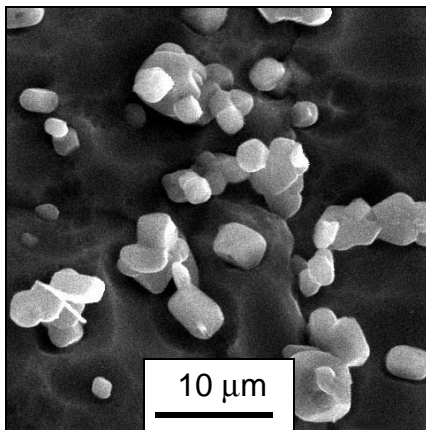
Figure 7.8: Deep-etched microstructure of T6 tensile specimen(12h/540°C).
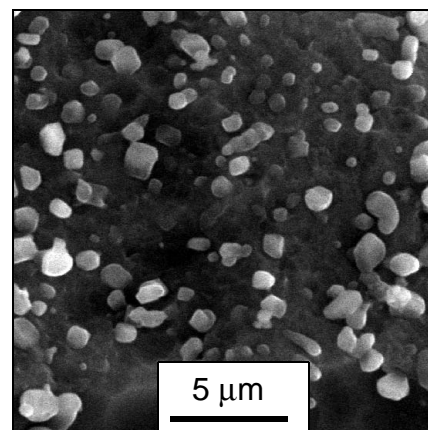
Figure 7.9: Deep-etched microstructure of T6x3 tensile specimen(3 min/540°C).

7.3.1.2 MODE OF FRACTURE OF SST TENSILE SPECIMENS

Different modes of fracture could be observed in T6 and T6x3 specimens, respectively. While the micrograph in conventional T6 condition (Fig. 7.10) reveals a typical intergranular crack propagation, the mode of fracture in T6x3 condition could be clearly identified as transgranular (Fig. 7.11). SEM pictures of both fracture surfaces can be seen in Figure 7.12 and Figure 7.13, respectively.
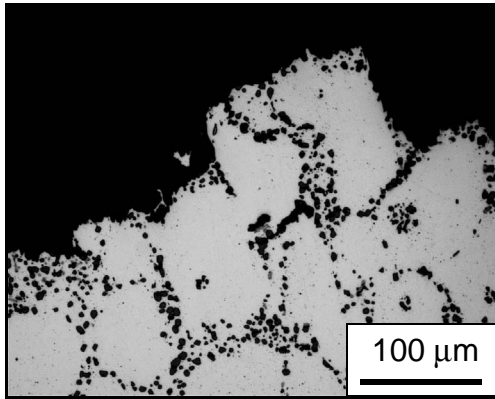
Figure 7.10: Intergranular fracture of T6.
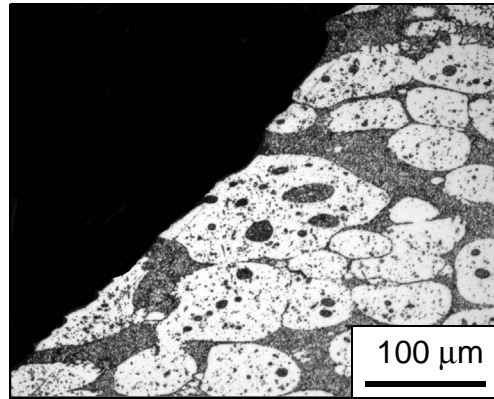
Figure 7.11: Transgranular fracture of T6x3.
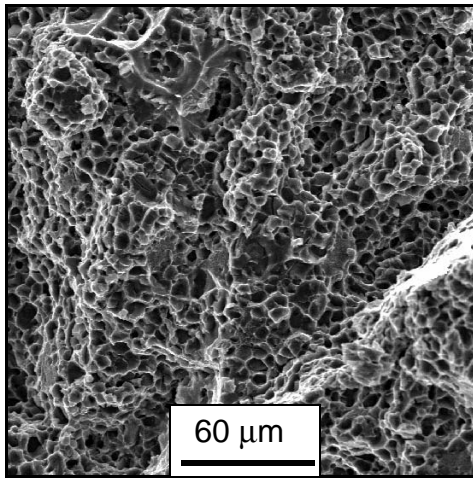
Figure 7.12: Fracture surface of T6.
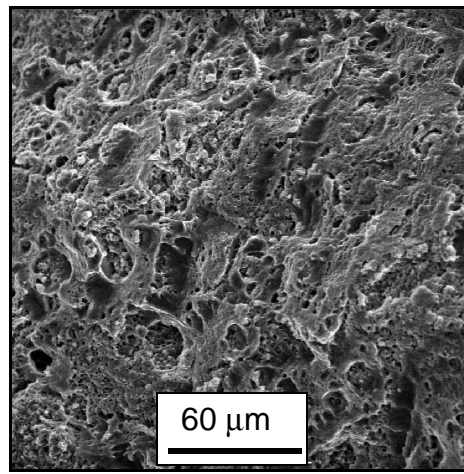
Figure 7.13: Fracture surface of T6x3.

Crack initiation in T6 specimens could be observed in the brittle eutectic region which can bee seen in Figure 7.14. The crack propagates through the eutectic and also through the silicon particles (Fig. 7.15). No cracked particles were found in T6x3 specimens.
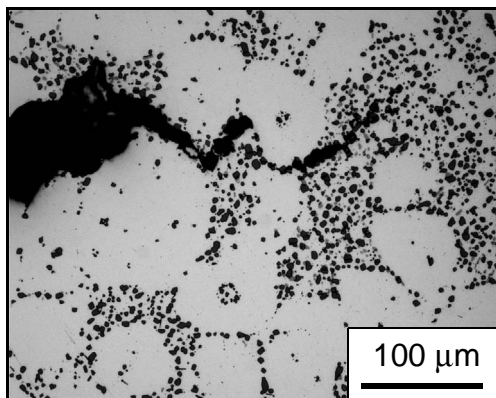
Figure 7.14: Crack initiation in the eutectic region of T6 specimen.
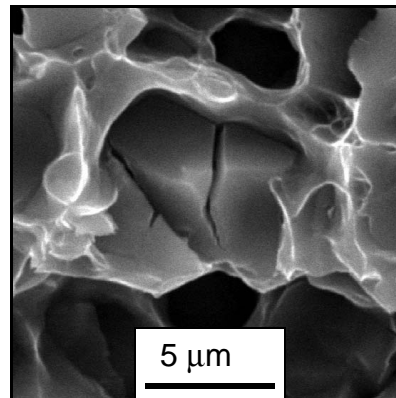
Figure 7.15: Cracked T6 silicon particle embedded in Al-matrix.

7.3.2 STATIC MECHANICAL PROPERTIES FOR VARIOUS Al-Si-Mg ALLOYS

SST was also applied to newly developed alloys described in Chapter 3. The results of tensile tests can be seen in Fig. 7.16. The difference between T5 and T6x3 treatment is 3 minutes of Silicon Spheroidization Treatment at 540°C. As a result of SST fracture elongation and yield strength were concurrently increased from T5 to T6x3 in all tested alloys.
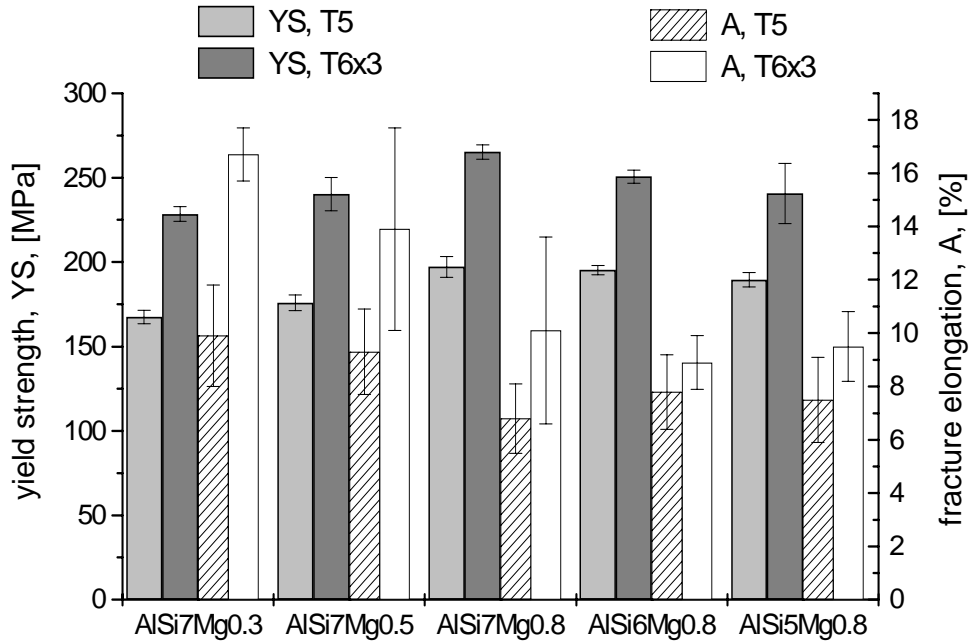
Figure 7.16: Influence of SST in comparison with T5 for various thixoformed AlSiMg alloys.

7.3.3 DYNAMIC MECHANICAL PROPERTIES OF A356

A thixoformed stepped plate of A356 (2mm, 4mm, 6mm and 11mm) shown in Figure 7.17 was used to make specimens for fatigue tests (Fig. 7.18). The fatigue tests were carried out on a servohydraulic testing machine from MTS Systems Corporation with a frequency of 50 Hz and a ratio of minimum stress to maximum stress of R = 0.1.
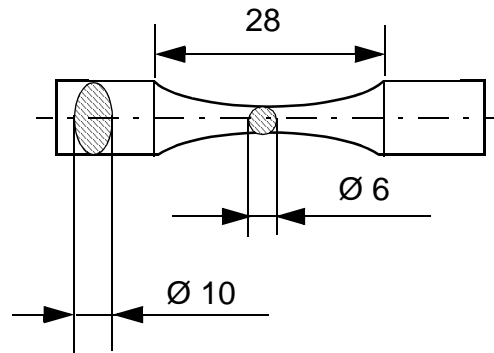
Figure 7.17: Thixoformed stepped plate.   *Figure 7.18: Specimen for fatigue testing.*

Results for A356 in T6 and T6x3 condition are depicted in Figure 7.19. The positive influence of the very small spheroidized silicon particles on the endurance of life is reflected by the increased fatigue stress level of the SST condition T6x3 compared to T6.
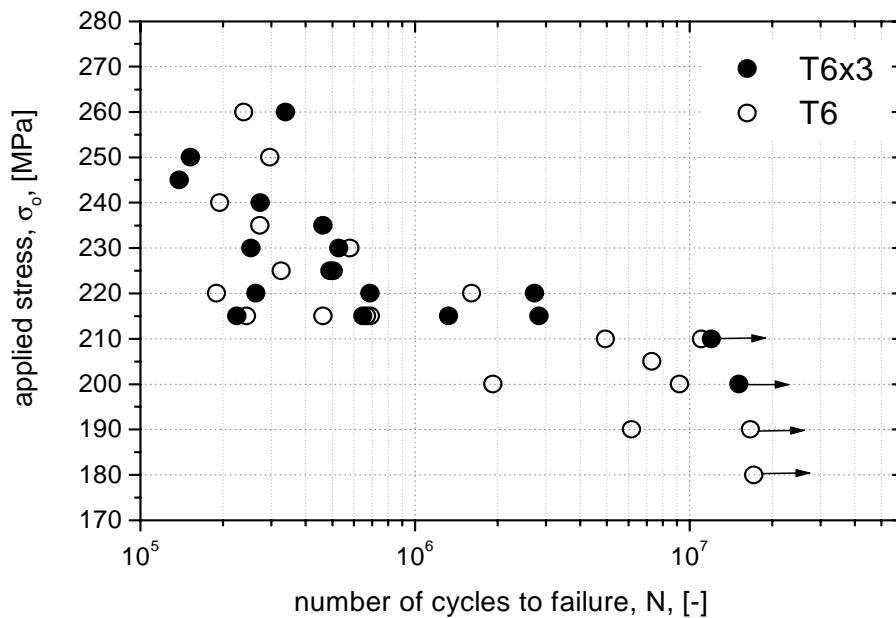
Figure 7.19: Dynamic mechanical properties of thixoformed A356 in conventional T6 and SST-T6x3 condition, R = 0.1.

7.3.3.1 MICROSTRUCTURE OF FATIGUE SPECIMENS

The microstructures of fatigue specimens of both T6 and T6x3 are illustrated in Figure 7.20 and Figure 7.21. The smaller and less sharp-edged silicon particles in T6x3 are responsible for the better fatigue stress values. The light grey intermetallic compounds in Figure 7.21 are β-phase needles which were not completely spheroidized. But due to the short high temperature treatment, they are rounded and partly disintegrated.
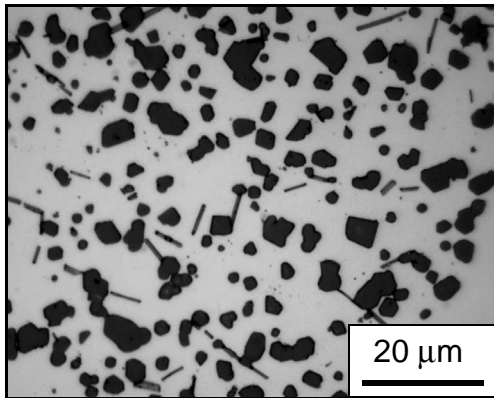
Figure 7.20: Microstructure of T6 fatigue specimen.
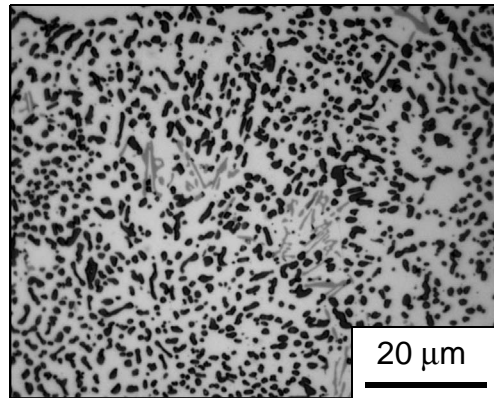
Figure 7.21: Microstructure of T6x3 fatigue specimen.

7.3.4 IMPACT PROPERTIES OF A356 AND A357

A modified thixoformed component was used for testing impact properties of SST. The core of a connecting pipe was removed and thixoformed at Thixalloy Components GmbH.
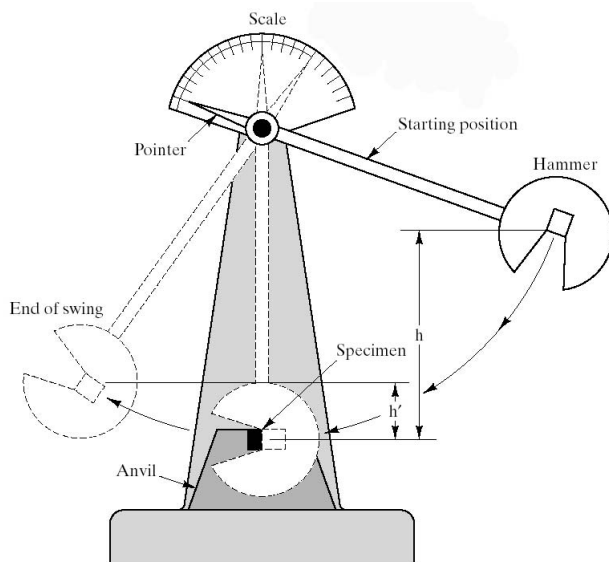
Figure 7.22: Charpy test of impact energy [SHA99].
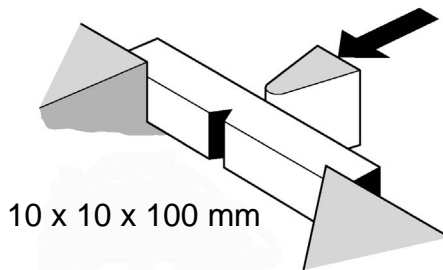
Figure 7.23: Thixoformed component (connecting pipe with removed core).

Impact energy specimens were cut out and T6 and T6x3 heat treated, respectively. Two different quenching media, namely water and air, were used for T6x3 specimens.

The results of impact energy tests are depicted in Figure 7.24. The values for impact energy of A356 and A357 are significantly increased by SST. Best results are obtained with air-quenched specimens. Compared to T6, the values of air quenched T6x3 specimens are almost doubled.
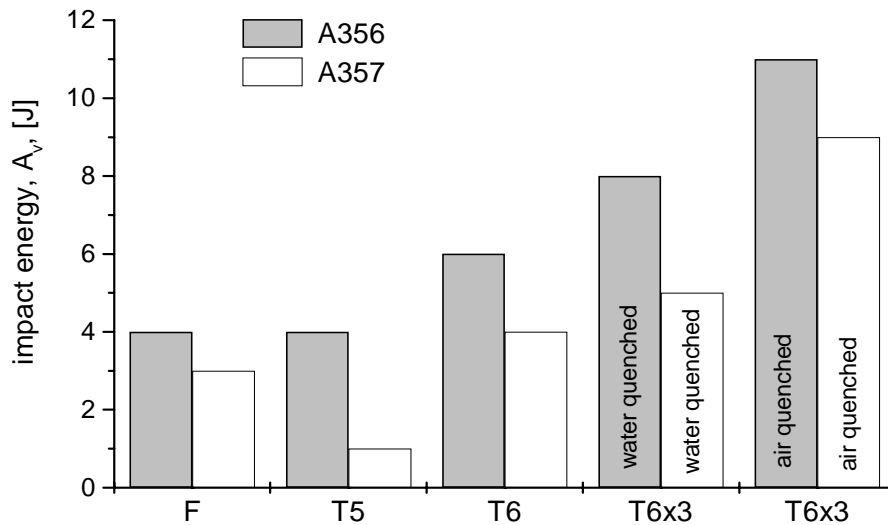
Figure 7.24: Impact energy of thixoformed A356 and A357. Similar results for thixoformed A356-T6 were found in [BLE01].

7.4 AGE HARDENING OF Al-Si-Mg ALLOYS

The precipitation sequence of the alloys system Al-Si-Mg from supersaturated solid solution (SSS) has been elucidated by various techniques, particularly X-ray techniques and transmission electron microscopy, as follows [CAH96]:

$$SSS \rightarrow GP\text{-}I_{spherical} \rightarrow GP\text{-}II(\beta'')_{needle} \rightarrow \beta'_{rod} \rightarrow \beta(Mg_2Si)_{platelet} \quad (7\text{-}1)$$
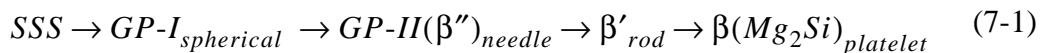
The decomposition process begins with the formation of two types of GP zones. One of them is coherent and spherical, called GP-I zone or pre-clusters, with no internal order. As ageing proceeds, the GP-I zones become ordered and acquire an acicular or needle

shape. At this stage, they are called GP-II zones or β''. The zones are orientated parallel to the <100> directions of the Al matrix and have coherency strain around the needles. Prolonged ageing results in the transformation of coherent β'' needles into semi-coherent β' rods. In the latter stages, β' loses coherency and the equilibrium $\beta_{(Mg_2Si)}$ phase is formed. The presence of Si, in excess of the quay-binary composition, is known to enhance the kinetics and age hardenability of the material [GUP95].

7.4.1 AGE HARDENING AFTER SST

The enormous increase of fracture elongation due to SST can be explained by the formation of very fine spheroidized silicon particles. However, the significant increase of yield strength in T6x3 compared to T5 values after only 3 minutes of annealing time is surprising. Age hardening curves of A356 after 12h and 3 min of soaking time at 540°C show only a minimal difference in peak hardness for ageing temperatures of 160° and 180°C, respectively. In addition the peak hardness shifts to shorter times with increasing ageing temperatures (Fig. 7.25).
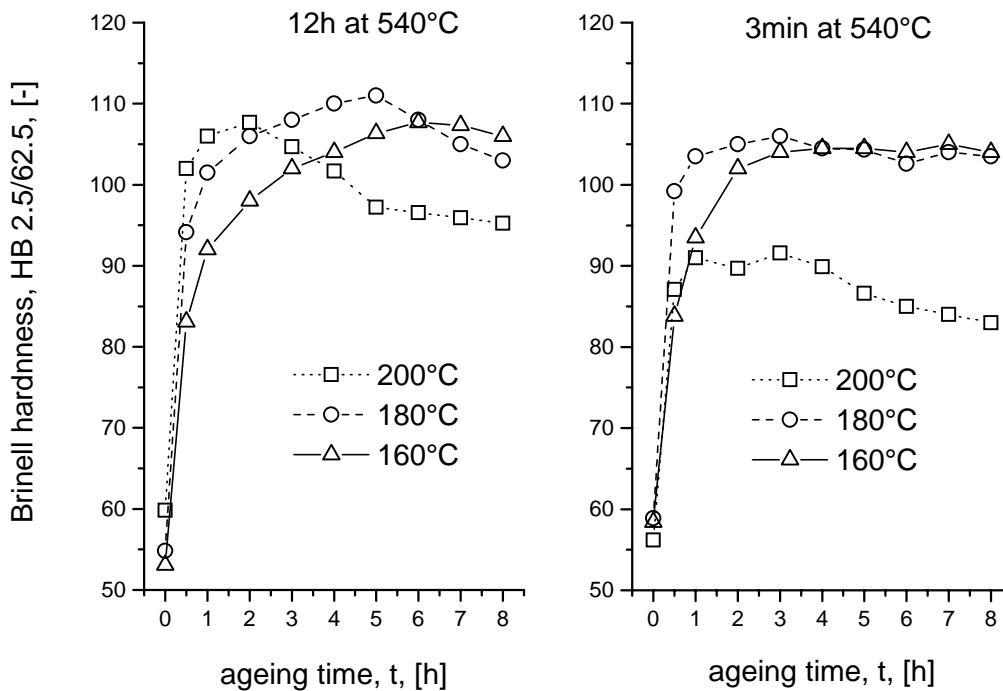
Figure 7.25: Course of hardness of A356 after conventional T6 treatment (12h) and SST (3min) at various ageing temperatures.

It was reported recently that solution treatments of less than 1 hour at 540°C are sufficient for most Al-Si-Mg foundry alloys to undergo full Mg_2Si dissolution and alloy homogenization [ROM99]. The results were obtained from numerical modelling and were verified by wavelength dispersive spectroscopy measurements. Modelling was performed for a secondary dendrite arm spacing (DAS) of 40µm for A356 and 55µm for A357, respectively. Some results are listed in Table 7.2. The model predicts a dissolution time for Mg_2Si in aluminum matrix of 3 minutes and a homogenization time of 5 minutes. However, the experimental verification of predicted values was carried out by method of spectroscopy, which is known to be quite uncertain, especially for low concentration profiles.

Table 7.2: Results of modelling dissolution and homogenization of Mg_2Si in Al-Si-Mg castings [ROM99].

Alloy and Condition	Numerical Model	Experimental Results
A356 Dissolution Time	3.0 min	2-4 min
A356 Homogenization Time	5.1 min	8-15 min
A357 Dissolution Time	38.7 min	< 50 min
A357 Homogenization Time	40.7 min	< 50 min

7.4.2 DIFFERENTIAL SCANNING CALORIMETRY (DSC)

A more precisely method which provides information about the amount of Mg_2Si in the aluminum matrix is Differential Scanning Calorimetry (DSC). By means of DSC exothermic and endothermic reactions can be detected. The exemplary result of a DSC trace of naturally aged A356 after several hours of solution treatment is illustrated in Figure 7.26. The endothermic peak at ~200°C represents the dissolution of GP-I zones which have been formed during natural ageing. The subsequent formation of GP-II zones (β″) can be seen at ~300°C. The dashed area is a measure for the amount of β″ particles which can precipitate in the aluminum matrix.
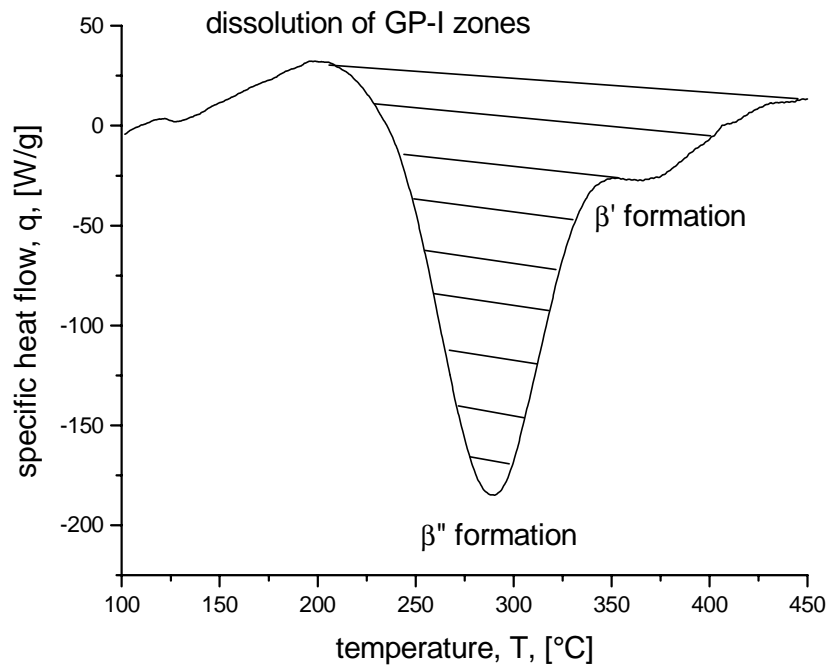
Figure 7.26: DSC trace of A356 in T4 condition.

.

7.4.2.1 EXPERIMENTAL PROCEDURE

DSC measurements were carried out on a Seiko DSC220 device. The measure principle of DSC is schematically illustrated in Figure 7.27. The heat flow passing through the thermal resistance material is proportional to the temperature difference between the heat conducting surface on one end and the sample holder on the other end. The heat conducting surface is controlled to maintain an uniform temperature level. Thus, the measured difference in heat flow through the sample holder is proportional to the sample and reference temperature differences.

Small samples of A356 were heated up in an IR-furnace to 500°C and 540°C, respectively. After soaking times of 0 min, 1 min, 3 min, 10 min and 12 h the samples were quenched and naturally aged at room temperature for 8 days. Then small cubes of ~40 mg were prepared and placed on the sample holder of the DSC device. The reference
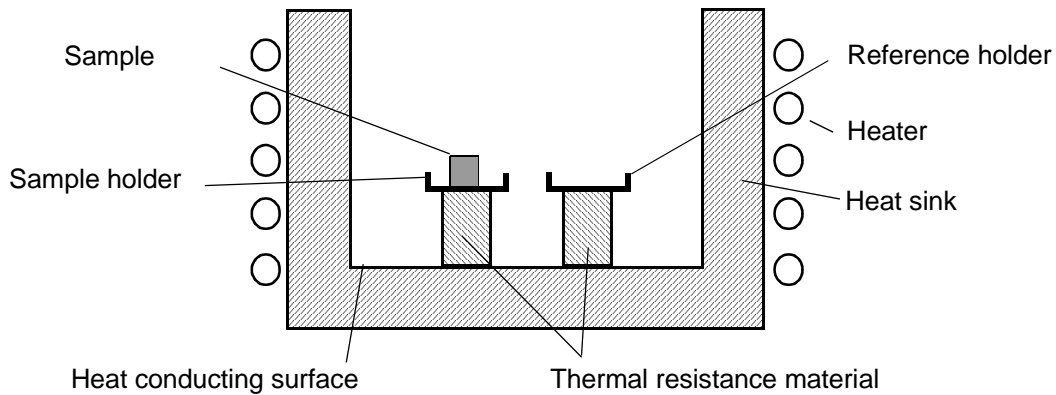
Figure 7.27: Measurement principle of Seiko DSC220, schematic.

holder was left blank. Prior to each measurement the whole heating unit was cooled down to -10°C. The samples were heated up to 470°C at a heating rate of 40 K/min, then instantly cooled down to -10°C with a maximal cooling rate of ~300 K/min, held for 10 minutes and reheated again to 470°C with 40 K/min. To prevent oxidation the experiment was carried out in an argon atmosphere.

7.4.2.2 RESULTS

DSC traces of experiments carried out at 540°C are depicted in Figure 7.28. The curves represent a rescan subtracted by the scan and have been offset for better visualization. The results show a distinct dissolution peak of GP-I zones at ~220°C which have already been formed during the natural T4 ageing procedure. The exothermic peak at ~300°C represents the formation of GP-II(β'') zones. The small peak at ~350°C marks the transition from β''-Mg_2Si to β'-Mg_2Si. The precipitated zones are dissoluted again at higher temperatures.

Figure 7.29 shows the results of experiments performed at 500°C. It can be seen that instead of the peak at ~350°C a small peak at ~270°C can be observed. This reaction takes place prior to β''-Mg_2Si formation whose peak is shifted to higher temperatures. Only the DSC trace after 12h at 500°C is different and shows a double peak at 320°C and 440°C, respectively.
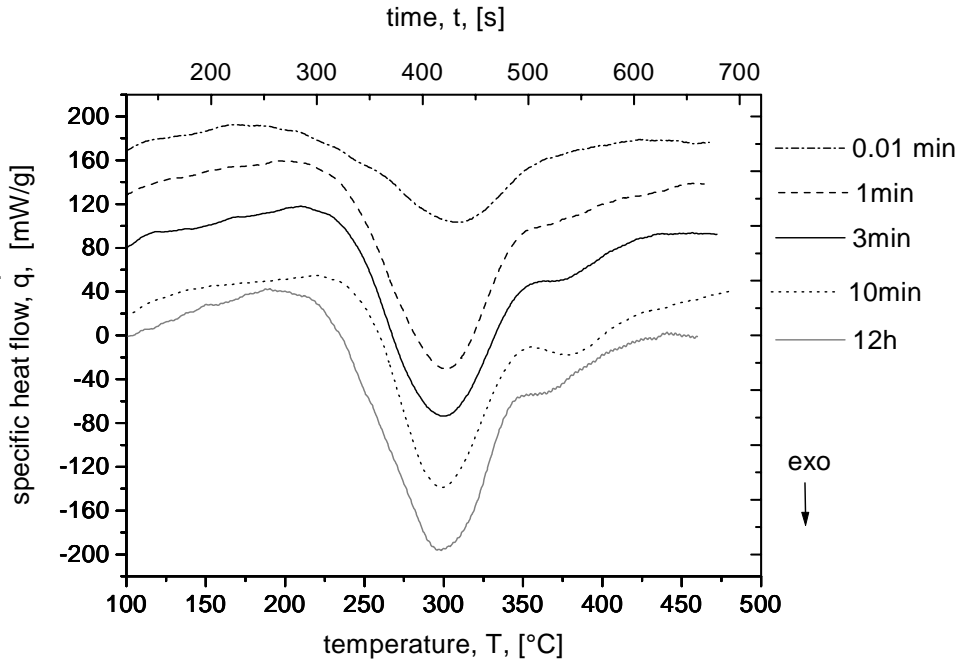
Figure 7.28: DSC curves from A356 after various soaking times at 540°C (dT/dt = 40K/min).

.
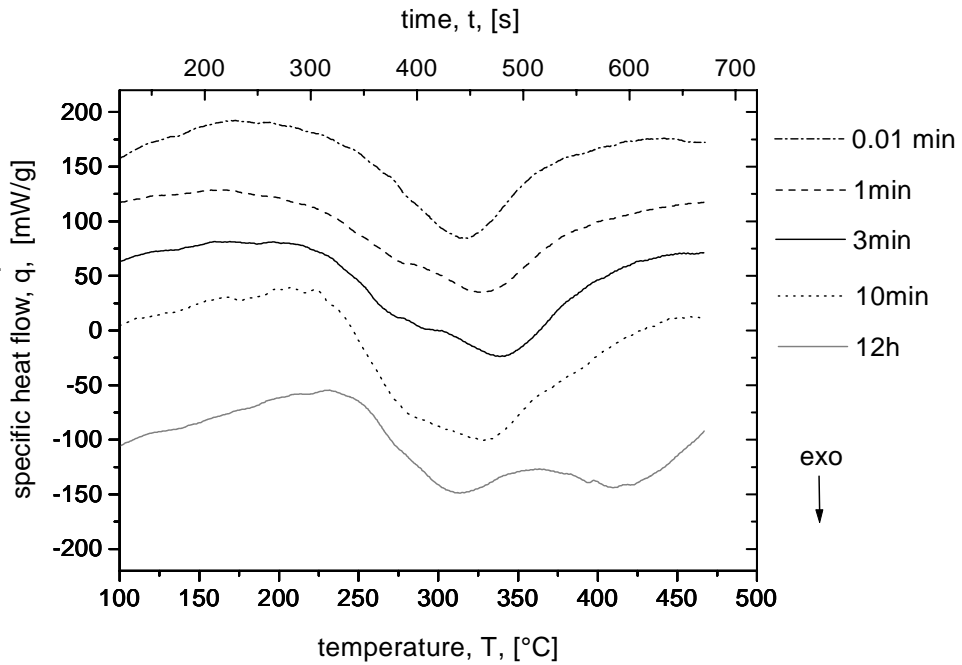
Figure 7.29: DSC curves from A356 after various soaking times at 500°C. (dT/dt = 40K/min).

The specific energy of formation of β″ zones was calculated as the area of β″ peak. Results of β″ formation in A356 at 500°C and 540°C can be seen in Figure 7.30.
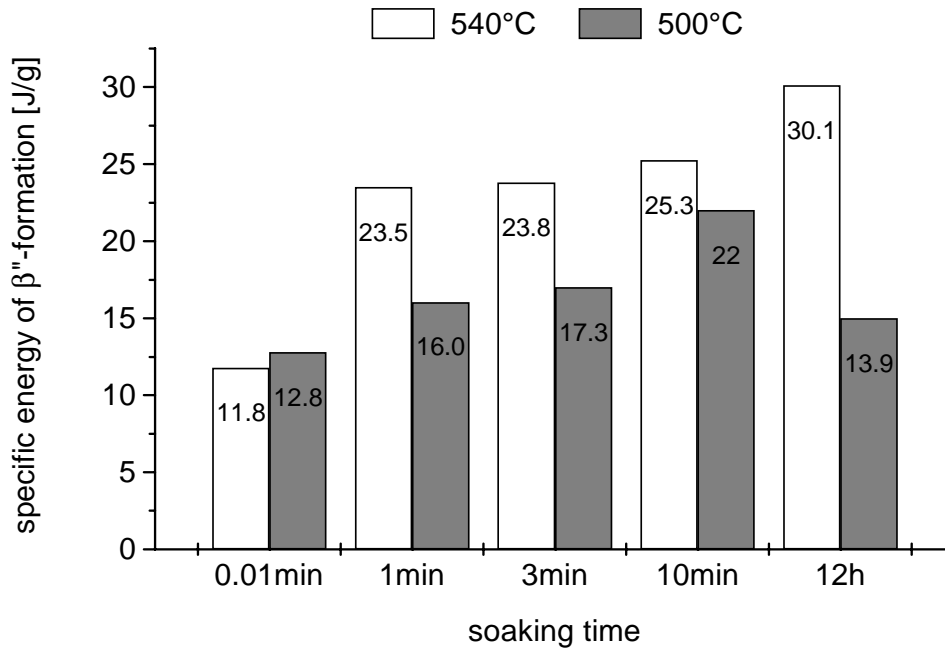
Figure 7.30: Specific energy of formation of GPII (β″) - zones after various soaking times at 500°C and 540°C, respectively, for A356.

7.4.2.3 DISCUSSION

The values for specific energy of β″ formation for A356 at 540°C reveal that most of the Mg diffusion occurs within the first minutes. From 0.01 minutes to 1 minute the energy of β″ formation is doubled. Up to 10 minutes of soaking time the values for β″ formation remain more or less constant. It is important to note that when the soaking time is dramatically increased from 10 minutes to 12 hours, the energy of β″ formation is only slightly increased from 25J/g to 30J/g. GP-II zones act as barriers for dislocations. According to Equation (2-4) the force to bypass the particles is proportional to the cubic root of the particles' volume fraction. As the volume fraction of formed particles is assumed to be proportional to the energy of formation, a comparison between the increase of yield strength from T6x3 to T6 and the increase of energy of formation from 3 minutes to 12 h at 540°C can be written as follows:

$$\frac{YS_{T6x3}}{YS_{T6}} = \sqrt[3]{\frac{E_{f,\,3min}}{E_{f,\,12h}}} \, . \tag{7-2}$$

Inserting 229 MPa for YS_{T6x3}, 260 MPa for YS_{T6}, 23.8 J/g for $E_{f,3min}$ and 30.1 J/g for $E_{f,12h}$, Equation (7-2) yields ~0.9 for both sides. Thus, the observed increase of yield strength from T6x3 to T6 of ~10% is in good accordance with the measured increase of formation energy of β'' particles.

At 500°C the diffusion processes are slower than at 540°C. Therefore the values for energy of formation of β'' particles are lower than corresponding values at 540°C up to 10 minutes of soaking time. At first sight the same amount of β'' particles after 12 h of soaking time was expected for A356 at 500°C and 540°C, respectively. From the pseudo-binary section of AlSi7Mg in Figure 3.3 can be deduced that the solubility of Mg for A356(AlSi7Mg0.3) at 500 and 540°C is ~0.3 wt%. However, it is surprising that after 12h at 500°C a significant lower value of energy formation is observed. One reason for that might be the enhanced formation of Mg and Fe containing $\pi(FeMg_3Si_6Al_8)$phase at 500°C in equilibrium condition while the amount of β-FeSiAl$_5$ phase is concurrently reduced (Table 7.3).

Table 7.3: Equilibrium calculation for iron containing intermetallic compounds in AlSi7Mg0.3Fe0.15 [wt %].

Temperature	Mg in α_{Al}	π-phase	β-phase
500°C	0.15	1.19	0.034
540°C	0.23	0.68	0.21

As a consequence of enhanced π-phase formation at 500°C in equilibrium, less Mg can be dissolved in the aluminum matrix at 500°C and therefore less Mg$_2$Si can be precipitated when the alloy is artificially aged.

7.5 SUMMARY OF SST

A new short heat treatment process, Silicon Spheroidization Treatment (SST), for modified Al-Si alloys was developed. SST spheroidizes the eutectic silicon within minutes between 500°C and 540°C. The effect of SST on the mechanical properties was tested on different thixoformed Al-Si-Mg components. The ductility was outstanding, maximum values of 18% fracture elongation and 230 MPa YS were obtained after 3 minutes of SST. Despite of the short SST annealing time the SST YS-level was very close to the T6 YS-level for A356. Figure 7.31 summarizes the values for yield strength and fracture elongation of thixoformed A356 and A357 in conventional and SST conditions. It can be clearly
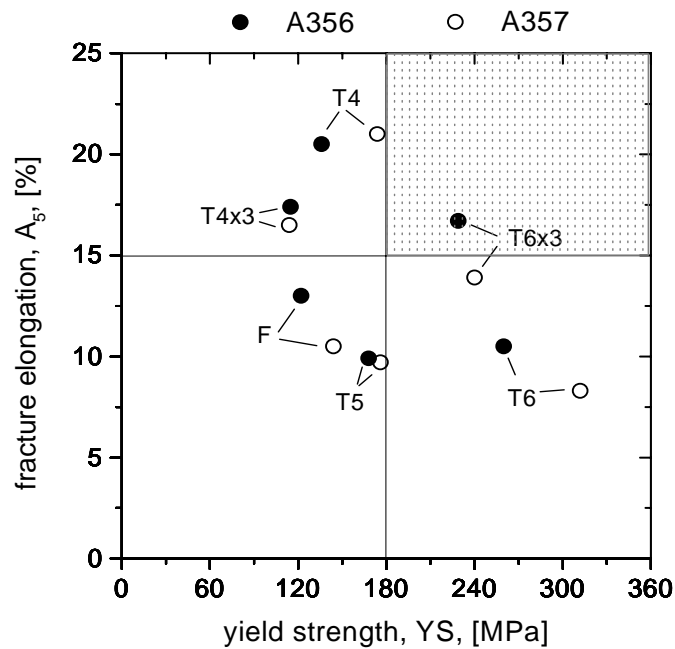
Figure 7.31: Fracture elongation to yield strength diagram for thixoformed A356 and A357 for various heat treatments. Note, that the margin of A=15% and YS=180 MPa can be crossed by newly developed Silicon Spheroidization Treatment (SST).

seen, that a high ductile state cannot be reached without any high temperature treatment (T5). Speroidized silicon seems to be a prerequisite for high ductility. The new SST condition T6x3 (3min at 540°C + 4h/160°C) is therefore a serious candidate for various safety components to satisfy these particular demands of the automotive industry.

Investigations of dynamic mechanical properties of thixoformed A356 revealed that T6x3 specimens have a higher endurance of life compared to specimens which are conventionally T6 treated.

The impact energy values of thixoformed A356 and A357 in T6x3 were significantly higher compared to T6. Best results were obtained when the specimens were quenched in air.

DSC experiments of A356 specimens after different soaking times at 500°C and 540°C were carried out. The energy of formation of β'' particles was calculated for each tested specimen. It was found that most part of Mg diffusion is completed after minutes of soaking time at 540°C for A356.

While the spheroidization which is responsible for excellent ductility occurs already at a temperature T > 500°C, a metal temperature of 540°C is essential for SST to maximize the yield strength.

8
APPLICATION OF SST

The conventional T6 solution heat treatment is expensive itself and causes subsequent process stages like straightening or X-ray control. The T6 solution treatment is the most expensive part of the post fabrication treatments as can be seen in Figure 8.1. By applying the Silicon Spheroidization Treatment instead of conventional T6 solution heat treatment, the effective soaking time and therefore costs can be dramatically reduced. As a consequence less warping and blistering is observed which also leads to cost savings. Therefore SST might be a substitute for conventional T6 heat treatment when good strength and high ductility are desired.
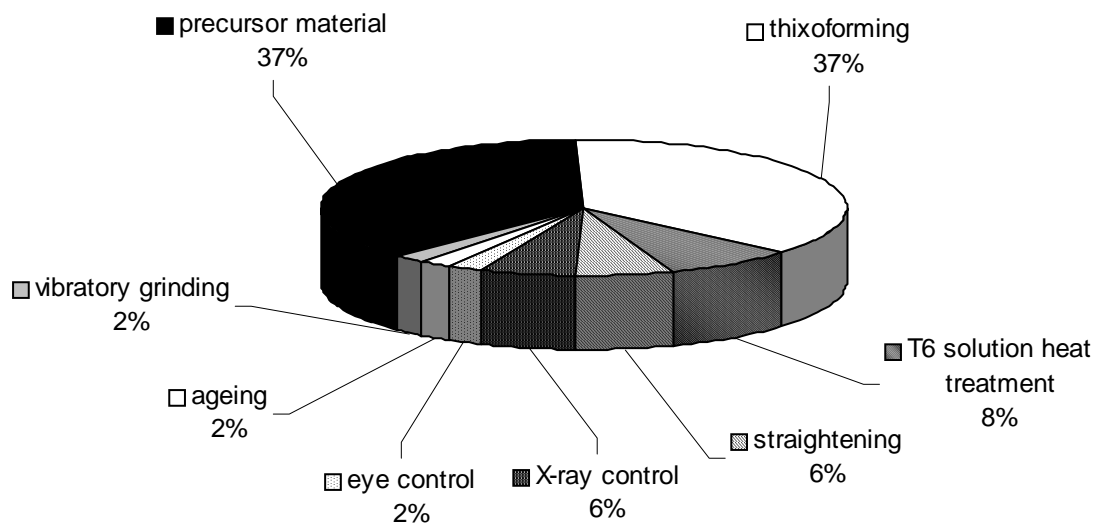
Figure 8.1: Cost splitting of different process stages for conventional thixoforming [WEN01].

8.1 SIMULATION OF THE HEATING PROCESS OF SST

The application of a short high temperature heat treatment to components with different wall thicknesses might be difficult. A light weight aluminum rim of A356 (Fig. 8.2) which is usually T6 heat treated was used to calculate the temperature distribution during SST. The wall thickness varies from 2 mm at the bead to 20 mm in the hub. A successful SST application requires a temperature of $T_{sphero} > 500°C$ (see Chapter 7.5). The effective time of a successful Silicon Spheroidization Treatment can therefore be divided into the time which is necessary to heat up the coldest spot of the component between 500°C and 540°C and the effective spheroidization time (Equation 8-1).

$$t_{SST} = t_{heating(500°C < T < 540°C)} + t_{spheroidization} \qquad (8\text{-}1)$$

In order to obtain a homogenous silicon spheroidization, it is desired that the temperature difference between the coldest and the hottest spot is as small as possible at any time.

.
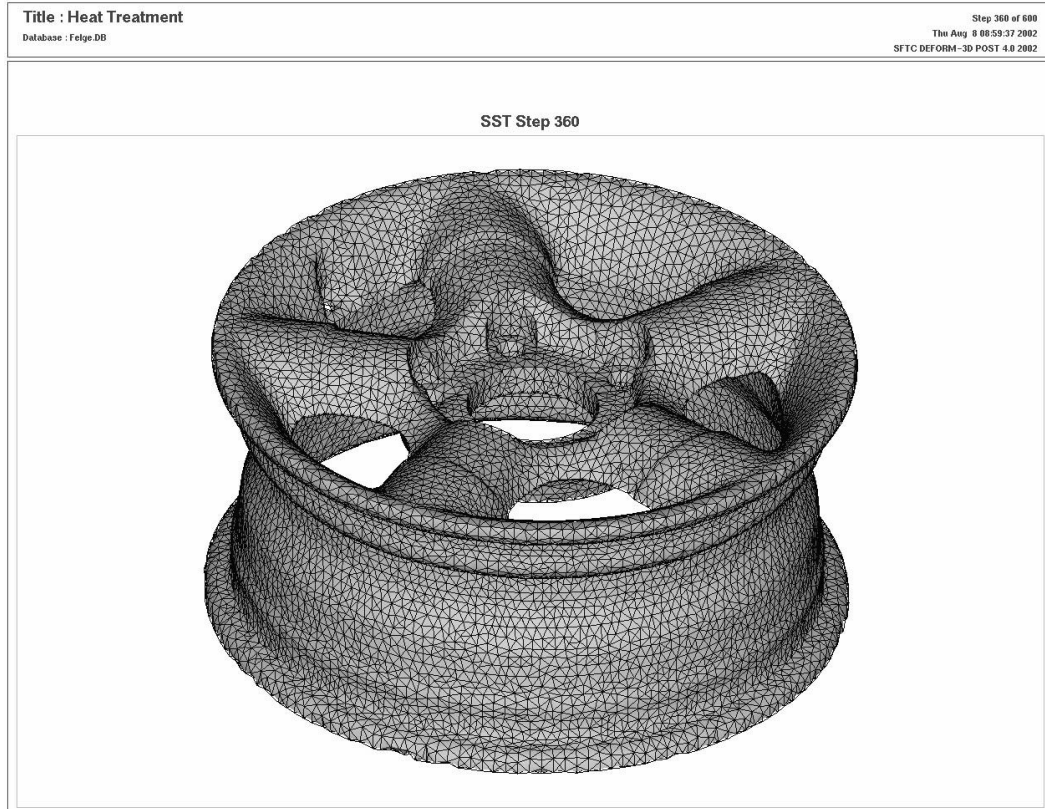
Figure 8.2: FEM simulated geometry of a light weight aluminum rim (A356).

8.1.1 EXPERIMENTAL PROCEDURE AND RESULTS

Specimens of thixoformed A356 with wall thicknesses of 3mm, 10mm and 20mm, respectively, were placed in a furnace heated up to 540°C. The temperature-time profile was recorded and can be seen in Figure 8.3. These experiments were used to determine unknown parameters needed for numeric simulation, i.e. the emissivity ε of the material and the heat transfer coefficient h to the furnace atmosphere. The simulation was performed with the commercial simulation software tool *DEFORM-3D*. Based on the finite element method it can simulate the complex behaviour of material flow and die fill as well as heat transfer problems between and within objects [DEF@]. The heat transfer cannot be only analyzed as a integral part of a deformation simulation but can also performed as a standalone process. After several iterations of the calibration simulations, most realistic results were obtained with an emissivity of $\varepsilon = 0.3$ and a heat transfer coefficient of $h = 40 \ W/m^2K$ (Fig. 8.3).
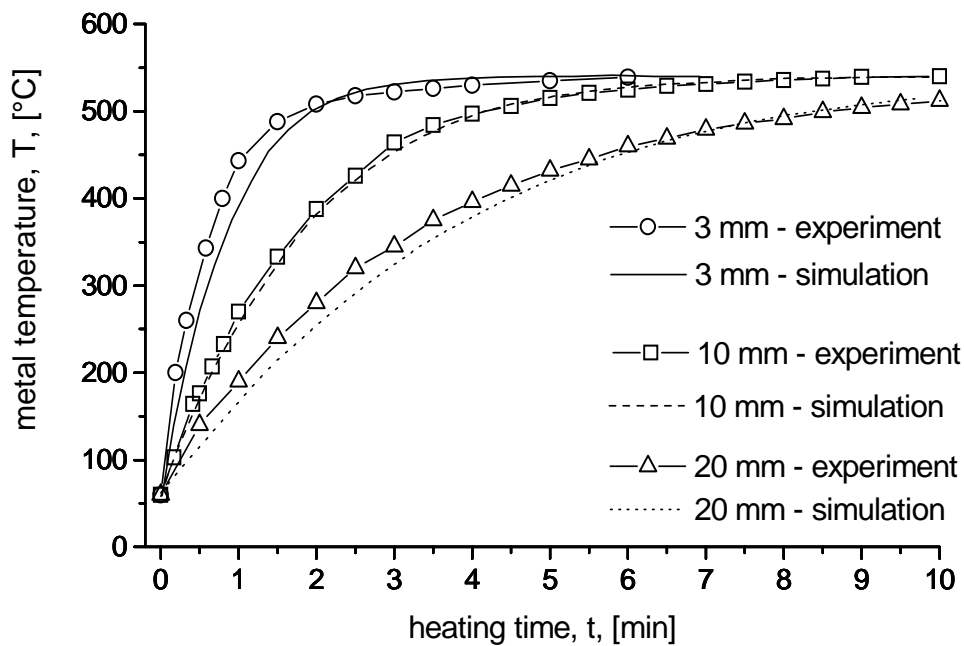
Figure 8.3: Calibration of the heat transfer at a furnace temperature of 540°C.

The temperature profile of the rim was calculated with a thermal conductivity of $k = 167 \ W/mK$ and a specific heat capacity of $cp = 0.963 \ J/gK$ [MAT@] for a furnace atmosphere of 540°C. The temperature distribution after 6 minutes of soaking time at 540°C is illustrated in Figure 8.4. It can be seen that after such a short soaking time the
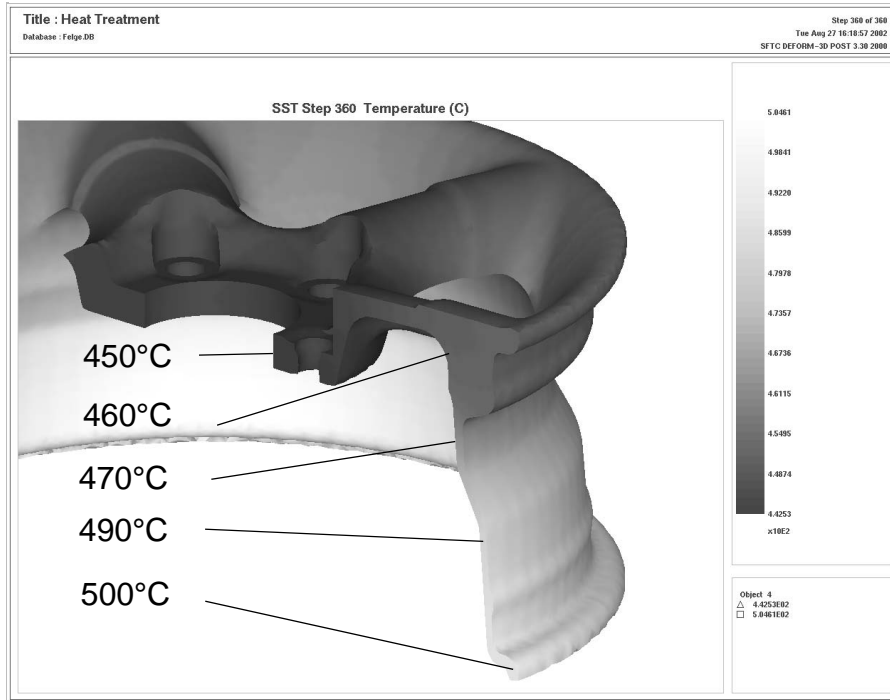
Figure 8.4: Temperature distribution in the rim after 6 min of soaking time at 540°C.
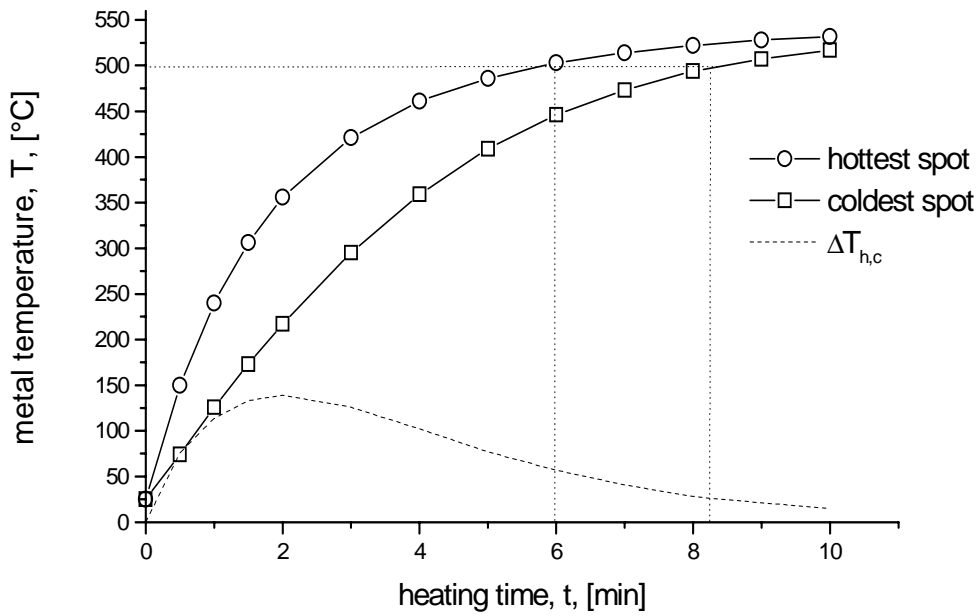
Figure 8.5: Simulated temperature evolution of the hottest and coldest spot, respectively, in the A356 rim.

temperature in the bead of the rim exceeds already 500°C, a temperature which is desired for successful SST. Naturally, the coldest area (~450°C) can be found in the rim's hub which is the thickest part of the rim (20 mm). Figure 8.5 shows the evolution of the temperature of the hottest and coldest spot, respectively. The hottest spot in the rim reaches 500°C after 6 minutes of soaking time whereas the coldest spot needs ~8 minutes to match the same temperature. The small temperature difference between the hottest and the coldest spot, $\Delta T_{h,c}$, after 10 minutes of soaking time indicates a sufficient homogeneous temperature distribution for SST. According to Equation (8-1), the heating time for advantageous SST can be indicated to less than 10 minutes for a component with considerable variations of wall thickness. The total process time for SST is therefore less than 15 minutes but might vary depending on the size and geometry of the particular component. It is important to note that the simulation was performed without the assumption of forced convection. Thus, the effective time for SST may be even shorter because of the enhanced heat transfer at forced convection in convection furnaces.

8.2 SST APPLICATION EXAMPLES

8.2.1 THIXOCOMPONENT REAR DOOR HINGE (A357)

SST was applied to a A357 rear door hinge (Fig. 8.6) of the Audi A2 in industrial environment at THIXALLOY® Components GmbH & Co KG in Lend, Austria. The particular requests for this component are: very high strength and elongation, surface quality and no machining before assembling. The rear door hinge is shot in 8 cavities with a shot
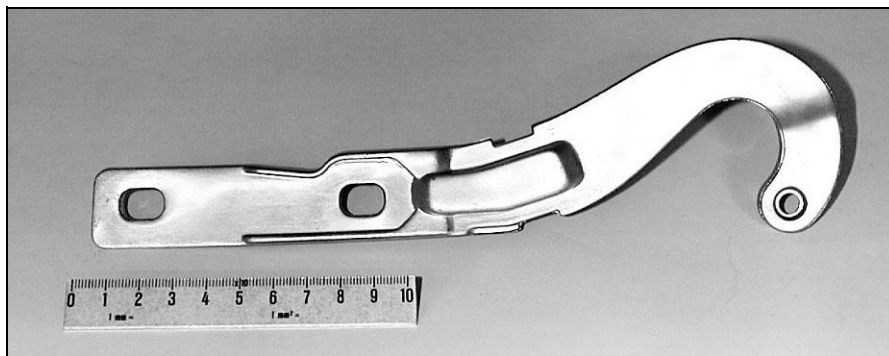
Figure 8.6: Thixocomponent rear door hinge (Audi A2), A357 (THIXALLOY 650).

weight of 2.8 kg. It has wall thicknesses from 2 mm to 20 mm, a part weight of 0.17 kg and a total length of 245 mm [WEN00]. The components were placed in a furnace which was preheated to ~530°C. One component was equipped with a thermocouple in order to measure the metal temperature. The metal temperature reached 520°C after ~15min. After 3 additional minutes of SST the components were water quenched and artificially aged for 4h at 160°C.

The static mechanical properties of specimens of the rear door hinge are illustrated in Figure 8.7. Due to SST, the fracture elongation is doubled from conventional T5 and T6 treatment to newly developed SST condition T6x3. The yield strength level is significantly increased from T5 (170 MPa) to T6x3 (245 MPa) and comes close to T6 level (270 MPa). Considering that the diffusion time of Mg in α-aluminum is much longer in A357 than in A356 (see Table 7.2), the SST yield strength level is a very good value compared to the T6 value after a 12h solution treatment at 530°C. However, the yield strength after SST might be improved if the furnace temperature was increased up to 540°C.
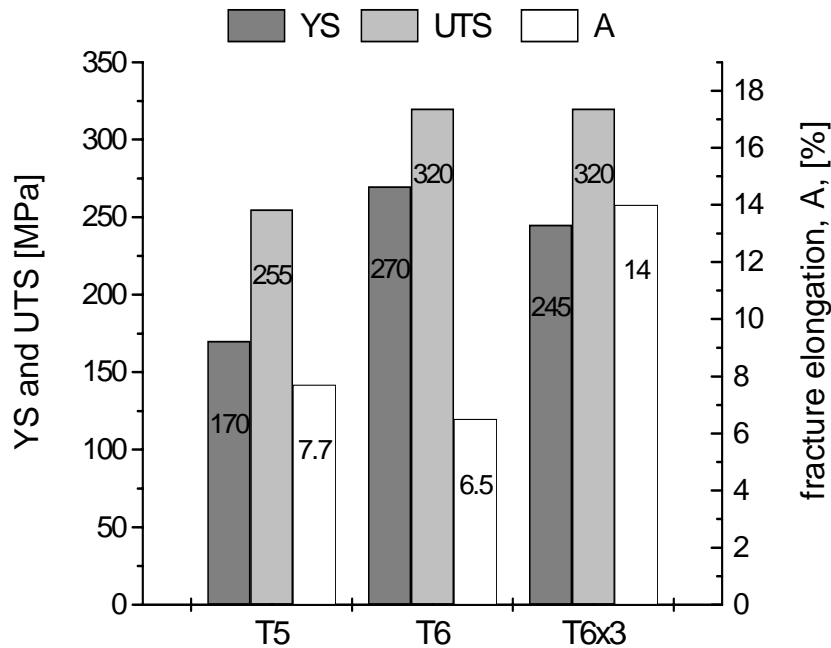
Figure 8.7: Mechanical properties of the A357 rear door hinge of the Audi A2 after SST (T6x3) in comparison to T5 (F+4h/160°C) and conventional T6 (12h/530°C + 4h/160°C) condition.

8.3 SST FOR VARIOUS ALLOYS

SST effectuates the spheroidization of the eutectic silicon. The spheroidization process can be accelerated if the eutectic silicon is modified. The application of SST is not limited to AlSiMg alloys. As a matter of principle it can be applied to all alloys containing aluminum-silicon eutectic. The following experiments intend to demonstrate the application of SST to common representatives of hypoeutectic-, eutectic and hypereutectic aluminum-silicon alloys.

8.3.1 HYPOEUTECTIC Al-Si ALLOYS

AlSi9Cu3 is a very frequently employed die-casting alloy. It is used in almost all fields of pressure die casting, especially in the fabrication of pumps, engine housings and gearings [WAB02].The microstructure of the unmodified as-cast condition is given in Figure 8.8. If
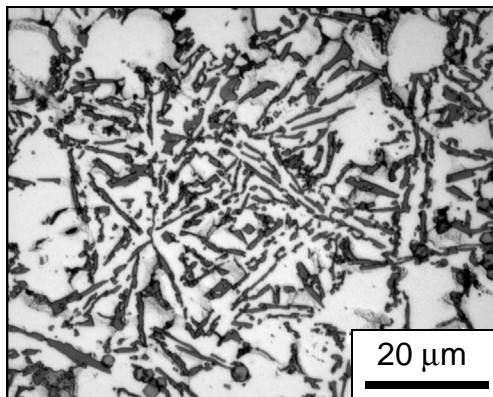
Figure 8.8: Micrograph of unmodified AlSi9Cu3, as-cast.
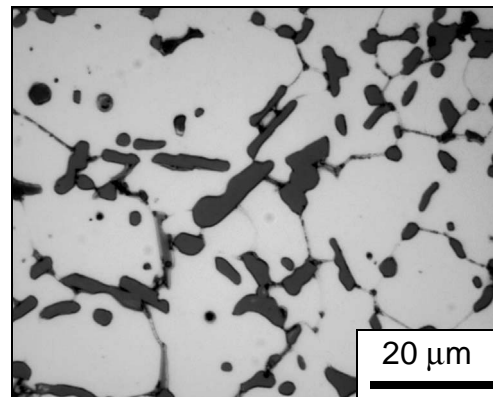
Figure 8.9: Micrograph of unmodified AlSi9Cu3, SST (3min/540°C).
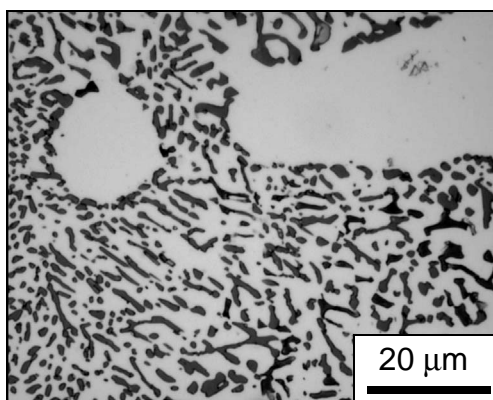
Figure 8.10: Micrograph of Sr-modified AlSi9Cu3, as-cast.
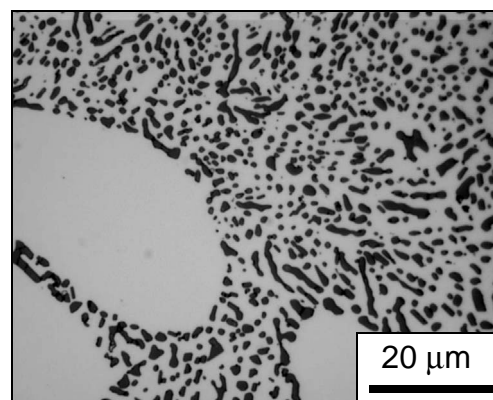
Figure 8.11: Micrograph of Sr-modified AlSi9Cu3, SST (3min/540°C).

the unmodified alloy is treated with SST, small silicon fragments spheroidize whereas the big silicon needles are preserved (Fig. 8.9). The same material modified with ~300ppm strontium shows a fine fibrous Al-Si eutectic (Fig. 8.10) which is totally spheroidized after 3 minutes of SST (Fig. 8.11).

8.3.2 EUTECTIC Al-Si ALLOYS

Alloy AlSi12 is notable for its very good castability and excellent weldability, which are due to its eutectic composition and low melting point. It combines moderate strength with relatively high fracture elongation and good corrosion resistance. The alloy is particularly suitable for intricate, thin walled, leak-proof, fatigue resistant castings [ALU98].
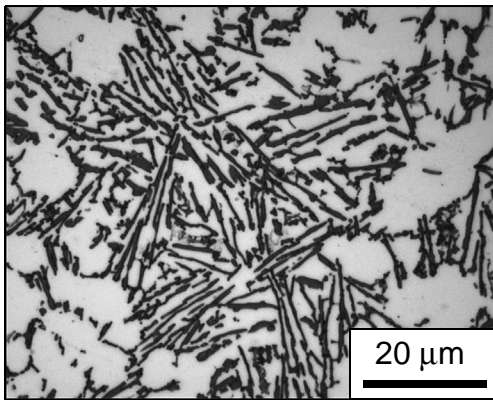
Figure 8.12: Micrograph of unmodified AlSi12, as-cast.
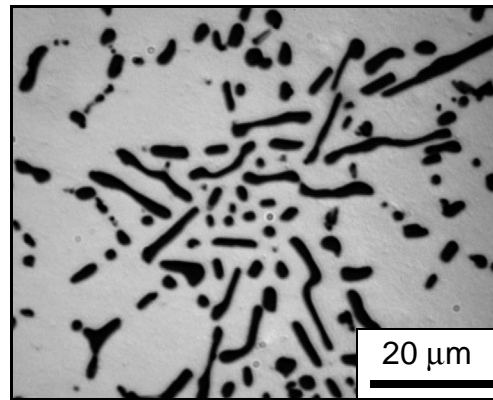
Figure 8.13: Micrograph of unmodified AlSi12, SST (3min/540°C).
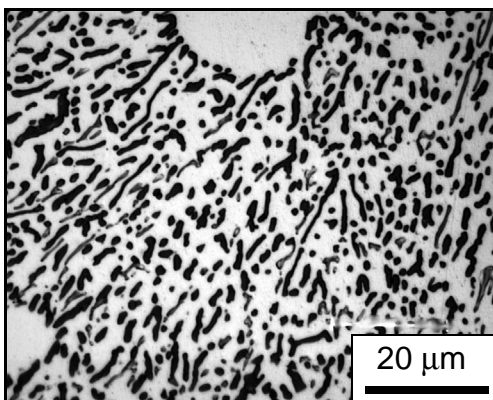
Figure 8.14: Micrograph of Sr-modified AlSi12, as-cast.
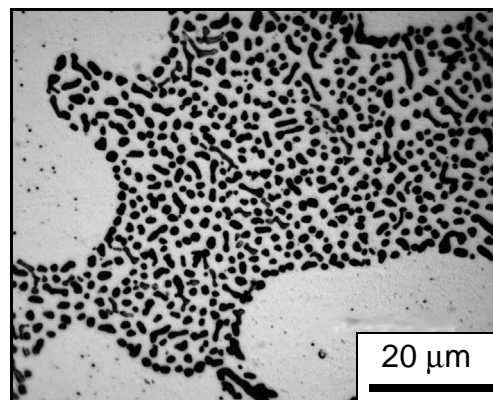
Figure 8.15: Micrograph of Sr-modified AlSi12, SST (3min/540°C).

The influence of Sr-modification on the microstructural evolution of the Al-Si eutectic during SST (Fig. 8.12-Fig. 8.15) is analogue to the results of hypoeutectic AlSi9Cu3.

8.3.3 HYPEREUTECTIC Al-Si ALLOYS

Hypereutectic aluminum silicon alloys are used in the automotive industry and other applications where good wear behaviour is necessary [VAL96]. Especially the alloy AlSi17Cu4 (A390) can be used for engine components like cylinder liners, pistons, connecting rods, oil pump gear wheels and control pistons for water- and oil pumps, respectively [HUM99].
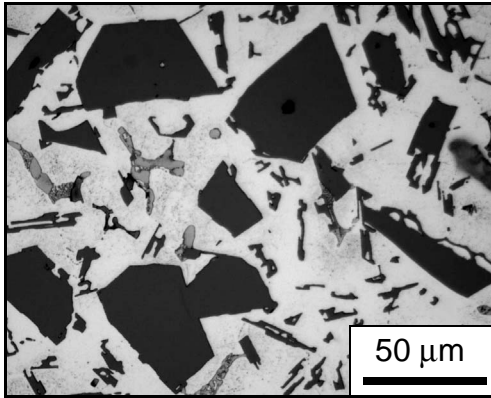
Figure 8.16: Micrograph of unmodified AlSi17Cu4, as-cast.
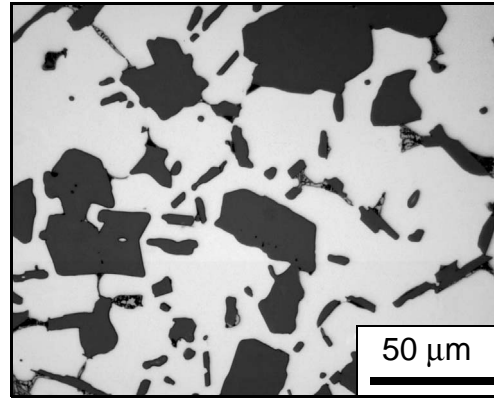
Figure 8.17: Micrograph of unmodified AlSi17Cu4, SST (3min/540°C).

Due to SST, the eutectic silicon is partly spheroidized and the sharp edges of the big polyhedral primary silicon (Fig. 8.16) are clearly smoothed in Figure 8.17. This might lead to an increase of wear resistance performance which was reported for a zinc-aluminum alloy reinforced by spheroidal silicon phase in [ZHA98].

8.3.4 ALLOY AlMg5.5Si2 (MAGSIMAL59)

The influence of a short high temperature treatment on the eutectic system Al-Mg$_2$Si was investigated. Small specimens of Magsimal59 were heated up to 580°C, soaked for 3 minutes and quenched. The microstructure in as-cast condition can be seen in Figure 8.18. After application of SST the morphology of eutectic Mg$_2$Si does not seem to be significantly altered which is illustrated in Figure 8.19. However, a possible positive influence of SST on the mechanical properties of Magsimal59 remains to be tested.
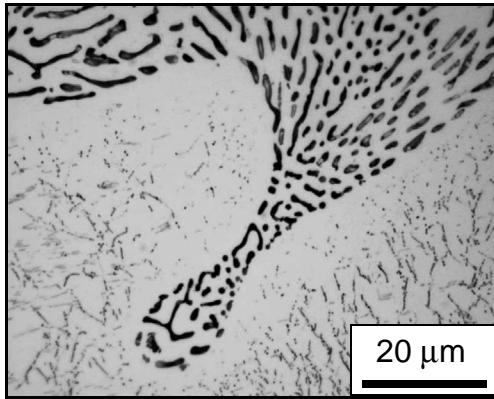
Figure 8.18: Micrograph of Magsimal59 in as-cast condition.
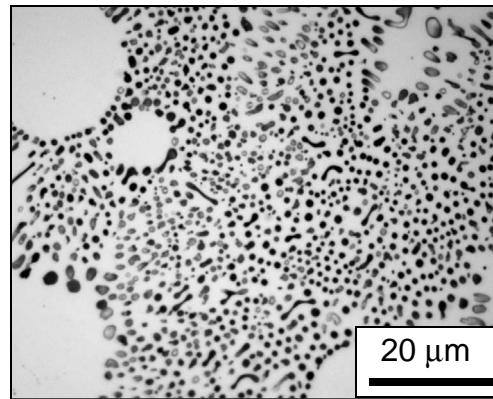
Figure 8.19: Micrograph of Magsimal59 in T6x3 (3min/580°C) condition.

8.4 SUMMARY

FEM simulation of the heating process has indicated that SST is possible for components with variable wall thicknesses. The heating time for reaching the starting temperature of 500°C for most effective SST was calculated to 8 minutes in a furnace atmosphere of 540°C for an aluminum rim with wall thicknesses ranging from 2mm to 20mm.

SST was applied to a thixocomponent in industrial environment at THIXALLOY® Components GmbH & Co KG in Lend, Austria. The mechanical properties of SST application in comparison to conventional T5 and T6 treatment were measured of this particular component. As a result the fracture elongation in T6x3 (SST) was more than doubled in comparison to conventional T6 condition.

SST was also applied to various alloys containing Al-Si eutectic phase. It seems that SST can be applied to hypoeutectic- as well as to eutectic- and even hypereutectic alloys. However, proper modification of the Al-Si eutectic in as-cast condition is a prerequisite for successful SST.

The benefits of SST are summarized in Table 8.1. It seems that SST can act as a substitute for conventional expensive T6 heat treatment for a broad spectrum of components. An application of SST can especially be recommended when highest ductility with moderate strength is required. Due to excellent ductility after SST its application for safety compo-

Table 8.1: Benefits of Silicon Spheroidization Treatment (SST).

Characteristics	Potential benefit or application
Very short high temperature heat treatment (SST)	- Time saving in comparison to T6 - Cost reduction in comparison to T6 - No gravity warping - Less straightening - Less surface oxidation - Can be realized in a continuous furnace
Less blistering	- Can be combined with various forming processes
Can be integrated in existing process sequences	- Time and cost reduction

nents in the transport industry seems to be possible. SST can be integrated in existing industrial process sequences. It can be applied to components fabricated by various conventional forming techniques like squeeze casting or die pressure casting. However, SST seems to work best with low porosity thixoformed components. SST has been patented by SAG-AG.

9
CONCLUSIONS

Ductility of Al-Si cast alloys is the crucial value to meet the requirements for many applications. The ductility of Al-Si cast alloys is highly determined by the morphology of the brittle eutectic silicon. It can be improved either by means of modifying agents like Sr or Na or by spheroidization of silicon.

The development of new Al-Si-Mg alloys for semi-solid forming has shown that the fracture elongation values are limited when no solution heat treatment is applied before ageing (T5). During the T6 solution heat treatment, the eutectic silicon spheroidizes which is responsible for good fracture elongation values in high strength T6 condition. Thus, a high temperature heat treatment seems to be unavoidable to attain high ductility (A > 15%) at elevated strength level (YS > 180 MPa) which are the demands of the automotive industry for light metal safety components.

It has been shown that the determining spheroidization process of eutectic silicon is completed within minutes of soaking time at 540°C in case of well modified eutectic in as-cast condition. The influence of this Silicon Spheroidization Treatment (SST) on the mechanical properties is outstanding.

Table 9.1: Static mechanical properties of AlSi6Mg0.8 in T5 and A356 in T6 and T6x3 (SST) condition, respectively.

Alloy	Condition	YS [MPa]	UTS [MPa]	A [%]	time for solution heat treatment at 540°C
AlSi6Mg0.8	T5	195	281	7.8	0 min
AlSi7Mg0.3	T6x3	229	317	16.7	3 min
AlSi7Mg0.3	T6	260	320	10.6	12 h

The static mechanical properties of AlSi6Mg0.8 in T5 and A356 in T6 and newly developed T6x3 conditions are summarized in Table 9.1.

The life of endurance benefits substantially from the very small spheroidized silicon particles which is reflected by the increased fatigue strength, σ_f, after SST (T6x3) in comparison to T6. The positive influence of SST on the dynamic mechanical properties of A356 can be seen in Table 9.2.

Table 9.2: Influence of SST on dynamic mechanical properties of A356.

Alloy	Condition	YS [MPa]	σ_f [MPa]	time for solution heat treatment at 540°C
A356	T6	260	180-190	12h
A356	T6x3	230	200-210	3min

The spheroidization process of eutectic silicon was successfully described by a dynamic analytic model. The modified eutectic silicon was approximated by small cylinders with fluctuating disturbances of their diameter. It has been shown that the spheroidization rate is highly dependent from the radius of the original cylinder, i.e. the degree of modification. By consideration of the specific diffusion problem at the Si-Al interface, the calculated spheroidization times for various temperatures were in good accordance with observed values as can be seen in Table 9.3.

Table 9.3: Comparison between calculated and experimentally observed spheroidization times of modified eutectic silicon with an original radius of $\rho = 0.15~\mu m$.

Temperature [°C]	$\tau_{calculated}$ [min]	$\tau_{experiment}$ [min]
540	2.4	2-3
500	3.88	3-5
450	8.08	~10
400	18.88	~20

FEM simulation of the SST heating process of a component with variable wall thicknesses has shown that the total process time for SST is somewhere between 10 and 15 minutes in a conventional convection furnace. Successful application of SST on thixoformed components has been already carried out in industrial environment. Apart from the enormous gain of ductility the potential economic savings of SST are also considerable since the costs of conventional solution heat treatment are typically around 11-22 cent/kg [APE90]. SST has been patented by SAG-AG and further industrial implementation and application of SST are currently the subjects of several studies and trials including various components and alloys.

9 Conclusions

10
APPENDIX

Table 10.1: Static mechanical properties of thixoformed alloys AlSi7Mg0.3, AlSi7Mg0.5 and AlSi7Mg0.8 in various temper conditions.

Alloy	Condition	YS [MPa]			UTS [MPa]			A [%]		
	F	122	±	3	246	±	4	13.0	±	1.6
	T4	138	±	3	265	±	4	20.5	±	5.5
	T4x3	115	±	10	232	±	19	17.4	±	1.9
AlSi7Mg0.3	T5	168	±	4	266	±	5	9.9	±	1.9
	T6	260	±	5	320	±	4	10.6	±	3.5
	T6x3	229	±	5	317	±	4	16.7	±	1.1
	F	144	±	4	256	±	6	10.4	±	2.4
	T4	174	±	3	301	±	3	21	±	1.1
	T4x3	114	±	7	232	±	14	16.5	±	2
AlSi7Mg0.5	T5	176	±	5	272	±	6	9.3	±	1.6
	T6	312	±	15	358	±	8	9.1	±	1.5
	T6x3	240	±	10	325	±	10	13.9	±	3.8
	F	160	±	2	263	±	9	8.3	±	3.4
	T4x3	118	±	24	207	±	11	9.7	±	2.8
AlSi7Mg0.8	T5	197	±	6	287	±	9	6.8	±	1.3
	T6	323	±	12	367	±	5	7.6	±	1.4
	T6x3	265	±	4	346	±	1	10.1	±	3.5

Table 10.2: Static mechanical properties of thixoformed alloys AlSi6Mg0.8 and AlSi5Mg0.8 in various temper conditions.

Alloy	Condition	YS [MPa]			UTS [MPa]			A [%]		
AlSi6Mg0.8	F	160	±	2	262	±	3	10.2	±	2.4
	T4x3	126	±	22	246	±	32	15.2	±	0.6
	T5	195	±	3	281	±	3	7.8	±	1.4
	T6	319	±	9	353	±	3	6.5	±	3.3
	T6x3	251	±	4	329	±	5	8.9	±	1.0
AlSi5Mg0.8	F	155	±	4	251	±	5	10.1	±	2
	T4x3	117	±	19	232	±	32	16	±	1.9
	T5	190	±	4	271	±	3	7.5	±	1.6
	T6	314	±	11	353	±	5	8.7	±	1.7
	T6x3	241	±	18	316	±	17	9.5	±	1.3

Table 10.3: Static mechanical properties of thixoformed alloys AlSi5Mg0.8Mn0.4 and AlSi5Mg0.8Mn0.8 in various temper conditions.

Alloy	Condition	YS [MPa]			UTS [MPa]			A [%]		
AlSi5Mg0.8Mn0.4	F	157	±	3	262	±	4	10.6	±	1.6
	T4x3	132	±	20	252	±	21	14.9	±	3.9
	T5	184	±	7	269	±	9	6.9	±	1.7
	T6	323	±	18	367	±	8	7.6	±	2.1
	T6x3	253	±	10	327	±	15	7.4	±	2.6
AlSi5Mg0.8Mn0.8	F	155	±	6	257	±	5	9.9	±	2.2
	T4x3	136	±	11	260	±	12	14	±	1.9
	T5	184	±	5	264	±	11	6.6	±	2.0
	T6	324	±	8	359	±	10	4.9	±	2.4
	T6x3	256	±	1	329	±	1	6.7	±	0.2

Table 10.4: Static mechanical properties of thixoformed alloys AlSi5Mg1.75, AlSi5Mg1.75Mn0.6Sr and AlSi5Mg1.75Mn0.6Ba in various temper conditions.

Alloy	Condition	YS [MPa]			UTS [MPa]			A [%]		
AlSi5Mg1.75	F	212	±	4	267	±	3	3.5	±	0.7
	T4x3	137	±	19	256	±	18	12.5	±	2.3
	T5	256	±	5	294	±	9	2.5	±	0.5
	T6	292	±	17	331	±	11	5.3	±	1.7
	T6x3	242	±	8	303	±	16	5.1	±	1.2
AlSi5Mg1.75 Mn0.6Sr	F	228	±	8	283	±	11	3.1	±	0.7
	T4x3	135	±	33	252	±	37	11.2	±	2.9
	T5	255	±	8	287	±	15	2.4	±	1.0
	T6	318	±	7	335	±	19	3.3	±	1.5
	T6x3	255	±	12	318	±	16	4.6	±	1.3
AlSi5Mg1.75 Mn0.6Ba8	F	218	±	5	287	±	15	5.3	±	1.7
	T4x3	124	±	17	245	±	23	14.9	±	1.4
	T5	246	±	7	305	±	8	5.0	±	1.2
	T6	324	±	9	357	±	9	6.3	±	2.6
	T6x3	248	±	5	326	±	9	8.9	±	2.3

10 Appendix

11
REFERENCES

[ABD98]   ABDOLLAHI A. and GRUZLESKI J.E.: *An evaluation of calcium as a eutectic modifier in A357 alloy,* Int. J. Cast Metals Res., 11, 1998, 145-155.

[ALT98]   ALTENPOHL D.G.: *Aluminium: Technology, Applications, and Environment,* The Aluminum Assiciation, Inc.,TMS, 1998.

[ALU95]   ALUMINIUM TASCHENBUCH, Aluminium-Verlag Düsseldorf, 1995, 229.

[ALU98]   THE ALUMINUM ASSOSIATION: *Aluminum Alloy: Selection and Applications,* The Aluminum Assosiation, Inc., Washington DC, USA, 1998.

[APE90]   APELIAN D., SHIVKUMAR S. and SIGWORTH G.: *Fundamental Aspects of Heat Treatment of Cast Al-Si-Mg Alloys*, AFS Transactions, 97, 1990, 727-742.

[ASM88]   ASM Metals Handbook Ninth Edition, Volume 15, *Casting*, ASM International, 1988.

[BAC83]   BACH F.-W., HAFERKAMP H. and LI B.: *Einfluss von Lanthan auf die mechanischen Eigenschaften und die Mikrostruktur der hochfesten Aluminium-Silizium-Magnesium-Legierung G-AlSi7Mg,* Metall, 37, (12) 1983, 1202-1208.

[BEN00]   EL-BENAWY T. and FREDRIKSSON H.: *Solidification Mechanism of Unmodified and Strontium Modified Al-Si Alloys,* Materials Transactions, 41, (4) 2000, 507-515.

[BIC98]   BICKFORD K.: *Fluidized Bed Heat Treating and Decoring of Aluminum Castings - A New Technology Advance,* Proc. 1st Int. Automotive Heat Treating Conf., Puerto Vallata, Mexico, 13-15 July, 1998, 385-388.

[BLE01]   BLECK W.: *Formgebung metallischer Werkstoffe im teilerstarrten Zustand und deren Eigenschaften, Projektbereich F, Werkstoff-/Bauteileigenschaften*, Arbeits- und Ergebnisbericht Sonderforschungsbereich 289, RWTH Aachen, 1999-2001, 625.

11 References

[CAC99]   CACERES C.H., DAVIDSON C.J., GRIFFITHS J.R. and WANG Q.G.: *The Effect of Mg on the Microstructure and Mechanical Behavior of Al-Si-Mg Casting Alloys,* Metallurgical and Materials Transactions A, 30A, (10) 1999, 2611-2618.

[CAH96]   CAHN R.W., HAASEN P. and KRAMER E.J.: *Materials Science and Technology, A Comprehensive Treatment, Volume 8, Structure and Properties of Nonferrous Alloys,* VCH Verlagsgesellschaft, Weinheim, 1996.

[CLO81]   CLOSSET B. and GRUZLESKI J.E.: *A Study on the Use of Pure Metallic Strontium in the Modification of Al-Si Alloys,* AFS Transactions, 89, 1981, 801-808.

[CLO82]   CLOSSET B. and GRUZLESKI J.E.: *Structure and Properties of Hypoeutectic Al-Si-Mg Alloys Modified with Pure Strontium,* Metallurgical Transactions A, 13A, (6) 1982, 945-951.

[DAH01]   DAHLE A.K.: *Heat Treatment of Aluminum Alloys*, Encyclopedia of Material Science and Technology, 3, (2) 2001, 1-3.

[DAV93]   DAVIS J.R. (edtr): *Aluminum and Aluminum Alloys*, ASM Specialty Handbook, ASM International® Materials Park, OH 440730002, USA, 1993.

[DEF@]   http://www.deform.com.

[DON00]   DONS A.L., PEDERSEN L. and BRUSETHAUG S.: *Modelling the microstructure of heat treated AlSi foundry alloys*, Aluminium, 76, (4) 2000, 294-297.

[EAA@]   EUROPEAN ALUMINIUM ASSOCIATION: *Aluminium in the Automotive Industry*, http://www.eaa.net.

[FAN02]   FAN Z.: *Semisolid metal processing,* International Materials Reviews, 47 (2), (4) 2002, 49-78.

[FLE00]   FLEMINGS M.C.: *SSM: Some thoughts on past milestones and on the path ahead*, Proc. 6th Int. Conf. on Semi-Solid Processing of Alloys and Components, Turin, Italy, Sept. 27-29, 2000, 11-14.

[FRA98]   FRANKE A.J. and KOCH H.: *Drei Jahre Erfahrungen mit eisenarmen Druckgusslegierungen, Giesserei-Praxis*, 2, 1998, 72-76.

[FUJ78]   FUJIKAWA S.-I., HIRANO K.-I. and FUKUSHIMA Y.: *Diffusion of Silicon in Aluminum,* Metall. Transactions A, 9A, (12) 1978, 1811-1815.

[FUN98]   FUNATANI K.: *Materials, Heat Treatment and Surface Modifications Applied for Automotive Components,* Proc. 1st Automotive Heat Treating Conf., Puerto Vallata, Mexico, 13-15 July, 1998, 283-290.

[GAB93]   GABATHULER J.-P., HUBER H.J. and ERLING J.: *Specific properties of produced parts using the thixocasting process,* Int. Conf. on „Aluminium Alloys: New Process Technologies", Marina di Ravenna, Italy, June 1993.

[GAR99]   GARAT M. and MAENNER L.: *Thixogiessen - Erweiterung der Legierungsreihen und Anwendungen*, Giesserei, 86, (5) 1999, 76-86.

[GLI00]   GLICKSMAN M.E.: *Diffusion in Solids: Field Theory, Solid-State Principles and Applications,* ISBN 0-471-23972-0, John Wiley & Sons Inc., New York, USA, 2000.

[GUI96]   GUINER A.: *On the Birth of GP Zones,* Proc. of 5th Int. Conf. on Aluminium Alloys, Grenoble, France, July 1-5, 1996, 3-6.

[GUL01]   GULLO G.-C.: *Thixotrope Formgebung von Leichtmetallen - Neue Legierungen und Konzepte,* Diss. ETH-Zürich, 2001.

[GUP95]   GUPTA A.K. and LLOYD D.J.: *Precipitation processes in long-term naturaly-aged AA6016 material,* Proc. Int. Symposium on Recent Metallurgical Advances in Light Metals Industries, August 20-24, Vancouver, British Columbia, 1995, 243-253.

[HAQ94]   HAQUE M.M.: *Effects of strontium on the structure and properties of aluminium-silicon alloys,* Journal of Materials Processing Technology, 55, 1995, 193-198.

[HAY65]   HAYDEN H.W., MOFFATT W.G. and WULFF J.: *The Structure and Properties of Materials,* Vol. 3: Mechanical Behavior, John Wiley & Sons, Inc., New York, 1965.

[HOG87]   HOGAN L.M. and SHAMSUZZOHA M.: *Crystallography of the Flake-Fibre Transition in the Al-Si Eutectic,* Metals Forum, 10 (4), 1987, 270-277.

[HÖG96]   HÖGERL J.: *Beeinflussung der Gefügemorphologie und der mechanischen Eigenschaften von AlSi7Mg-Legierungen,* Diss. TU München, Fortschr.-Ber. VDI Reihe 5 Nr. 457, VDI Verlag, Düsseldorf, 1996.

[HOR01]   HORNBOGEN E.: *Hundred years of precipitation hardening,* Journal of Light Metals, 1, 2001, 127-132.

[HUM99]   HUMMERT K., FRECH W. and SCHWAGEREIT M.: *Industriell hergestellte sprühkompaktierte Aluminiumlegierungen,* Metall, 53, (9) 1999, 496-500.

[JOE91]   JOENOES A. and GRUZLESKI J.E: *Magnesium Effects on the Microstructure of Unmodified and Modified Al-Si Alloys,* Cast Metals, 4 (2), 1991, 62-71.

11 References

[KAS93]   KASHYAP K.T., MURALI S., RAMAN K.S. and MURTHY K.S.S.: *Casting and heat treatment variables of Al-7Si-Mg alloy,* Materials Science and Technology, 9, (3) 1993, 189-203.

[KAU00]   KAUFMANN H., WABUSSEG H. and UGGOWITZER P.J.: *Metallurgical and Processing Aspects of the NRC Semi-Solid Casting Technology*, Aluminium, 76, (1/2) 2000, 70.

[KEE94]   KEEFFE M.E., UMBACH C.C. and BLAKELY J.M.: *Surface self-diffusion on Si from the evolution of periodic atomic step arrays, J. Phys. Chem. Solids, 55, (10) 1994, 965-973.*

[KIM63]   KIM C.B. and HEINE R.W.: *Fundamentals of Modification in the Aluminum-Silicon System,* Journal of the Institute of Metals, 92, 1963-64, 367-376.

[KNU01]   KNUUTINEN A., NOGITA K., McDONALD S.D. and DAHLE A.K.: *Modification of Al-Si alloys with Ba, Ca, Y and Yb,* Journal of Light Metals, 1, 2001, 229-240.

[KOC98]   KOCH H.: *Use of an aluminium alloy for pressure die casting*, EP0853133, Rheinfelden Aluminium GmbH, 1998.

[KUC72]   KUCZYNSKI G.C.: *Sintering and Related Phenomena,* Proc. of the Third Int. Conf. on Sintering and Related Phenomena, University of Notre Dame, Notre Dame, Indiana, USA, June 5-7, 1972,

[KUR86]   KURZ W. and FISHER D.J.: *Fundamentals of Solidification,* Trans Tech Publications LTD, Switzerland, 1986.

[LI 97]   LI S., ZHAO S., PAN M., ZHAO D., CHEN X., BARABASH O.M. and BARABASH R.I.: *Solidification and Structural Characteristics of $\alpha(Al)$-Mg_2Si Eutectic,* Materials Transactions, JIM, 38 (6), 1997, 553-559.

[LU85]   LU S.-Z. and HELLAWELL A.: *Growth mechanism of Silicon in Al-Si Alloys,* Journal of Crystal Growth, 73, 1985, 316-328.

[LU 87]   LU S.-Z. and HELLAWELL A.: *The Mechanism of Silicon Modification in Aluminum-Silicon Alloys: Impurity Induced Twinning,* Metallurgical Transactions A, 18A, (10) 1987, 1721-1733.

[MAK01]   MAKHLOUF M.M. and GUTHY H.V.: *The aluminum-silicon eutectic reaction: mechanisms and crystallography*, Journal of Light Metals, 1, 2001, 199-218.

[MAR70]   MARICH S.: *Structural Stability of the Rod-like Iron-Iron Sulfide Eutectic at Elevated Temperatures,* Metall. Trans, 1, (10) 1970, 2953-2958.

[MAS95]   MASBAUM N.: *Ostwald-Reifung in zwei Dimensionen: Numerische Simulation von Teilchen-Teilchen-Korrelationen,* Diss. Universität Köln, 1995.

[MAT@]   http://www.matweb.com

[MEY74]   MEYER W.: *Vergleich der Einflüsse von Strontium, Antimon oder Natrium auf das Aluminium-Silizium-Eutektikum in Abhängigkeit von der Abkühlungsgeschwindigkeit,* Aluminium, 50, (7) 1974, 699-703.

[MEY85]   MEYERS C. W.: *Solution Heat Treatment Effects in A357 Alloys*, AFS Transactions, 93, 1995, 741-750.

[MÜR80]   MÜRRLE U., EXNER H. E. and STÖCKEL D.: *Gefügeinstabilität von Silber-Nickel-Faserverbundwerkstoffen*, Metall, 34, 1980, 617-621.

[NAK72]   NAKAGAWA Y.G. and WEATHERLY G. C.: *The Thermal Stability of the Rod Al₃Ni-Al Eutectic,* Acta Metall., 20, 1972, 345-350.

[NIE00]   NIEDICK I.: *Eignungsbewertung und Optimierung von Vormaterial für Thixoforming,* Diss. RWTH Aachen, Fortschr.-Ber. VDI Reihe 5 Nr. 607, VDI Verlag, Düsseldorf, 2000.

[OGR01]   OGRIS E., WAHLEN A., UGGOWITZER P.J. and KRALY A.; Semi-solid backward extrusion of Al-7075, Proc. of the Int. Symp. on Light Metals, COM 2001, Toronto, Ontario, Canada, August 26-29, 2001, 107-118.

[OGR02]   OGRIS E., LÜCHINGER H. and UGGOWITZER P.J.: Silicon Spheroidization Treatment of Thixoformed Al-Si-Mg Alloys, Materials Science Forum, 396-402, 2002, 149-154.

[PAC21]   PACZ A.: U.S. patent 1387900, 1921.

[PAR93]   PARAY F. and GRUZLESKI J.E.: *Modification - a Parameter to Consider in the Heat Treatment of Al-Si Alloys,* Cast Metals, 5 (4), 1993, 187-198.

[PAR96]   PARAY F. and GRUZLESKI J.E.: *Einfluss von Wärmebehandlung und Veredelung auf die mechanischen Eigenschaften der Legierung G-AlSi7Mg*, Giesserei-Praxis, 15/16, 1996, 300-312.

[PAR00]   PARAY F., KULUNK B. and GRUZLESKI J.E.: *Impact properties of Al-Si foundry alloys*, Int. J. Cast Metals Res., 13, 2000, 17-37.

[PÁR00]   PÁRAMO V., COLÁS R., VELASCO E. and VALTIERRA S.: *Spheroidization of the Al-Si Eutectic in a Cast Aluminum Alloy*, Journal of Materials Engineering and Performance, 9(6), (12) 2000, 616-622.

11 References

[PAU82]   PAUL J., EXNER H.E. and MÜLLER-SCHWELLING D.: *Gefügeausbildung und mechanische Eigenschaften von gegossenen und wärmebehandelten eutektischen Al-Si-Legierungen*, Z. Metallkunde, 73, 1982, 50-55.

[PEN98]   PENNORS L., SAMUEL A.M., SAMUEL F.H. and DOTY H.W.: *Precipitation of β-Al_5FeSi Iron Intermetallic in Al-6% Si-3.5% Cu (319) Type Alloys: Role of Sr and P*, AFS Transactions, 105, 1998, 251-264.

[QIY81]   QIYUN Z., CHAOGUI Z. and WANSHU H.: *The Modification of Al-Si Eutectic Alloys with Rare-Earth Elemets*, Acta Metallurgica Sinica, 17 (2), 1981, 136.

[RAV98]   RAVI M., PILLAI U.T.S., PAI B.C., DAMODARAN A.D. and DWARAKADASA E.S.: *Mechanical properties of cast Al-7Si-0.3Mg (LM 25/356) alloy*, Int. J. Cast Metals Res., 11, 1998, 113-125.

[RAY$_{18}$78]   LORD RAYLEIGH, Proc. Lond. math. Soc. 10, 4, 1878.

[RHI86]   RHINES F.N. and ABALLE M.: *Growth of Silicon Particles in an Aluminum Matrix*, Metallurgical Transactions A, 17A, (12) 1986, 2139-2152.

[ROB98]   ROBERGE J.L. and RICHARD M.: *Action des terres rares sur les alliages aluminum-silicon*, Fonderie, Fondeur d'aujourd'hui, 171(1), 1998, 15-35.

[ROM99]   ROMETSCH P.A., ARNBERG L. and ZHANG D.L.: *Modelling dissolution of Mg_2Si and homogenisation in Al-Si-Mg casting alloys*, Int. J. Cast Metals Res., 12, 1999, 1-8.

[RÖH41]   RÖHRIG H. and KÄPERNICK E.: *Über die beim Glühen von Al-Si Legierungen eintretenden Gefügeveränderungen*, Alumin., 23, 1941, 235-239.

[SAH99]   SAHM P.R., EGRY I. and VOLKMANN T. (Edt.): *Schmelze, Erstarrung, Grenzflächen - Eine Einführung in die Physik und Technologie flüssiger und fester Metalle*, Viehweg, Braunschweig/Wiesbaden, 1999.

[SHA99]   SHACKELFORD J. F.: *Introduction to Materials Science for Engineers*, Prentice Hall College Div, ISBN: 0130112879, 5th edition, 1999.

[SHI89]   SHIVKUMAR S., RICCI Jr. S., STEENHOFF B., APELIAN D. and SIGWORTH G.: *An Experimental Study to Optimize the Heat Treatment of A356 Alloy*, AFS Transactions, 97, 1989, 791-810.

[SHI90]   SHIVKUMAR S., RICCI Jr. S. and APELIAN D.: *Influence of Solution Parameters and Simplified Supersaturation Treatment on Tensile Properties of A356 Alloy*, AFS Transactions, 98, 1990, 913-922.

[SHI98]   SHIH T.-S. and SHIH F.-S.: *Effects of silicon, magnesium and strontium content on the qualities of Al-Si-Mg alloys*, Int. J. Cast Metals Res., 10, 1998, 273-282.

[SPE71]   SPENCER D.B. : PhD thesis, MIT, Cambridge, MA, USA, 1971.

[STÜ88]   STÜWE H.P. and KOLEDNIK O.: *Shape Instability of Thin Cylinders*, Acta metall., 36, 1988, 1705-1708.

[SUN97]   SUNDMAN B.: *Thermo-Calc Users' Guide*, Royal Inst. of Technology, KTH-Stockholm, Version M, 1997.

[TAY00]   TAYLOR J.A., JOHN D.H., BARRESI J. and COUPER M.J.: *Influence of Mg Content on the Microstructure and Solid Solution Chemistry of Al-7%Si-Mg Casting Alloys During Solution Treatment,* Materials Science Forum, 331-337, 2000, 277-282.

[TEN99]   TENSI H.M., SEIBOLD P., HÖGERL L.J., HALDENWANGER H.-G., LIPOWSKY H. and SCHNEIDER W.: *Optimization of Mechanical Properties of Advanced Aluminum Casting Alloys by Heat Treatment and Definition of a 'Ductility Value' for Safe Life Aluminum Casting Parts in the Automotive Industry*, Proc. of the 1st intern. Automotive Heat Treating Conference, Ohio ASM, 1999, 9-16.

[UBE96]   European Patent EP 745694: *Method and apparatus for shaping semisolid metals,* UBE Industries Ltd., 1996.

[UGG00a]   UGGOWITZER P.J., GULLO G.-C. and WAHLEN A.: *Metallkundliche Aspekte bei der semi-solid Formgebung von Leichtmetallen*, Vom Werkstoff zum Bauteil, ed. H. Kaufmann and P.J. Uggowitzer, LKR-Verlag Ranshofen, (5) 2000, 95-107.

[UGG00b]   UGGOWITZER P.J. and WAHLEN A.: *On the formation of eutectic phase in magnesium alloys during cooling from the semi-solid state,* Proc. 6th Int. Conf. on Semi-Solid Processing of Alloys and Components, Turin, Italy, Sept. 27-29, 2000, 429-435.

[VAL96]   VALER GONI J., RODRIGUEZ-IBABE J.M. and URCOLA J.J.: *Strength and Toughness of Semi-Solid Processed Hypereutectic Al/Si Alloys,* Scripta Materialia, 34 (3), 1996, 483-489.

[VEN91]   VENKATESWARAN S., MALLYA R.M. and SESHADRI R.: *The Effect of Trace Elements on the Cooling Curves, Microstructure and Mechanical Properties of Eutectic Aluminum-Silicon Alloy,* Cast Metals, 4(2), 1991, 72-82.

[VOJ01]   VOJE J. and DONS A.L.: *The type of Fe- and Mn-bearing particles in Al-7%Si foundry alloys, and the effect on the brittleness,* Aluminium, 77, (4) 2001, 284-287.

[VOL89]   VOLLERTSEN F. and VOGLER S.: *Werkstoffeigenschaften und Mikrostruktur,* München, Wien, Hanser, 1989, 280.

[WAB02]   WABUSSEG H.: *Process and alloy development for high quality alumin-ium components for lightweight construction - The New Rheocasting Process,* Diss. ETH Zürich, Shaker Verlag, Aachen, 2002.

[WAH01]   WAHLEN A.: *Processing of Aluminum Alloys in the Semi-Solid State - Basic Principles and Constitutive Models,* Diss. ETH-Zürich, 2001.

[WAL73]   WALTER J.L. and CLINE H.E.: *Stability of the Directionally Solidified Eutectics NiAl-Cr and NiAl-Mo,* Metall. Trans., 4, 1973, 33-38.

[WAL93]   WALY M.A.W.: *Vorgänge im Zusammenhang mit der Veredelung von Aluminium-Silizium-Legierungen am Beispiel AlSi7,* Diss. TU Berlin, 1993.

[WEN00]   WENDINGER B.: *Serial Production of Net Shaped and Weldable Struc-tural Components by Processing Thixalloy®,* Proc. 6th Int. Conf. on Semi-Solid Processing of Alloys and Components, Turin, Italy, Sept. 27-29, 2000, 103-108.

[WEN01]   WENDINGER B.: Personal communications, SAG - Thixalloy Compo-nents GmbH & Co KG, Lend, Austria, 2001.

[WER89]   WERNER E.: *The Spheroidization of Thin Plates*, Acta metall., 37 (7), 1989, 2047-2053.

[WER90a]   WERNER E.: *Thermal Shape Instabilities of Lamellar Structures,* Z. Metallkunde, 81, (11) 1990, 790-798.

[WER90b]   WERNER E.: *On the Kinetics of Pearlite Spheroidization,* Z. Metallkunde, 81, 1990, 668-671.

[WIL06]   WILM A.: DRP 244554 (German patent), 1906.

[WIL11]   WILM A.: *Physikalisch - metallurgische Untersuchungen über magne-siumhaltige Aluminiumlegierungen*, Metallurgie, 8, 1911.

[WOO@]   WOODS K.I.: *Aladar Pacz, Developer of Nonsag Tungsten,* http://www.frognet.net/~ejcov/pacz.html.

[YOU83]   YOUNG K.P., KYONKA C.P. and CURTOIS J.A.: *Fine grained metal composition,* US Patent 4415374, 1983.

[ZHA98]   ZHAO H. and WANG X.: *The morphology of cast zinc-based alloy rein-forced by spheroidal silicon phase and its wear resistance,* Int. J. Cast Metals Res., 11, 1998, 39-42.

[ZHU85]   ZHU P.Y., LIU Q.Y. and HOU T.X.: *Spheroidization of Eutectic Silicon in Al-Si Alloys*, AFS Transactions, 93, 1985, 609-614.

CURRICULUM VITAE

PERSONAL PARTICULARS

Name: Erhard Ogris

Date of Birth: 26.02.1975

Place of Birth: Klagenfurt (Austria)

Citizenship: Austrian

Civil Status: Married

EDUCATION

1985 - 1993: Bundesrealgymnasium Völkermarkterstrasse, Klagenfurt

1993:   Matura

1994-1999:   Student of Process Technology-Chemical Engineering, Technical University of Vienna (TU-Wien)

2000-2002:   Research scientist and Sc.D. student, Institute of Metallurgy, Swiss Federal Institute of Technology Zurich (ETH-Zürich)

PATENT

E. OGRIS, P.J. UGGOWITZER, J. WÖHRER: Aluminium-Silizium-Legierungen mit verbesserten mechanischen Eigenschaften, AT 20011733, 5.11.2001.

SELECTED PUBLICATIONS

OGRIS E., WAHLEN A., UGGOWITZER P.J. and KRALY A.: *Semi-solid backward extrusion of Al-7075*, Proc. of the Int. Symposium on Light Metals, COM 2001, Toronto, Ontario, Canada, August 26-29, 2001, 107-118.

OGRIS E., LÜCHINGER H. and UGGOWITZER P.J.: *Entwicklung eines neuen Wärmebehandlungsverfahrens für Aluminium-Silizium-Legierungen und insbesondere für Formteile aus Thixowerkstoffen*, Druckguss-Praxis, (1) 2002, 23-27.

OGRIS E., LÜCHINGER H. and UGGOWITZER P.J.: *Silicon Spheroidization Treatment (SST) - ein neues neuen Wärmebehandlungsverfahren für Aluminium-Silizium-Legierungen und insbesondere für Formteile aus Thixowerkstoffen*, Proc. of 2. Ranshofener Leichtmetalltage 2002, ISBN-3-902092-01-7, LKR-Verlag, Ranshofen, Austria, April 25-26, 2002, 58-69.

OGRIS E., LÜCHINGER H. and UGGOWITZER P.J.: *Silicon Spheroidization Treatment of Thixoformed Al-Si-Mg Alloys*, Materials Science Forum, 396-402, 2002, 149-154.

OGRIS E., LÜCHINGER H. and UGGOWITZER P.J.: SST - Ein Fortschritt im Wärmebehandeln von Al-Si Legierungen, Giessereiforschung, 54/3, 2002, 97-99.

OGRIS E., LÜCHINGER H. and UGGOWITZER P.J.: *On the High Ductility of Al-Si-Mg SSM Components*, Proc. of the 7th Intern. Conf. On Semi-Solid Processing of Alloys and Composites, Tsukuba, Japan, Sept. 24-28, 2002, 713-718.

OGRIS E., WAHLEN A., LÜCHINGER H. and UGGOWITZER P.J.: On the Silicon Spheroidization in Al-Si Alloys, Journal of Light Metals, in print.

OGRIS E., WAHLEN A., LÜCHINGER H. and UGGOWITZER P.J.: SST für Al-Si Legierungen - Entwicklung und Anwendung, Giessereiforschung, in print.

GAMMER K., OGRIS E., UGGOWITZER P.J. and HUTTER H.: SIMS Investigations on the Distribution of Trace Elements in Modified Aluminium-Silicon-Magnesium Alloys, Microchimica Acta, in print.